THE UNIVERSITY of EDINBURGH

Edinburgh Research Explorer

Petrogenesis of lavas from Detroit Seamount: Geochemical differences between Emperor Chain and Hawaiian volcanoes

Citation for published version:
Huang, S, Regelous, M, Thordarson, T & Frey, FA 2005, 'Petrogenesis of lavas from Detroit Seamount: Geochemical differences between Emperor Chain and Hawaiian volcanoes' Geochemistry, Geophysics, Geosystems, vol 6, no. 1, Q01L06, pp. 1-52., 10.1029/2004GC000756

Digital Object Identifier (DOI):
10.1029/2004GC000756

Link:
Link to publication record in Edinburgh Research Explorer

Document Version:
Publisher final version (usually the publisher pdf)

Published In:
Geochemistry, Geophysics, Geosystems

Publisher Rights Statement:
Published in Geochemistry, Geophysics, Geosystems by the American Geophysical Union (2005)

General rights
Copyright for the publications made accessible via the Edinburgh Research Explorer is retained by the author(s) and / or other copyright owners and it is a condition of accessing these publications that users recognise and abide by the legal requirements associated with these rights.

Take down policy
The University of Edinburgh has made every reasonable effort to ensure that Edinburgh Research Explorer content complies with UK legislation. If you believe that the public display of this file breaches copyright please contact openaccess@ed.ac.uk providing details, and we will remove access to the work immediately and investigate your claim.

OPEN ACCESS

Download date: 20. Feb. 2015

Geochemistry Geophysics Geosystems G3
AN ELECTRONIC JOURNAL OF THE EARTH SCIENCES
Published by AGU and the Geochemical Society

Article
Volume 6, Number 1
28 January 2005
Q01L06, doi:10.1029/2004GC000756
ISSN: 1525-2027

Petrogenesis of lavas from Detroit Seamount: Geochemical differences between Emperor Chain and Hawaiian volcanoes

S. Huang
Department of Earth, Atmospheric and Planetary Sciences, Massachusetts Institute of Technology, Cambridge, Massachusetts 02139, USA (huangs@mit.edu)

M. Regelous
Department of Earth Sciences, University of Bristol, Bristol, UK

Max-Planck Institut für Chemie, Postfach 3060, 55020 Mainz, Germany

T. Thordarson
Department of Geology and Geophysics, University of Hawaii at Manoa, Honolulu, Hawaii 96822, USA

F. A. Frey
Department of Earth, Atmospheric and Planetary Sciences, Massachusetts Institute of Technology, Cambridge, Massachusetts 02139, USA

[1] The Hawaiian Ridge and Emperor Seamount Chain define a hot spot track that provides an 80 Myr record of Hawaiian magmatism. Detroit Seamount (~76 to 81 Ma) is one of the oldest Emperor Seamounts. Volcanic rocks forming this seamount have been cored by the Ocean Drilling Program at six locations. Only tholeiitic basalt occurs at Site 884 on the eastern flank and only alkalic basalt, probably postshield lavas, occurs at Sites 883 and 1204 on the summit plateau. However, at Site 1203 the basement core (453 m penetration) includes four thick flows of pahoehoe alkalic basalt underlying ~300 m of volcaniclastic rocks interbedded with submarine erupted tholeiitic basalt. The geochemical characteristics of these alkalic lavas indicate that phlogopite was important in their petrogenesis; they may represent preshield stage volcanism. The surprising upward transition from subaerial to submarine eruptives implies rapid subsidence of the volcano, which can be explained by the inferred near-ridge axis setting of the seamount at ~80 Ma. A near-ridge axis setting with thin lithosphere is also consistent with a shallow depth of melt segregation for Detroit Seamount magmas relative to Hawaiian magmas, and the significant role for plagioclase fractionation as the Detroit Seamount magmas evolved in the crust. An important long-term trend along the hot spot track is that $^{87}Sr/^{86}Sr$ decreases in lavas erupted from ~40 to 80 Ma. Tholeiitic basalt at Site 884 on Detroit Seamount is the extreme and overlaps with the $^{87}Sr/^{86}Sr$-$^{143}Nd/^{144}Nd$ field of Pacific mid-ocean ridge basalts (MORB). Complementary evidence for a depleted component in Detroit Seamount lavas is that relative to Hawaiian basalt, Detroit Seamount lavas have lower abundances of incompatible elements at a given MgO content. These lavas, especially from Sites 883 and 884, trend to extremely unradiogenic Pb isotopic ratios which are unlike MORB erupted at the East Pacific Rise. A component with relatively low $^{87}Sr/^{86}Sr$ and $^{206}Pb/^{204}Pb$ is required. Lavas erupted from a spreading center in the Garrett transform fault, 13°28′S on the East Pacific Rise, have this characteristic. A plausible hypothesis is mixing of a plume-related component with a component similar to that expressed in lavas from the Garrett transform fault. However, basaltic glasses from Detroit Seamount also have relatively high Ba/Th, a distinctive characteristic of Hawaiian lavas. We argue that all Detroit Seamount lavas, including those from Site 884, are related to the Hawaiian hot spot. Rejuvenated stage Hawaiian lavas also have high Ba/Th and define a trend to low $^{87}Sr/^{86}Sr$ and $^{206}Pb/^{204}Pb$. We speculate that rejuvenated stage lavas and Detroit Seamount lavas sample a depleted mantle component, intrinsic to the plume, over the past 80 Myr.

Copyright 2005 by the American Geophysical Union

Components: 26,724 words, 19 figures, 10 tables.

Keywords: geochemical composition; Hawaiian hot spot; mantle heterogeneity; mantle plume; ODP.

Index Terms: 1025 Geochemistry: Composition of the mantle; 1040 Geochemistry: Radiogenic isotope geochemistry; 1065 Geochemistry: Major and trace element geochemistry; 1212 Geodesy and Gravity: Earth's interior: composition and state (7207, 7208, 8105, 8124); 9355 Geographic Location: Pacific Ocean.

Received 10 May 2004; **Revised** 16 October 2004; **Accepted** 18 November 2004; **Published** 28 January 2005.

Huang, S., M. Regelous, T. Thordarson, and F. A. Frey (2005), Petrogenesis of lavas from Detroit Seamount: Geochemical differences between Emperor Chain and Hawaiian volcanoes, *Geochem. Geophys. Geosyst.*, *6*, Q01L06, doi:10.1029/2004GC000756.

Theme: Movement, Dynamics, and Geochemical Evolution of the Hawaiian Hot Spot
Guest Editors: R. Duncan, J. A. Tarduno, D. Schull, and T. Davies

1. Introduction

[2] The linear intraplate Hawaiian Ridge and Emperor Seamount Chain define an approximately 6000 km long, age-progressive hot spot track [*Wilson*, 1963], ranging from active volcanoes at the southeastern end of the Hawaiian Ridge to >80 Myr old extinct volcanoes at the northern end of the Emperor Seamount Chain (Figure 1a). Hawaiian volcanoes are predominantly constructed by eruptions of basaltic magma with major and trace element compositions and radiogenic isotopic ratios that distinguish them from mid-ocean ridge basalt (MORB) [e.g., *Basaltic Volcanism Study Project*, 1981]. An understanding of the origin and evolution of Hawaiian magmatism requires documentation and understanding of geochemical variations in hot spot-derived lavas on both short-term (<1 Myr) and long-term (>10 Myr) time scales. On a time scale of ~1 Myr, volcanoes forming the Hawaiian islands evolve through a sequence of growth stages, characterized by the transition from alkalic to tholeiitic and back to alkalic magmatism [e.g., *Clague and Dalrymple*, 1987]. These transitions are consistent with passage of the Pacific plate over the hot spot [e.g., *Chen and Frey*, 1985]. Although there have been numerous studies of young volcanoes exposed on the Hawaiian Islands [e.g., *Rhodes and Lockwood*, 1995] (see Hawaii Scientific Drilling Project theme at http://www.agu.org/journals/gc/), much less is known about the geochemistry of lavas forming the older volcanoes of the submarine Emperor Seamount Chain. Are lavas forming the Emperor Seamounts geochemically similar to lavas forming Hawaiian volcanoes, and did these old volcanoes evolve through a similar sequence of growth stages?

[3] Detailed study of lavas forming the Emperor Seamounts requires drilling to penetrate the thick sedimentary cover and to obtain samples whose relative ages are known. The first detailed sampling of the Emperor Seamounts was during Deep Sea Drilling Project Leg 55, which penetrated 387 m of basalt at Suiko Seamount (Figure 1a). *Dalrymple et al.* [1980] and *Sharp and Clague* [2002] reported ages of 64.7 ± 1.1 Ma and 61.3 ± 0.5 Ma, respectively, for Suiko Seamount lavas. Important results are that: (1) like Hawaiian volcanoes, Suiko Seamount has shield stage lavas of tholeiitic basalt overlain by alkalic basalt [*Kirkpatrick et al.*, 1980]; (2) Initial $^{87}Sr/^{86}Sr$ ratios of tholeiitic basalt decrease from Daikakuji Seamount at the Hawaiian-Emperor bend to Suiko Seamount, which represent over 20 Myr of hot spot activity (~42–61 Ma, Figure 1a) [*Lanphere et al.*, 1980].

[4] More recently, the Ocean Drilling Program (ODP) Leg 145 drilled and cored the older Detroit Seamount (~76–81 Ma, Table 1, Figures 1a and 1b) [*Keller et al.*, 1995; *Duncan and Keller*, 2004]. The basaltic core from Site 883 and especially Site 884 of ODP Leg 145 yielded surprising results. Relative to primitive mantle and tholeiitic basalt from younger volcanoes on the Hawaiian Ridge-Emperor Seamount Chain, the ~81 Ma basalt from Site 884 has lower ratios of highly to moderately incompatible elements, lower initial $^{87}Sr/^{86}Sr$ and higher initial $^{143}Nd/^{144}Nd$ ratios; in fact, Site 884 lavas are similar to MORB [*Keller et al.*, 2000; *Regelous*

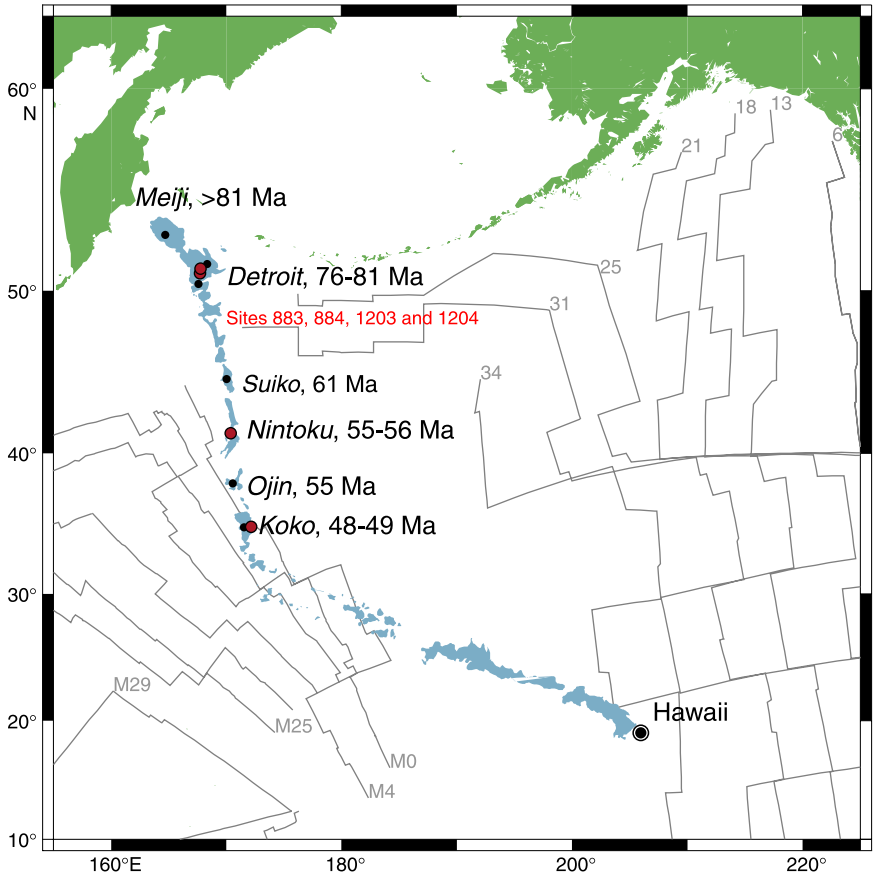

Figure 1a. The Hawaii-Emperor Seamount Chain and the location of Detroit Seamount. Modified from *Tarduno et al.* [2002] by adding new ^{40}Ar-^{39}Ar ages for Detroit Seamount, Nintoku Seamount, and Koko Seamount from *Duncan and Keller* [2004] and for Suiko Seamount from *Sharp and Clague* [2002]. Magnetic anomaly identifications are following *Mueller et al.* [1997].

et al., 2003]. These results have led to two contrasting interpretations for the origin and evolution of magma forming Detroit Seamount. *Keller et al.* [2000] noted that at ~80 Ma, the Hawaiian hot spot was located near an active mid-ocean ridge [see *Cottrell and Tarduno*, 2003, Figure 5c]. They suggest that the MORB-like isotopic signature of Detroit Seamount lavas from Site 884 resulted from entrainment of MORB-related upper mantle (i.e., hot low viscosity asthenosphere and hot thin lithosphere) by the rising mantle plume. In contrast, *Regelous et al.* [2003] propose that the depleted characteristics of Site 884 lavas reflect sampling of a depleted and refractory plume component by unusually high extents of mantle melting beneath young and thin oceanic lithosphere.

[5] During ODP Leg 197 three additional cores with basement penetrations of 61 to 453 m were recovered from Detroit Seamount (Table 1) [*Tarduno et al.*, 2002]. Lavas from Site 1203 yield ^{40}Ar-^{39}Ar ages of 76 ± 1 Ma [*Duncan and Keller*, 2004]. In this paper, we report major and trace element abundances for basaltic whole rocks recovered during ODP Leg 197 and basaltic glasses recovered during ODP Legs 197 and 145. In addition, Sr, Nd and Pb isotopic ratios are reported for whole-rock samples from Leg 197. We use these geochemical data, along with the petrographic and volcanological information to constrain the magmatic evolution at Detroit Seamount and to evaluate the two alternative hypotheses for the origin of its magmas.

[6] Important results are that (1) alkalic basalt at Sites 883 and 1204 may reflect postshield stage lavas, but the upward transition from intercalated alkalic and tholeiitic basalt to solely tholeiitic basalt at Hole 1203A may reflect the preshield to shield stage transition; (2) compared with Hawaiian shield stage lavas, tholeiitic basalt mag-

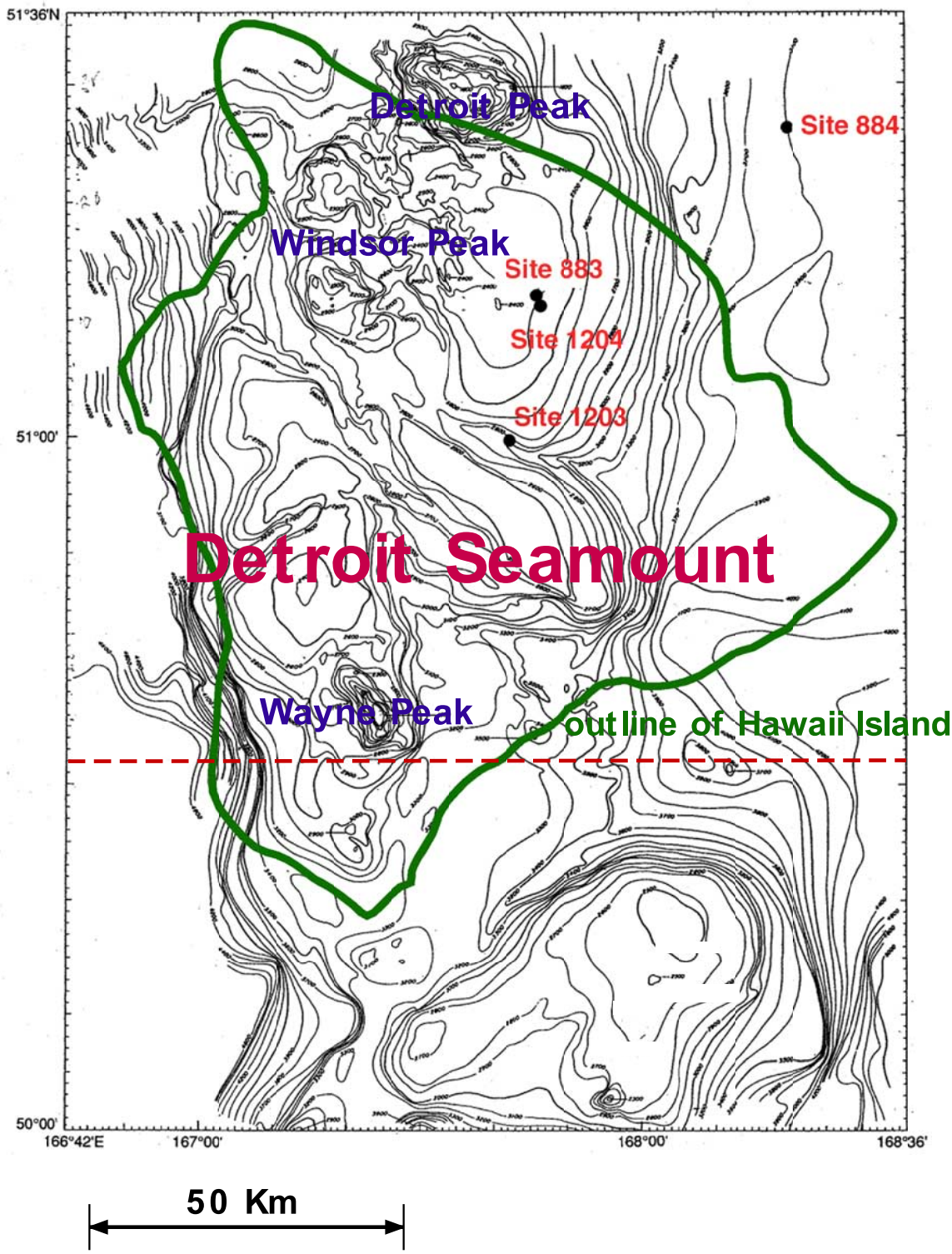

Figure 1b. Bathymetry of Detroit Seamount and drill site locations. Detroit Seamount refers to the region north of the red dashed line. Also shown is the outline of the Big Island of Hawaii (thick green line).

mas erupted at Detroit Seamount segregated at a lower mean pressure; (3) Detroit Seamount lavas sampled a depleted component (i.e., low $^{87}Sr/^{86}Sr$, Pb isotopic ratios and high $^{143}Nd/^{144}Nd$) that is not present in Hawaiian shield stage lavas or East Pacific Rise (EPR) MORB. It is also present in Hawaiian rejuvenated stage and North Arch lavas [*Frey et al.*, 2005]. We speculate that this depleted

Table 1. Sampling of Detroit Seamount

Hole	Penetration Into Basement, m	Basement Recovery, %
883E	37.8	63
883F	26.7	41
884E	87	76
1203A	452.6	56.5
1204A	60.8[a]	52
1204B	140.5	37.9

[a] The penetration of basement was 60.8 m at Hole 1204A. However, there was no recovery in the lower 22.4 m due to a clogged bit. The basement recovery rate is based on the upper 38.4 m. See *Shipboard Scientific Party* [2002b] for details.

component has been associated with the Hawaiian hot spot for ~80 Myr.

2. Detroit Seamount

2.1. Bathymetry

[7] A region of shallow seafloor, depths of 2400 to 3000 m, centered at 51°N in the northern part of the Emperor Seamount Chain has been referred to as Detroit Tablemount or Detroit Plateau [*Lonsdale et al.*, 1993]. We refer to this region as Detroit Seamount (Figures 1a and 1b). The area, 10,000 km^2, of the Detroit Seamount is similar to the subaerial part of the Big Island of Hawaii

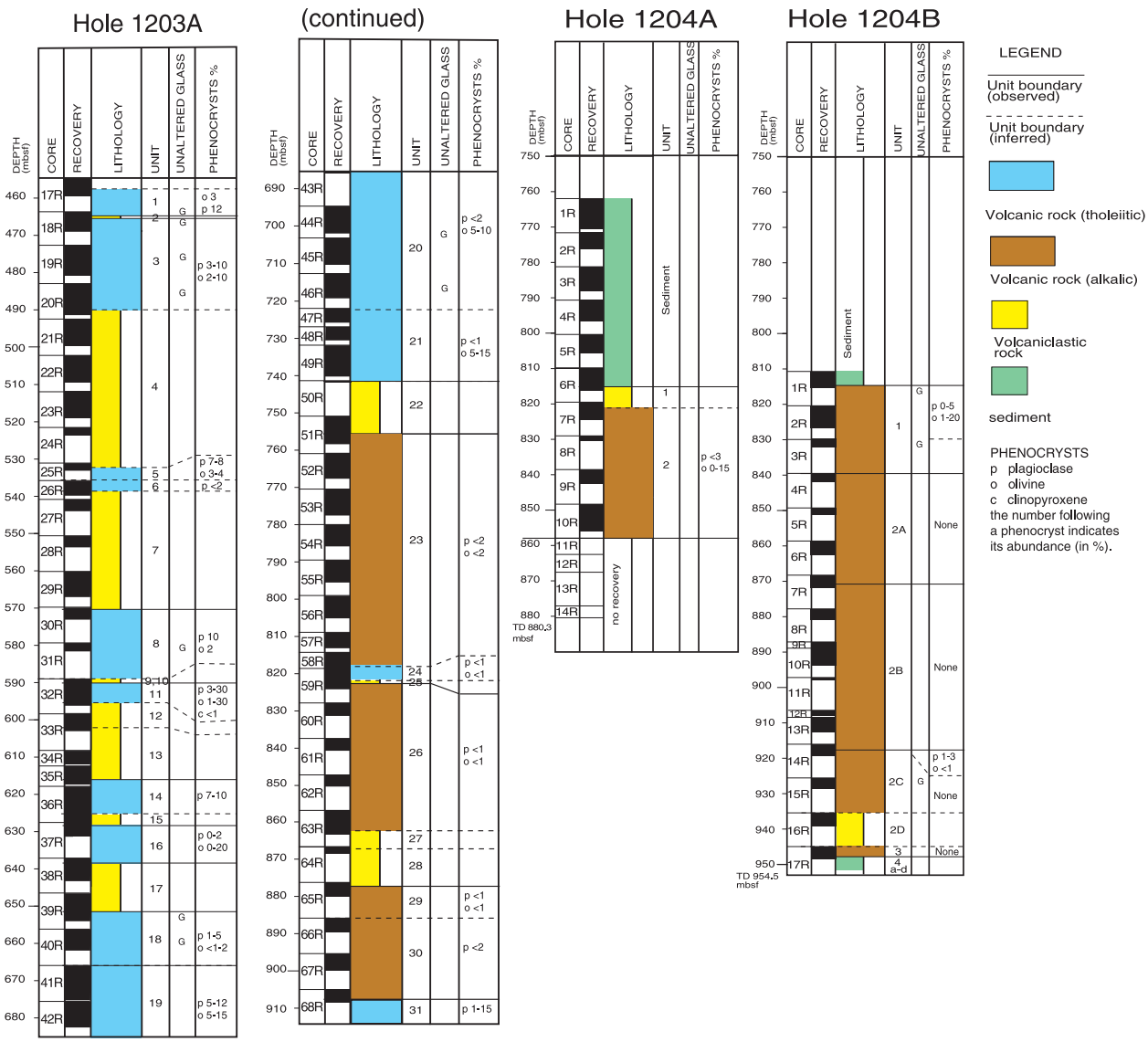

Figure 2. Stratigraphy of basement core at Holes 1203A, 1204A, and 1204B. Unit boundaries, rock types, presence of glass, and phenocryst abundance are indicated. Modified from *Tarduno et al.* [2002].

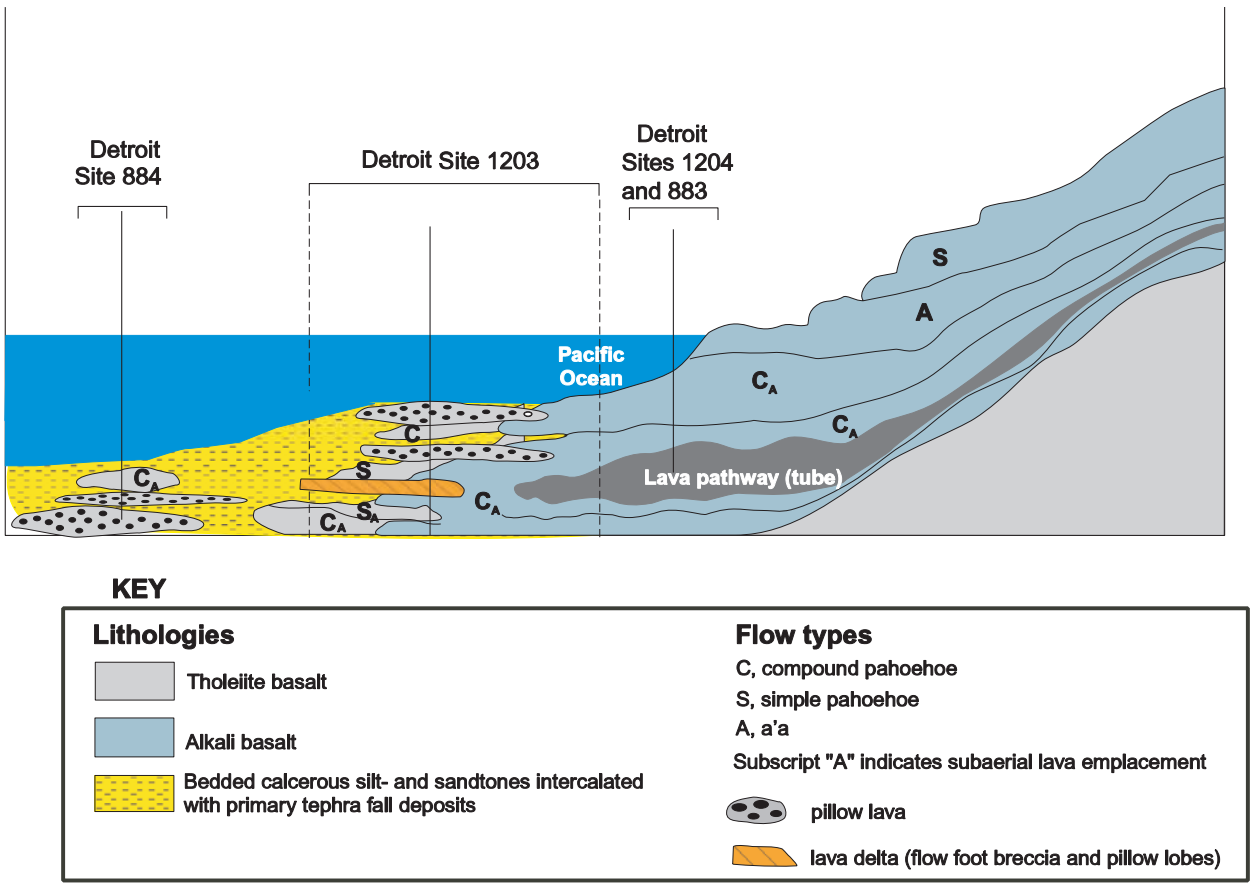

Figure 3. Inferred volcanic environment of four drill sites at Detroit Seamount. Modified from T. Thordarson et al. (manuscript in preparation, 2004). See text for details.

(Figure 1b). Like the Big Island, Detroit Seamount probably represents several coalesced volcanic shields [*Duncan and Keller*, 2004]. Three peaks, Detroit, Windsor and Wayne, reach shallower depths, up to 1388m (Figure 1b). Dredging of the northerly peak recovered lapilli hyalotuffs that included nepheline and perovskite-bearing lava fragments that were interpreted as rejuvenated stage volcanism, analogous to the highly alkalic rejuvenated stage of some Hawaiian volcanoes [*Lonsdale et al.*, 1993]. These unsedimented peaks were avoided during ODP drilling whose objective was to sample lavas erupted during the shield construction stage; such lavas are buried beneath 460 to 850 m of sediment.

2.2. Stratigraphy and Petrography

2.2.1. Hole 1203A

[8] Hole 1203A, located in a valley on the eastern flank of Detroit Seamount, penetrated 452.6 m into basement, and recovered parts of 18 lava flow units (Figures 1b and 2). Five samples from four tholeiitic units (Units 11, 14, 16 and 24) have been dated using the ^{40}Ar-^{39}Ar technique, and yield an age of 76 ± 1 Ma [*Duncan and Keller*, 2004]. From top to bottom, these lava flow units range from dominantly non-vesicular pillow lavas to dominantly vesicular compound pahoehoe lavas. Glassy lobe margins are present in all lava units except for Units 6 and 24 whose lobe margins were not recovered. Unaltered glass occurs in the lobe margins throughout the upper pillow lava units; but only altered glass occurs in the lower pahoehoe lava units. Vesicles are variably filled with secondary minerals, such as carbonate, zeolites and sulfides. The vesicular compound pahoehoe lavas are inferred to have been erupted subaerially, whereas the upper non-vesicular pillow lavas and some of the associated volcaniclastic rocks (Figure 2) are inferred to be submarine eruptives [*Shipboard Scientific Party*, 2002a] (Figure 3). Volatile analyses of glasses from lobe margins of these pillow lavas indicate that they

Table 2a. Whole-Rock Sample Information

Sample Name	Unit	Unit Name[a]	Basalt Type[b]	Lava Flow Type[a]	Unit Thickness,[a] m	Depth,[a] mbsf	Phenocryst,[c] %		
							PLAG	OL	CPX
1203A 17R4W 43-47	1	highly plagioclase-olivine-phyric basalt	tholeiitic	pillow lava	7.95	457.99	10	4	0
1203A 18R3W 116-119	3	highly plagioclase-olivine-phyric basalt	tholeiitic	pillow lava	24.60	467.96	10	3	1[d]
1203A 20R3W 10-14	3			pillow lava		486.1	9	4	9
1203A 25R1W 37-41	5	moderately plagioclase-olivine-phyric basalt	tholeiitic	sheet lobe	1.94	531.47	0	0	0
1203A 26R2W 5-9	6	sparsely plagioclase-phyric basalt	tholeiitic	sheet lobe	4.78	535.84	0	0	0
1203A 26R3W 97-101	6			sheet lobe		537.4	0	0	0
1203A 30R1W 108-112	8	highly plagioclase-olivine-phyric basalt	tholeiitic	pillow lava	18.70	570.88	2	0.5	0
1203A 31R1W 46-50	8			pillow lava		579.86	5	1	0
1203A 32R2W 32-36	11	plagioclase-olivine-phyric basalt	tholeiitic	sheet lobe	4.58	590.6	2	2	0
1203A 32R3W 58-62	11			sheet lobe		592.36	25	35	5
1203A 32R4W 76-80	11			sheet lobe		593.82	20	15	0
1203A 32R5W 60-64	11			sheet lobe		594.77	3	0.5	0
1203A 36R3W 25-29	14	moderately plagioclase-phyric basalt	tholeiitic	vesicular pillow lava	9.49	620.55	7	0	0
1203A 36R6W 18-22	14			vesicular pillow lava		624.18	8	0	0
1203A 37R2W 87-91	16	aphyric to highly-olivine-phyric basalt	tholeiitic	sheet lobe	10.37	629.87	0.5	16	0
1203A 37R3W 103-107	16			sheet lobe		631.53	0.5	45	0
1203A 38R1W 123-126	16			sheet lobe		638.33	1	4	0
1203A 39R5W 98-102	18	moderately plagioclase-olivine-phyric basalt	tholeiitic	vesicular pillow lava	14.57	653.14	5	3	0
1203A 42R1W 88-92	19	vesicular moderately olivine-phyric basalt	tholeiitic	compound pahoehoe	19.63	676.38	10	7	1
1203A 42R5W 40-44	19			compound pahoehoe		681.59	17	11	2
1203A 44R1W 75-79	20	moderately olivine-phyric basalt	tholeiitic	vesicular pillow lava	36.73	695.45	1	5	0
1203A 45R1W 35-39	20			vesicular pillow lava		703.45	1	5	0
1203A 46R4W 50-54	20			vesicular pillow lava		717.48	1	2	0
1203A 47R3W 50-54	21	moderately olivine-phyric basalt	tholeiitic	vesicular pillow lava	19.05	725.48	2	2	0
1203A 48R2W 96-100	21			vesicular pillow lava		729.4	2	0	0
1203A 49R3W 50-54	21			vesicular pillow lava		735.05	0	0	0
1203A 52R 6W 23-27	23	vesicular sparsely olivine-plagioclase-phyric to aphyric basalt	alkalic	compound pahoehoe	63.39	768.09	4	1	0
1203A 53R6W 123-127	23			compound pahoehoe		779.13	2	1	0
1203A 54R4W 74-78	23			compound pahoehoe		785.09	2	1	0
1203A 55R1W 109-113	23			compound pahoehoe		790.79	2	trace	0[e]
1203A 58R2W 94-98	23			compound pahoehoe		816.95	3	1	1
1203A 58R4W 37-41	24	vesicular aphyric basalt	tholeiitic	pahoehoe sheet lobe	3.38	819.24	1	0.5	0
1203A 59R2W 69-73	24			pahoehoe sheet lobe		820.55	0.5	0	0
1203A 62R1W 101-105	26	vesicular aphyric basalt	alkalic	compound pahoehoe	40.55	848.41	0	0	0
1203A 62R2W 88-92	26			compound pahoehoe		849.78	trace	0	0
1203A 63R4W 19-22	26			compound pahoehoe		861.65	0	0	0
1203A 65R4W 9-13	29	vesicular aphyric basalt	alkalic	compound pahoehoe	8.38	880.03	2	1	0
1203A 66R2W 8-10	30	vesicular, sparsely plagioclase-phyric basalt	alkalic	compound pahoehoe	23.76	887.38	1	4	0
1203A 67R4W 10-14	30			compound pahoehoe		899.9	0.5	0.5	0
1203A 68R4W 40-43	31b	highly plagioclase-phyric basalt	tholeiitic	pillow lava	$\gg$0.2	909.86	15	0.5	0

Table 2a. (continued)

Sample Name	Unit	Unit Name[a]	Basalt Type[b]	Lava Flow Type[a]	Unit Thickness,[a] m	Depth,[a] mbsf	Phenocryst,[c] %		
							PLAG	OL	CPX
1204A 7R3W 12-16	2	aphyric basalt	alkalic	vesicular pillow lava	35.49	822.44	0.5	0	0
1204A 8R1W 73-77	2			vesicular pillow lava		829.73	0.5	0	0
1204A 9R2W 55-59	2			vesicular pillow lava		840.65	0	0	0
1204A 9R2W 76-80	2			vesicular pillow lava		840.86	0.5	0	0
1204A 9R3W 25-27	2			vesicular pillow lava		841.85	0	0	0
1204A 10R2W 89-93	2			vesicular pillow lava		850.66	0	trace	0
1204A 10R2W 108-112	2			vesicular pillow lava		850.85	0	trace	0
1204A 10R3W 77-81	2			vesicular pillow lava		851.68	0	0	0
1204A 10R5W 44-48	2			vesicular pillow lava		854.26	0.5	0.5	0
1204B 1R4W 51-53	1	aphyric basalt	alkalic	vesicular pillow lava	27.07	815.26	<1	0	0
1204B 2R2W 76-80	1			vesicular pillow lava		822.36	<1	0	0
1204B 2R4W 102-105	1			vesicular pillow lava		824.82	<1	0	0
1204B 2R5W 11-15	1			vesicular pillow lava		825.26	<1	0	0
1204B 3R2W 41-44	1			vesicular pillow lava		831.76	<1	0	0
1204B 4R2W 49-53	2A	aphyric basalt	alkalic	vesicular pillow lava	30.53	841.59	0	0	0
1204B 6R1W 44-47	2A			vesicular pillow lava		859.04	0	0	0
1204B 7R2W 39-43	2A			vesicular pillow lava		870.06	0	0	0
1204B 7R3W 68-72	2A			vesicular pillow lava		871.85	0	0	0
1204B 8R2W 85-89	2B	diabase	alkalic	sheet lobe/internal pathway	46.22	880.15	0	0	0
1204B 9R3W 28-32	2B			sheet lobe/internal pathway		888.97	0	0	0
1204B 10R1W 11-14	2B			sheet lobe/internal pathway		888.91	0	0	0
1204B 10R2W 50-54	2B			sheet lobe/internal pathway		890.8	0	0	0
1204B 10R4W 43-47	2B			sheet lobe/internal pathway		892.79	0	0	0
1204B 12R1W 65-69	2B			sheet lobe/internal pathway		906.95	0	0	0
1204B 13R1W 118-122	2B			sheet lobe/internal pathway		909.48	0	0	0
1204B 14R1W 18-22	2B			sheet lobe/internal pathway		916.08	0	0	0
1204B 14R1W 87-91	2B			sheet lobe/internal pathway		916.77	0	0	0
1204B 17R1W 107-110	3	aphyric basalt	alkalic	vesicular pillow lava	2.33	945.97	0	0	0
1204B 17R2W 11-15	3			vesicular pillow lava		946.19	0	0	0

[a] Taken from *Tarduno et al.* [2002] with modification.
[b] See section 5.1 for details.
[c] Phenocryst content is estimated in volume%.
[d] Phenocrysts are low first-order yellow to gray and biaxial. They may be orthopyroxene.
[e] This sample contains a single clinopyroxene phenocryst (2.5 mm in diameter), which is attached to a plagioclase phenocryst.

Table 2b. Glass Sample Information

Sample Name	Unit[a]	Depth, mbsf
1203A 18R-2 17-21	1f: base of Unit 1 overlying sediment	465.47
1203A 18R-2 21-27	1f: glass at the top of Unit 2 sediment	465.51
1203A 19R-2 38-42	3k: glass in middle of lobe 3k	475.28
1203A 20R-1 106-107	3x: base of lobe, overlying 3y	484.06
1203A 20R-2 58-61	3ab top of lobe	485.08
1203A 31R-1 105-108	8k: glass in middle of lobe	580.45
1203A 31R-2 1-6	8m top of lobe	580.91
1203A 39R-6 57-63	18f top of lobe	653.97
1203A 40R-1 0-3	18h top of lobe	656.2
1203A 40R-1 65-70	18h bottom of lobe	656.85
1203A 40R-2 102-105	18i base of lobe	657.92
1203A 40R-2 142-146	18j base of lobe	658.32
1203A 40R-4 57-65	18n top of lobe	660.29
1203A 40R-4 80-90	18o top/side of lobe	660.52
1203A 45R-2 32-35	20s top of lobe	704.92
1203A 46R-4 0-4	20aj top of lobe	716.98
1204B 1R-3 69-81	Unit 1 glass fragments	814.39
1204B 3R-2 97-100	Unit 1 lobe boundary	832.2
1204B 3R-2 100-106	Unit 1 lobe boundary	832.35
1204B 3R-2 106-110	Unit 1 lobe boundary	832.41
1204B 15R-1 112-116	Unit 2c lobe margin	926.72
883E 20R-5 46-50	Unit 8 top	
883E 22R-2 105-110	Unit 17 lobe margin	
883E 22R-4 112-120	Unit 19-20 boundary	
884E 10R-5 59-62	Unit 11 top	
884E 10R-6 38-40	Unit 11 base	
884E 10R-6 118-121	Unit 13 top	

[a] Most units are multilobed, and are divided into subunits. Letters after numbers refer to subunits. See *Tarduno et al.* [2002] for a detailed documentation of subunits.

were erupted at variable water depths. In detail, uppermost pillow lavas, Units 3 and 8, are undegassed; hence they were erupted in water depths greater than 500 m. In contrast, the deeper pillow lavas, Units 14 and 18, are partially degassed, and inferred eruption water depths are less than 500 m (T. Thordarson et al., manuscript in preparation, 2004).

[9] The subsidence indicated by the upward transition from subaerial to submarine eruptives differs from that of a typical Hawaiian volcano. For example, submarine lavas underlie subaerial lavas in the drill core for Mauna Kea volcano recovered by the Hawaii Scientific Drilling Project (HSDP) [*DePaolo et al.*, 1999]. That is, the accumulation rate, 9 to 18 mm/yr (W. D. Sharp and P. Renne, $^{40}Ar/^{39}Ar$ dating of core recovered by the Hawaii Scientific Drilling Project (phase 2) Hilo, Hawaii, submitted to *Geochemistry, Geophysics, Geosystems*, 2004), for the HSDP drill core from Mauna Kea was greater than subsidence rate of the Big Island, ~2.4 mm/yr [*Moore*, 1987]. The dominance of subsidence rate over accumulation rate at Detroit Seamount can be explained by a lower accumulation rate and the proximity of the seamount to an active spreading center at ~80 Ma [*Rea and Dixon*, 1983; *Mammerickx and Sharman*, 1988; *Cottrell and Tarduno*, 2003]. The relatively thin and weak oceanic lithosphere close to a spreading center subsides rapidly [e.g., *Parsons and Sclater*, 1977; *Stein and Stein*, 1992], so it is possible that during the growth of Detroit Seamount the subsidence rate was greater than the volcano accumulation rate.

[10] Lava flows from Hole 1203A are aphyric to olivine-and/or-plagioclase-phyric basalt (Table 2a). Plagioclase and olivine phenocrysts commonly occur as glomerocrysts. Large plagioclase phenocrysts/glomerocrysts, up to 1.3 cm in length, occur in Units 14 and 31. Trace amounts (<5%) of clinopyroxene phenocrysts occur in several units (Table 2a). Some plagioclase phenocrysts have rounded or embayed margins, which suggests that they are not in equilibrium with surrounding groundmass. Olivine rich zones, containing >10% olivine by volume, occur in Units 11 and 16. Some olivine phenocrysts are unaltered, but many are altered to clay, iddingsite, Fe-oxyhydroxide and carbonate, and they are recognized by their equant form and characteristic fracture patterns. The groundmass of these lavas consists of plagioclase,

clinopyroxene, opaque minerals (mostly titanomagnetite) and glass (usually devitrified).

2.2.2. Holes 883E, 883F, 1204A, and 1204B

[11] Site 1204 is ~27 km north of Site 1203, and within ~0.5 km of Site 883. Both sites are located on the edge of a summit plateau (Figure 1b). Holes 1204A and 1204B were drilled within ~100 m of each other. Five samples from Site 1204 and two from Site 883 yield no reliable ^{40}Ar-^{39}Ar ages [*Keller et al.*, 1995; *Duncan and Keller*, 2004]. However, nannofossils in the sediment overlying and intercalated within the basalt from Site 1204 imply a minimal age of 71–76 Ma (cc22-23 [*Shipboard Scientific Party*, 2002b]). At Hole 1204A the basement penetration was 60.8 m, but a clogged bit limited recovery to 38.4 m of one vesicular pillow lava flow unit (Table 1; Figure 2). Hole 1204B penetrated 140.5 m into basement, and recovered 3 lava flow units; Unit 2 is ~77 m thick (Figure 2). These lava flow units, except for subunit 2B, are multilobed vesicular pillow lavas, and unaltered glass was recovered from several glassy margins. Subunit 2B is composed of coarse grained (up to 6 mm) diabase: From the upper and lower margins toward the center of this subunit, grain size ranges from highly vesicular aphanitic to fine-grained to sparsely vesicular medium-grained with ophitic to subophitic texture. This subunit may be a submarine sheet lobe or it may represent an internal transport system that fed an active flow front (Figure 3; T. Thordarson et al., manuscript in preparation, 2004). On the basis of their high vesicularity, Site 1204 lavas, and nearby Site 883 lavas, were classified as subaerially erupted pahoehoe flows by *Shipboard Scientific Party* [2002b]. However, volatile analyses of glasses associated with these lavas indicate that these lavas were only partially degassed upon eruption. They probably erupted at relatively shallow water depths (<500–1000 m) (Figure 3; T. Thordarson et al., manuscript in preparation, 2004).

[12] The four lava flow units from Site 1204 are nearly aphyric, with some units containing trace amounts (<5%) of plagioclase phenocrysts and olivine and plagioclase microphenocrysts. These lava flows range from highly vesicular (up to 30% close to lobe margins) to non-vesicular (in diabase). Vesicles are variably filled with secondary minerals, such as carbonate, zeolites, sulfides and green clay. Olivine, in groundmass or as microphenocrysts, is altered to Fe-oxyhydroxide, iddingsite and carbonate. Glass in groundmass is altered to green and brown clays and Fe-oxyhydroxide.

2.2.3. Hole 884E

[13] In contrast to the relatively shallow water depth of Sites 1203, 1204 and 883 (2370–2593 m), Site 884 is located in deeper water (3284 m) on the northeastern flank of Detroit Seamount (Figure 1b). Only one of three samples from this drill site yields a meaningful ^{40}Ar-^{39}Ar plateau age: 81 ± 1 Ma [*Keller et al.*, 1995]. Hole 884E was drilled 87 m into basement and recovered 13 cooling units [*Shipboard Scientific Party*, 1993]. From top to bottom, these lava flow units range from variably vesicular (0–30%) pahoehoe lavas to non-vesicular pillow lavas. Unaltered glass only occurs in the lobe margins of lower pillow lavas, and their volatile contents require eruption at deep water depth (>500 m) (Figure 3; T. Thordarson et al., manuscript in preparation, 2004). No volcaniclastic rock was recovered from Hole 884E.

[14] At Site 884 the upper pahoehoe lavas range from aphyric to highly plagioclase-phyric to megaphyric basalt. Lower pillow lavas range from highly plagioclase-phyric to megaphyric to highly plagioclase-olivine basalt [*Shipboard Scientific Party*, 1993]. The compositional zonation of cm-size plagioclase reflects magma mixing [*Kinman and Neal*, 2002].

3. Samples and Sample Preparation

[15] All lava flow units recovered from Detroit Seamount during ODP Leg 197 were sampled and multiple samples were collected from thick units. Table 2a shows the unit number, name and thickness, basalt type, lava flow type and phenocryst proportions for each sample. Unaltered glass was obtained from 12 units at Sites 883, 884, 1203 and 1204 (Table 2b).

[16] Highly altered regions, such as amygdules and veins, were removed from all samples selected for whole-rock analysis. The trimmed whole-rock samples were wrapped in plastic and crushed with a hammer into small pieces (<0.5 cm). Again, pieces containing filled vesicles and/or veins were removed. The remaining chips were rinsed with deionized water several times before pulverizing in an agate shatter box. Fragments of unaltered glass were hand-picked using a binocular microscope. To remove alteration phases, these fragments were

Table 3a. Whole-Rock Analyses[a]

Sample Name	Unit	Unit Name	Depth, mbsf	LOI[b]	SiO_2	TiO_2	Al_2O_3	Fe_2O_3*[c]	MnO	MgO	CaO	Na_2O	K_2O	P_2O_5	Total[d]
1203A 17R4W 43-47	1	highly plagioclase-olivine-phyric basalt	457.99	2.13	49.4	1.99	16.0	11.0	0.16	6.01	12.1	2.36	0.56	0.21	99.7
1203A 18R3W 116-119	3	highly plagioclase-olivine-phyric basalt	467.96	2.18	48.6	1.95	15.3	12.7	0.17	5.90	11.7	2.39	0.64	0.20	99.5
1203A 20R3W 10-14	3	highly plagioclase-olivine-phyric basalt	486.1	1.39	49.3	1.95	15.6	11.3	0.16	7.00	11.9	2.10	0.17	0.19	99.7
1203A 25R1W 37-41	5	moderately plagioclase-olivine-phyric basalt	531.47	3.18	48.1	2.04	16.1	12.4	0.17	8.71	9.12	2.67	0.33	0.22	99.9
1203A 26R2W 5-9	6	sparsely plagioclase-phyric basalt	535.84	4.49	47.7	2.00	16.1	12.4	0.18	10.0	8.26	2.32	0.27	0.21	99.4
1203A 26R3W 97-101	6	sparsely plagioclase-phyric basalt	537.4	4.13	47.9	1.91	15.7	12.5	0.21	9.99	8.45	2.38	0.36	0.23	99.7
1203A 30R1W 108-112	8	highly plagioclase-olivine-phyric basalt	570.88	0.370	49.0	1.95	15.6	12.2	0.21	5.63	12.5	2.17	0.27	0.20	99.8
1203A 31R1W 46-50	8	highly plagioclase-olivine-phyric basalt	579.86	1.55	49.5	1.94	15.9	10.3	0.24	6.46	12.3	2.51	0.25	0.19	99.6
1203A 32R2W 32-36	11	plagioclase-olivine-phyric basalt	590.6	2.32	50.1	2.01	15.7	11.3	0.12	8.59	8.22	3.05	0.37	0.20	99.7
1203A 32R3W 58-62	11	plagioclase-olivine-phyric basalt	592.36	1.56	44.7	0.94	9.94	13.3	0.20	21.9	7.15	1.06	0.14	0.10	99.5
1203A 32R4W 76-80	11	plagioclase-olivine-phyric basalt	593.82	1.99	48.4	1.54	16.3	11.7	0.15	7.89	11.5	2.06	0.15	0.16	99.8
1203A 32R5W 60-64	11	plagioclase-olivine-phyric basalt	594.77	2.27	49.3	1.89	15.7	11.3	0.13	8.11	9.87	2.80	0.29	0.17	99.5
1203A 36R3W 25-29	14	moderately plagioclase-phyric basalt	620.55	1.52	48.9	1.68	17.9	9.80	0.17	5.74	12.9	2.37	0.10	0.16	99.7
1203A 36R6W 18-22	14	moderately plagioclase-phyric basalt	624.18	1.37	49.8	1.77	18.0	9.10	0.13	6.11	11.8	2.71	0.15	0.17	99.7
1203A 37R2W 87-91	16	aphyric to highly-olivine-phyric basalt	629.87	3.23	47.3	1.23	14.4	11.8	0.16	13.3	9.68	1.34	0.10	0.10	99.5
1203A 37R3W 103-107	16	aphyric to highly-olivine-phyric basalt	631.53	1.51	43.8	0.72	7.78	12.4	0.18	28.4	5.41	0.86	0.08	0.06	99.7
1203A 38R1W 123-126	16	aphyric to highly-olivine-phyric basalt	638.33	1.78	48.7	1.44	15.4	12.1	0.17	8.31	11.3	1.74	0.16	0.12	99.4
1203A 39R5W 98-102	18	moderately plagioclase-olivine-phyric basalt	653.14	3.08	48.4	1.74	15.9	11.0	0.24	6.58	13.3	2.20	0.27	0.19	99.8
1203A 42R1W 88-92	19	vesicular moderately olivine-phyric basalt	676.38	5.35	47.9	1.56	15.5	11.0	0.17	8.49	11.9	2.02	1.14	0.14	99.7
1203A 42R5W 40-44	19	vesicular moderately olivine-phyric basalt	681.59	3.59	47.9	1.54	15.3	11.0	0.19	9.89	11.4	2.50	0.08	0.15	100.0
1203A 44R1W 75-79	20	moderately olivine-phyric basalt	695.45	5.23	47.3	2.17	15.2	11.8	0.21	6.26	13.0	2.19	1.25	0.20	99.5
1203A 45R1W 35-39	20	moderately olivine-phyric basalt	703.45	8.01	45.6	2.13	16.1	14.6	0.22	3.10	11.5	4.05	2.19	0.35	99.8
1203A 46R4W 50-54	20	moderately olivine-phyric basalt	717.48	10.9	44.3	2.21	15.2	12.5	0.30	3.65	16.2	3.26	1.67	0.27	99.5
1203A 47R3W 50-54	21	moderately olivine-phyric basalt	725.48	3.28	49.1	2.21	15.9	11.9	0.20	9.43	8.51	2.25	0.31	0.20	100.0
1203A 48R2W 96-100	21	moderately olivine-phyric basalt	729.4	2.93	48.1	2.17	15.4	13.3	0.19	8.33	9.50	2.47	0.25	0.20	99.8
1203A 49R3W 50-54	21	moderately olivine-phyric basalt	735.05	1.83	47.8	2.19	14.9	13.5	0.20	8.34	10.3	2.07	0.08	0.20	99.6
1203A 52R 6W 23-27	23	vesicular sparsely olivine-plagioclase-phyric to aphyric basalt	768.09	3.02	48.2	2.59	16.0	11.6	0.18	8.01	8.98	3.19	0.30	0.47	99.5
1203A 53R6W 123-127	23	vesicular sparsely olivine-plagioclase-phyric to aphyric basalt	779.13	2.52	47.6	2.58	15.3	12.7	0.19	6.90	10.8	2.90	0.18	0.48	99.6
1203A 54R4W 74-78	23	vesicular sparsely olivine-plagioclase-phyric to aphyric basalt	785.09	1.48	48.1	2.88	15.7	12.4	0.19	5.98	11.1	2.94	0.13	0.54	99.9
1203A 55R1W 109-113	23	vesicular sparsely olivine-plagioclase-phyric to aphyric basalt	790.79	1.98	47.5	2.69	15.5	12.6	0.20	6.42	10.8	2.76	0.40	0.51	99.4
1203A 58R2W 94-98	23	vesicular sparsely olivine-plagioclase-phyric to aphyric basalt	816.95	1.96	47.8	2.66	15.0	13.1	0.25	7.02	10.4	2.54	0.45	0.49	99.7
1203A 58R4W 37-41	24	vesicular aphyric basalt	819.24	1.83	49.0	1.72	15.5	11.8	0.18	7.75	11.2	2.63	0.24	0.17	100.1
1203A 59R2W 69-73	24	vesicular aphyric basalt	820.55	1.98	48.5	1.76	15.5	11.9	0.15	7.56	11.5	2.41	0.09	0.17	99.5
1203A 62R1W 101-105	26	vesicular aphyric basalt	848.41	4.85	45.2	3.30	13.7	13.1	0.30	5.45	14.4	2.53	1.00	0.68	99.7
1203A 62R2W 88-92	26	vesicular aphyric basalt	849.78	3.97	47.4	2.93	15.1	12.5	0.19	9.16	8.21	3.12	0.36	0.56	99.4
1203A 63R4W 19-22	26	vesicular aphyric basalt	861.65	3.23	49.0	3.05	15.6	11.8	0.16	9.28	7.16	3.28	0.35	0.58	100.2
1203A 65R4W 9-13	29	vesicular aphyric basalt	880.03	3.79	47.6	3.60	15.1	14.0	0.18	6.77	7.62	2.75	1.51	0.65	99.8
1203A 66R2W 8-10	30	vesicular, sparsely plagioclase-phyric basalt	887.38	4.83	46.5	3.44	14.8	15.4	0.15	7.56	6.76	2.74	1.79	0.63	99.7
1203A 67R4W 10-14	30	vesicular, sparsely plagioclase-phyric basalt	899.9	3.62	47.5	3.19	14.6	13.4	0.16	6.06	9.94	2.62	1.50	0.51	99.5
1203A 68R4W 40-43	31b	highly plagioclase-phyric basalt	909.86	3.22	48.8	1.40	19.3	10.4	0.10	5.72	10.8	2.09	1.05	0.10	99.8

Table 3a. (continued)

Sample Name	Unit	XRF	Nb	Zr	Y	Sr	Rb	Zn	Ni	Cr	V	ICP-MS	Sc	Rb	Sr	Y	Zr	Nb	Ba	La	Ce	Pr	Nd
1203A 17R4W 43-47	1		8.2	124	27.3	249	9.0	108	80	271	265		40.6	9.21	244	30.9	124	8.69	41.0	7.41	19.4	3.08	14.3
1203A 18R3W 116-119	3		8.1	123	26.2	238	11.6	109	71	247	297		38.8	11.4	229	29.2	120	8.69	35.2	7.02	18.4	2.95	14.0
1203A 20R3W 10-14	3		8.0	122	26.5	246	0.4	113	98	236	305		39.8	0.731	232	29.0	118	8.60	30.1	6.80	18.4	2.90	13.8
1203A 25R1W 37-41	5		8.2	129	24.9	231	3.8	88	130	232	257		35.1	3.81	227	28.2	128	9.02	54.9	7.40	19.4	3.07	14.6
1203A 26R2W 5-9	6		7.7	123	24.2	227	1.3	85	133	259	244		33.8	1.46	214	26.9	122	8.52	51.9	6.97	18.3	2.95	13.8
1203A 26R3W 97-101	6		8.1	128	25.6	215	2.8	84	150	238	215		30.9	2.98	201	28.1	127	8.98	55.0	7.47	20.0	3.05	14.6
1203A 30R1W 108-112	8		7.5	117	26.2	243	3.2	111	89	260	298		40.1	3.53	230	28.9	112	8.03	25.0	6.65	17.5	2.84	13.5
1203A 31R1W 46-50	8		7.4	117	26.5	253	1.0	110	97	250	303		43.4	1.22	252	29.5	114	8.15	37.9	6.67	17.7	2.81	13.5
1203A 32R2W 32-36	11		7.4	117	25.2	238	3.4	109	76	290	304		43.2	3.44	232	28.4	115	8.35	48.4	6.95	18.0	2.90	13.7
1203A 32R3W 58-62	11		3.4	55	12.8	164	1.7	86	812	651	140		21.1	1.87	150	13.7	54	3.91	23.5	3.25	8.2	1.36	6.5
1203A 32R4W 76-80	11		5.9	92	20.7	235	1.2	81	120	264	200		33.1	1.31	223	22.5	89	6.26	29.9	5.25	14.0	2.24	10.6
1203A 32R5W 60-64	11		6.8	107	22.0	229	1.6	106	76	262	298		40.7	1.62	217	24.0	104	7.47	40.6	5.95	15.7	2.54	12.1
1203A 36R3W 25-29	14		6.4	97	22.3	266	0.3	87	77	272	263		36.9	0.390	257	24.3	94	6.76	27.1	5.69	14.7	2.43	11.7
1203A 36R6W 18-22	14		6.7	103	22.1	271	0.4	79	81	306	284		38.1	0.689	257	24.3	100	7.24	36.5	6.10	15.9	2.53	12.1
1203A 37R2W 87-91	16		3.0	65	17.5	155	1.1	84	376	895	187		31.1	1.21	144	18.9	65	3.43	17.3	3.11	8.55	1.47	7.39
1203A 37R3W 103-107	16		1.9	41	10.7	90	1.2	85	1322	1442	124		20.0	0.990	83	11.7	41	2.09	11.5	1.95	5.29	0.914	4.67
1203A 38R1W 123-126	16		4.0	81	21.1	195	1.3	89	164	353	232		34.5	1.51	186	23.5	80	4.34	25.4	4.04	10.9	1.87	9.33
1203A 39R5W 98-102	18		6.8	103	23.2	260	5.3	89	112	268	249		34.7	5.15	240	24.8	101	7.33	26.5	6.15	16.1	2.56	12.2
1203A 42R1W 88-92	19		5.3	85	20.0	201	16.6	85	174	372	203		31.9	16.8	197	22.5	84	5.73	27.5	4.84	12.8	2.13	10.1
1203A 42R5W 40-44	19		5.3	85	20.3	242	0.6	84	212	487	231		32.7	0.794	233	22.4	85	5.67	16.1	4.85	12.5	2.03	10.0
1203A 44R1W 75-79	20		7.2	119	28.2	208	15.9	105	119	247	297		44.8	17.3	222	33.7	126	8.24	37.3	6.52	17.6	2.91	14.1
1203A 45R1W 35-39	20		6.7	113	27.7	244	27.4	97	99	245	339		48.2	30.9	272	35.3	125	8.15	51.9	6.79	17.6	2.86	13.8
1203A 46R4W 50-54	20		6.7	113	27.3	324	20.6	105	93	277	336		47.0	23.2	356	34.3	122	7.89	48.4	6.45	16.9	2.80	13.7
1203A 47R3W 50-54	21		7.3	122	27.6	191	1.2	102	114	242	306		46.8	1.23	206	34.1	132	8.67	33.0	6.60	18.3	2.95	14.5
1203A 48R2W 96-100	21		7.3	121	29.2	189	2.3	102	102	238	296		47.4	2.80	198	35.5	129	8.39	43.5	6.74	17.8	2.90	14.1
1203A 49R3W 50-54	21		7.1	121	29.4	197	0.0	97	115	273	299		49.7	0.302	206	35.8	128	8.33	27.7	6.64	17.9	2.93	14.3
1203A 52R 6W 23-27	23		13.6	214	35.4	235	0.8	112	104	183	299		44.0	0.844	250	43.4	229	15.4	46.4	12.3	32.9	4.98	23.6
1203A 53R6W 123-127	23		13.9	216	39.7	232	0.0	126	92	183	295		42.8	0.481	244	48.3	232	15.6	47.0	12.7	34.5	5.29	25.2
1203A 54R4W 74-78	23		15.5	244	45.3	254	0.0	137	85	200	328		49.2	0.343	260	54.8	256	17.3	52.2	14.4	38.3	5.88	28.0
1203A 55R1W 109-113	23		14.6	228	41.8	237	3.7	131	94	187	305		44.0	4.36	245	50.6	239	16.1	46.4	13.6	36.1	5.52	26.6
1203A 58R2W 94-98	23		14.1	222	40.1	228	0.5	121	82	180	298		38.1	1.28	229	46.8	225	15.5	50.2	12.8	34.7	5.34	25.4
1203A 58R4W 37-41	24		5.8	103	24.2	221	2.8	84	107	267	238		38.5	3.02	211	27.0	100	6.38	44.0	5.67	14.9	2.46	11.9
1203A 59R2W 69-73	24		5.9	107	24.8	233	0.0	86	106	249	239		36.9	0.386	219	27.1	103	6.53	32.6	5.63	15.3	2.51	12.0
1203A 62R1W 101-105	26		18.5	284	54.1	219	8.0	137	66	129	335		38.1	8.01	210	62.3	283	19.4	62.3	17.6	46.1	6.94	33.1
1203A 62R2W 88-92	26		15.9	246	41.6	225	0.5	120	86	136	310		33.7	0.913	216	46.7	245	16.8	55.2	14.4	38.1	5.68	26.8
1203A 63R4W 19-22	26		16.7	255	38.1	239	0.8	108	95	145	331		34.0	0.893	225	42.9	257	17.8	61.3	14.9	39.2	5.87	27.3
1203A 65R4W 9-13	29		15.8	211	41.2	236	17.8	150	75	179	363		39.0	17.8	230	46.1	203	16.2	62.7	14.0	37.2	5.61	26.8
1203A 66R2W 8-10	30		14.9	199	38.3	225	24.1	142	63	167	384		35.1	23.0	211	42.1	192	15.0	57.6	13.4	34.8	5.19	24.6
1203A 67R4W 10-14	30		14.0	185	36.9	234	9.4	140	92	160	337		36.5	9.37	226	41.8	185	15.0	58.4	12.3	32.7	5.09	24.4
1203A 68R4W 40-43	31b		4.6	79	19.9	218	27.4	93	72	277	217		31.3	27.7	212	21.8	76	4.83	28.9	5.19	13.3	2.18	10.6

Table 3a. (continued)

Sample Name	Unit	ICP-MS	Sm	Eu	Gd	Tb	Dy	Ho	Er	Tm	Yb	Lu	Hf	Ta	Pb	Th	U
1203A 17R4W 43-47	1		4.25	1.55	5.05	0.881	5.30	1.09	2.94	0.428	2.65	0.386	3.13	0.609	0.834	0.560	0.769
1203A 18R3W 116-119	3		4.13	1.51	4.89	0.845	5.05	1.05	2.85	0.425	2.54	0.361	3.12	0.613	0.708	0.552	0.286
1203A 20R3W 10-14	3		4.00	1.46	4.84	0.826	5.00	1.02	2.78	0.409	2.51	0.374	3.01	0.589	0.814	0.542	0.149
1203A 25R1W 37-41	5		4.15	1.52	4.77	0.823	4.90	1.00	2.76	0.412	2.51	0.359	3.14	0.590	0.674	0.555	0.182
1203A 26R2W 5-9	6		3.98	1.47	4.60	0.787	4.71	0.974	2.67	0.390	2.42	0.352	3.08	0.553	0.633	0.527	0.172
1203A 26R3W 97-101	6		4.13	1.49	4.80	0.819	4.88	1.00	2.73	0.419	2.45	0.363	3.15	0.575	0.937	0.561	0.182
1203A 30R1W 108-112	8		4.07	1.50	4.87	0.845	5.10	1.05	2.91	0.423	2.58	0.371	3.00	0.551	0.726	0.512	0.183
1203A 31R1W 46-50	8		3.98	1.47	4.69	0.812	4.90	1.01	2.80	0.399	2.52	0.357	2.90	0.521	0.690	0.496	0.266
1203A 32R2W 32-36	11		4.03	1.50	4.88	0.843	5.08	1.02	2.86	0.430	2.57	0.374	3.01	0.599	0.991	0.521	0.179
1203A 32R3W 58-62	11		1.88	0.710	2.29	0.399	2.41	0.500	1.34	0.202	1.25	0.185	1.41	0.273	0.336	0.241	0.0809
1203A 32R4W 76-80	11		3.12	1.18	3.74	0.647	3.90	0.799	2.20	0.328	1.99	0.288	2.28	0.437	0.603	0.394	0.134
1203A 32R5W 60-64	11		3.57	1.36	4.25	0.726	4.41	0.889	2.41	0.367	2.22	0.323	2.77	0.526	0.602	0.467	0.548
1203A 36R3W 25-29	14		3.45	1.32	4.06	0.709	4.22	0.876	2.41	0.346	2.12	0.303	2.49	0.495	0.576	0.449	0.164
1203A 36R6W 18-22	14		3.51	1.35	4.20	0.714	4.26	0.888	2.40	0.366	2.15	0.312	2.59	0.526	0.646	0.469	0.236
1203A 37R2W 87-91	16		2.39	0.937	3.04	0.533	3.32	0.691	1.88	0.281	1.72	0.250	1.73	0.244	0.702	0.205	0.0726
1203A 37R3W 103-107	16		1.45	0.580	1.85	0.331	2.06	0.428	1.20	0.175	1.08	0.160	1.07	0.262	0.295	0.124	0.0460
1203A 38R1W 123-126	16		2.98	1.16	3.76	0.660	4.02	0.835	2.30	0.349	2.06	0.303	2.16	0.335	0.482	0.257	0.0902
1203A 39R5W 98-102	18		3.57	1.34	4.19	0.725	4.36	0.908	2.46	0.370	2.20	0.325	2.56	0.505	0.597	0.469	0.241
1203A 42R1W 88-92	19		3.10	1.18	3.74	0.646	4.02	0.830	2.26	0.329	2.04	0.300	2.29	0.397	0.480	0.369	0.234
1203A 42R5W 40-44	19		3.01	1.17	3.65	0.645	3.87	0.810	2.21	0.323	1.98	0.290	2.17	0.468	0.796	0.351	0.146
1203A 44R1W 75-79	20		4.22	1.56	5.27	0.912	5.54	1.17	3.20	0.474	2.93	0.432	3.20	0.580	0.677	0.525	0.266
1203A 45R1W 35-39	20		4.27	1.55	5.20	0.902	5.52	1.17	3.24	0.482	2.97	0.439	3.12	0.640	0.626	0.505	0.394
1203A 46R4W 50-54	20		4.10	1.53	5.07	0.892	5.39	1.13	3.08	0.466	2.88	0.431	3.02	0.566	0.545	0.485	0.233
1203A 47R3W 50-54	21		4.40	1.61	5.29	0.925	5.60	1.18	3.26	0.481	2.95	0.437	3.36	0.584	0.825	0.547	0.185
1203A 48R2W 96-100	21		4.34	1.62	5.32	0.937	5.64	1.18	3.30	0.503	2.97	0.448	3.23	0.542	1.21	0.521	0.172
1203A 49R3W 50-54	21		4.38	1.60	5.38	0.942	5.76	1.19	3.29	0.493	2.99	0.446	3.21	0.566	0.591	0.518	0.174
1203A 52R 6W 23-27	23		6.53	2.23	7.32	1.22	7.22	1.48	4.04	0.602	3.64	0.531	5.12	0.961	0.895	0.891	0.451
1203A 53R6W 123-127	23		6.95	2.36	8.03	1.34	7.80	1.60	4.39	0.646	3.86	0.579	5.20	0.988	0.947	0.923	0.318
1203A 54R4W 74-78	23		7.77	2.63	8.97	1.49	8.82	1.83	4.93	0.719	4.40	0.636	5.70	1.08	1.02	0.990	0.380
1203A 55R1W 109-113	23		7.28	2.46	8.37	1.40	8.32	1.72	4.68	0.675	4.03	0.603	5.42	1.03	0.977	0.948	0.409
1203A 58R2W 94-98	23		6.98	2.37	8.10	1.35	7.93	1.64	4.44	0.648	3.89	0.572	5.18	0.988	0.877	0.893	0.353
1203A 58R4W 37-41	24		3.55	1.34	4.36	0.749	4.56	0.932	2.57	0.387	2.37	0.353	2.64	0.427	1.23	0.393	0.131
1203A 59R2W 69-73	24		3.64	1.36	4.45	0.765	4.57	0.960	2.66	0.394	2.40	0.345	2.69	0.440	0.573	0.396	0.134
1203A 62R1W 101-105	26		8.99	2.96	10.5	1.73	10.3	2.12	5.76	0.838	4.96	0.739	6.49	1.27	1.59	1.15	1.13
1203A 62R2W 88-92	26		7.28	2.44	8.23	1.37	8.07	1.65	4.46	0.658	4.01	0.597	5.57	1.10	0.958	1.00	0.467
1203A 63R4W 19-22	26		7.28	2.46	8.03	1.36	7.84	1.61	4.42	0.659	4.04	0.586	5.91	1.16	1.04	1.07	0.635
1203A 65R4W 9-13	29		7.42	2.58	8.50	1.41	8.25	1.66	4.51	0.637	3.86	0.568	5.08	1.10	1.06	0.977	0.460
1203A 66R2W 8-10	30		6.75	2.38	7.65	1.28	7.50	1.53	4.11	0.609	3.63	0.532	4.69	1.03	0.940	0.893	0.453
1203A 67R4W 10-14	30		6.75	2.37	7.65	1.29	7.44	1.53	4.17	0.582	3.58	0.504	4.60	1.01	0.953	0.880	0.628
1203A 68R4W 40-43	31b		3.17	1.23	3.82	0.655	3.88	0.810	2.13	0.321	1.88	0.278	2.01	0.347	0.612	0.295	0.280

Table 3a. (continued)

Sample Name	Unit	Unit Name	Depth, mbsf	LOI	SiO_2	TiO_2	Al_2O_3	Fe_2O_3*	MnO	MgO	CaO	Na_2O	K_2O	P_2O_5	Total
1204A 7R3W 12-16	2	aphyric basalt	822.44	8.17	44.1	2.29	15.1	10.2	0.16	3.58	20.5	2.79	0.79	0.30	99.8
1204A 8R1W 73-77	2	aphyric basalt	829.73	8.99	42.9	2.32	14.9	10.2	0.15	3.42	22.1	2.81	0.84	0.30	99.9
1204A 9R2W 55-59	2	aphyric basalt	840.65	8.39	42.0	2.19	14.6	13.4	0.20	3.64	20.1	2.64	0.75	0.28	99.8
1204A 9R2W 76-80	2	aphyric basalt	840.86	3.43	46.8	2.19	15.0	13.9	0.18	6.84	10.5	2.92	0.97	0.24	99.6
1204A 9R3W 25-27	2	aphyric basalt	841.85	6.02	45.1	2.53	14.0	12.5	0.23	4.73	16.4	2.65	0.92	0.26	99.4
1204A 10R2W 89-93	2	aphyric basalt	850.66	3.85	47.5	2.33	16.2	12.3	0.17	7.55	10.2	2.99	0.62	0.26	100.2
1204A 10R2W 108-112	2	aphyric basalt	850.85	3.44	48.3	2.19	16.7	11.7	0.14	9.09	8.15	3.05	0.40	0.24	99.9
1204A 10R3W 77-81	2	aphyric basalt	851.68	3.11	47.6	2.34	15.8	13.7	0.16	8.68	7.71	2.81	0.45	0.30	99.5
1204A 10R5W 44-48	2	aphyric basalt	854.26	3.91	47.5	2.41	15.4	13.1	0.19	8.09	9.30	3.07	0.72	0.26	100.0
1204B 1R4W 51-53	1	aphyric basalt	815.26	4.06	46.3	2.33	17.4	12.9	0.15	2.76	14.4	2.77	0.72	0.28	100.0
1204B 2R2W 76-80	1	aphyric basalt	822.36	6.80	44.3	2.33	15.8	11.6	0.17	3.44	18.6	2.54	0.56	0.27	99.7
1204B 2R4W 102-105	1	aphyric basalt	824.82	3.62	45.9	2.56	17.9	13.8	0.20	2.14	12.5	3.08	1.06	0.56	99.8
1204B 2R5W 11-15	1	aphyric basalt	825.26	3.16	45.7	2.40	16.5	14.8	0.23	3.01	12.5	2.93	1.16	0.34	99.6
1204B 3R2W 41-44	1	aphyric basalt	831.76	2.63	46.0	2.50	17.7	14.5	0.19	2.30	11.6	3.54	1.17	0.71	100.2
1204B 4R2W 49-53	2A	aphyric basalt	841.59	5.18	46.6	2.27	15.7	12.7	0.16	3.44	14.1	2.91	1.22	0.33	99.4
1204B 6R1W 44-47	2A	aphyric basalt	859.04	4.67	46.6	2.36	15.9	13.0	0.12	3.80	13.5	3.01	1.17	0.33	99.8
1204B 7R2W 39-43	2A	aphyric basalt	870.06	4.45	46.5	2.58	14.4	13.0	0.18	5.57	13.4	2.87	0.99	0.31	99.8
1204B 7R3W 68-72	2A	aphyric basalt	871.85	2.67	47.6	2.26	16.0	13.1	0.19	6.25	10.1	2.66	1.51	0.36	100.1
1204B 8R2W 85-89	2B	diabase	880.15	4.05	47.0	2.39	15.4	12.9	0.17	6.17	11.7	2.21	1.13	0.32	99.4
1204B 9R3W 28-32	2B	diabase	888.97	2.87	47.4	2.20	15.5	13.3	0.17	8.74	8.98	2.63	0.39	0.25	99.6
1204B 10R1W 11-14	2B	diabase	888.91	2.59	47.8	2.29	15.9	13.0	0.15	8.35	9.08	2.74	0.38	0.25	99.9
1204B 10R2W 50-54	2B	diabase	890.8	3.20	47.3	2.27	15.3	13.4	0.16	7.41	9.77	3.01	1.09	0.27	99.9
1204B 10R4W 43-47	2B	diabase	892.79	2.17	47.7	2.24	15.5	12.7	0.18	7.73	9.88	2.80	0.43	0.31	99.4
1204B 12R1W 65-69	2B	diabase	906.95	3.10	47.6	2.46	15.0	13.5	0.20	6.61	10.6	3.10	0.93	0.31	100.2
1204B 13R1W 118-122	2B	diabase	909.48	3.15	47.5	2.44	15.1	13.6	0.19	6.06	11.0	2.91	0.99	0.33	100.0
1204B 14R1W 18-22	2B	diabase	916.08	3.33	47.5	2.25	16.0	12.1	0.17	8.34	10.0	2.92	0.51	0.25	100.1
1204B 14R1W 87-91	2B	diabase	916.77	3.76	45.6	2.16	14.5	16.1	0.25	7.18	9.80	2.73	1.08	0.24	99.6
1204B 17R1W 107-110	3	aphyric basalt	945.97	4.56	47.4	2.20	15.3	12.7	0.19	5.56	12.3	2.82	1.25	0.26	99.9
1204B 17R2W 11-15	3	aphyric basalt	946.19	6.27	46.1	2.36	15.4	12.2	0.20	4.59	15.0	2.79	1.07	0.31	100.0

Table 3a. (continued)

Sample Name	Unit	XRF	Nb	Zr	Y	Sr	Rb	Zn	Ni	Cr	V	ICP-MS	Sc	Rb	Sr	Y	Zr	Nb	Ba	La	Ce	Pr	Nd
1204A 7R3W 12-16	2		8.2	134	30.7	243	11.0	95	40	144	283		35.9	10.5	226	32.8	129	8.58	69.9	7.78	20.2	3.23	15.8
1204A 8R1W 73-77	2		8.5	132	29.9	230	8.6	95	40	153	295		37.6	8.31	216	32.0	123	8.71	66.0	7.65	20.6	3.26	15.7
1204A 9R2W 55-59	2		8.0	135	29.3	248	17.2	88	51	138	300		35.3	16.4	236	32.5	132	8.63	74.5	7.57	19.6	3.14	15.2
1204A 9R2W 76-80	2		8.1	135	29.3	189	21.8	92	86	185	264		39.4	20.9	181	32.9	133	8.69	65.8	7.52	20.0	3.17	15.4
1204A 9R3W 25-27	2		8.4	143	33.0	224	62.0	99	40	174	352		44.1	61.5	211	36.8	141	9.27	88.7	8.15	21.1	3.42	16.6
1204A 10R2W 89-93	2		8.5	142	31.0	206	9.3	87	75	414	278		36.9	8.99	192	33.9	137	9.19	66.0	7.86	21.0	3.35	16.1
1204A 10R2W 108-112	2		8.1	136	28.3	205	3.6	89	95	154	299		35.6	3.51	194	31.2	131	8.55	59.3	7.55	20.0	3.11	14.9
1204A 10R3W 77-81	2		10.2	164	35.2	193	3.5	100	79	127	283		34.6	3.54	182	39.0	161	10.8	70.3	9.49	25.2	3.89	18.7
1204A 10R5W 44-48	2		8.9	147	32.5	196	21.9	94	75	284	296		41.0	21.5	184	36.9	148	9.69	89.0	8.43	22.3	3.56	17.1
1204B 1R4W 51-53	1		9.1	147	32.2	284	9.3	106	62	166	325		37.5	9.17	266	35.7	141	9.46	67.3	8.26	21.9	3.48	16.9
1204B 2R2W 76-80	1		8.6	145	32.3	287	7.8	99	74	160	288		38.9	7.44	277	35.3	138	9.16	57.9	7.92	21.5	3.35	16.1
1204B 2R4W 102-105	1		9.8	159	35.4	291	14.1	139	70	148	373		40.5	13.7	277	39.2	155	10.3	115	9.24	24.4	3.88	18.6
1204B 2R5W 11-15	1		9.2	154	31.8	253	19.0	126	79	164	380		41.1	18.4	241	35.7	152	9.79	92.6	8.53	22.8	3.56	17.3
1204B 3R2W 41-44	1		9.7	157	36.8	286	13.6	142	72	155	400		42.2	13.1	267	40.7	151	9.96	97.9	9.36	23.5	3.71	18.1
1204B 4R2W 49-53	2A		8.9	145	31.0	239	30.2	172	64	149	272		37.0	30.2	233	34.9	142	9.51	80.3	8.20	21.6	3.42	16.4
1204B 6R1W 44-47	2A		9.1	149	32.3	239	22.7	167	55	154	305		38.4	22.4	229	35.6	143	9.63	75.6	8.29	21.9	3.46	16.8
1204B 7R2W 39-43	2A		10.0	165	36.3	209	36.8	125	63	148	331		42.6	36.6	197	40.6	161	10.6	81.1	9.22	24.4	3.83	18.6
1204B 7R3W 68-72	2A		8.3	142	32.6	222	56.0	177	111	182	334		40.0	54.2	204	35.9	137	9.12	78.2	8.22	20.8	3.39	16.4
1204B 8R2W 85-89	2B		8.7	145	32.5	209	34.2	166	145	128	304		35.4	32.9	195	35.9	142	9.52	76.6	8.44	22.6	3.56	17.3
1204B 9R3W 28-32	2B		8.5	141	30.2	194	3.5	88	85	149	285		36.7	3.47	172	32.8	136	8.95	58.5	7.76	20.7	3.27	15.9
1204B 10R1W 11-14	2B		8.5	143	30.3	203	3.5	90	94	149	292		38.5	3.51	186	33.9	138	9.12	60.3	7.99	21.1	3.35	16.2
1204B 10R2W 50-54	2B		8.5	143	30.0	191	25.2	210	140	162	299		37.2	24.3	177	32.8	140	9.32	66.6	7.79	21.1	3.34	16.2
1204B 10R4W 43-47	2B		9.9	160	33.6	202	3.8	99	105	146	285		36.4	3.62	184	36.5	153	10.1	65.3	8.75	23.6	3.75	18.2
1204B 12R1W 65-69	2B		10.1	169	35.8	198	20.0	107	81	176	334		38.4	19.3	186	39.8	160	10.8	97.8	9.41	25.3	3.93	18.9
1204B 13R1W 118-122	2B		10.1	168	37.0	211	30.9	134	79	148	293		36.9	29.1	192	40.2	163	11.0	84.8	9.86	26.1	4.11	19.8
1204B 14R1W 18-22	2B		8.6	142	31.4	197	3.6	95	96	151	285		37.5	3.46	184	34.0	138	9.08	62.1	7.93	21.0	3.34	16.0
1204B 14R1W 87-91	2B		8.0	135	29.8	181	23.4	80	77	150	267		37.5	22.5	170	32.8	133	8.69	151	7.46	19.8	3.12	15.1
1204B 17R1W 107-110	3		8.4	139	29.4	215	72.5	148	179	139	283		36.8	73.6	209	33.5	138	8.91	85.2	7.84	20.7	3.32	15.7
1204B 17R2W 11-15	3		8.9	147	31.4	239	40.8	140	67	146	274		38.2	42.5	242	35.5	142	9.57	80.4	8.17	22.1	3.45	16.3

Table 3a. (continued)

Sample Name	Unit	ICP-MS	Sm	Eu	Gd	Tb	Dy	Ho	Er	Tm	Yb	Lu	Hf	Ta	Pb	Th	U
1204A 7R3W 12-16	2		4.65	1.69	5.44	0.942	5.73	1.21	3.32	0.497	2.97	0.454	3.36	0.606	0.903	0.581	0.394
1204A 8R1W 73-77	2		4.53	1.63	5.35	0.917	5.59	1.16	3.15	0.475	2.93	0.429	3.34	0.618	1.24	0.601	0.262
1204A 9R2W 55-59	2		4.44	1.61	5.29	0.913	5.55	1.17	3.22	0.492	3.00	0.439	3.24	0.583	0.747	0.577	0.351
1204A 9R2W 76-80	2		4.54	1.62	5.44	0.925	5.56	1.18	3.19	0.482	2.93	0.433	3.38	0.593	0.787	0.588	0.176
1204A 9R3W 25-27	2		4.88	1.77	5.87	1.03	6.17	1.31	3.62	0.535	3.24	0.484	3.62	0.624	0.869	0.613	1.06
1204A 10R2W 89-93	2		4.69	1.71	5.54	0.952	5.79	1.22	3.33	0.506	3.10	0.462	3.53	0.637	0.634	0.604	0.218
1204A 10R2W 108-112	2		4.32	1.59	5.04	0.873	5.32	1.13	3.10	0.472	2.89	0.418	3.32	0.587	0.480	0.587	0.233
1204A 10R3W 77-81	2		5.39	1.91	6.36	1.08	6.62	1.39	3.76	0.566	3.52	0.519	3.92	0.732	0.522	0.743	0.222
1204A 10R5W 44-48	2		5.00	1.81	5.97	1.04	6.24	1.32	3.65	0.540	3.28	0.485	3.74	0.628	0.726	0.632	0.241
1204B 1R4W 51-53	1		4.94	1.79	5.89	1.02	6.06	1.29	3.50	0.529	3.18	0.481	3.63	0.640	0.775	0.637	0.522
1204B 2R2W 76-80	1		4.70	1.72	5.57	0.980	5.77	1.22	3.40	0.506	3.06	0.458	3.51	0.617	0.781	0.620	1.79
1204B 2R4W 102-105	1		5.43	1.98	6.47	1.13	6.65	1.40	3.89	0.585	3.51	0.528	4.02	0.696	0.934	0.701	0.583
1204B 2R5W 11-15	1		5.07	1.84	6.01	1.03	6.11	1.29	3.46	0.525	3.16	0.468	3.85	0.672	0.899	0.652	0.385
1204B 3R2W 41-44	1		5.23	1.90	6.30	1.09	6.48	1.39	3.83	0.584	3.52	0.527	3.90	0.690	0.978	0.681	0.608
1204B 4R2W 49-53	2A		4.80	1.72	5.70	0.977	5.90	1.23	3.39	0.512	3.07	0.458	3.54	0.636	0.852	0.622	0.321
1204B 6R1W 44-47	2A		4.90	1.78	5.79	1.01	6.02	1.27	3.44	0.530	3.17	0.479	3.63	0.650	0.966	0.648	0.318
1204B 7R2W 39-43	2A		5.50	1.94	6.47	1.12	6.71	1.41	3.90	0.583	3.54	0.535	4.03	0.701	1.07	0.689	0.705
1204B 7R3W 68-72	2A		4.73	1.73	5.78	1.00	5.97	1.28	3.51	0.537	3.22	0.481	3.54	0.614	0.423	0.612	0.671
1204B 8R2W 85-89	2B		5.08	1.85	6.03	1.05	6.20	1.32	3.57	0.538	3.24	0.497	3.63	0.631	0.411	0.643	1.40
1204B 9R3W 28-32	2B		4.62	1.69	5.44	0.956	5.74	1.19	3.26	0.494	3.00	0.452	3.47	0.597	0.834	0.605	0.184
1204B 10R1W 11-14	2B		4.68	1.72	5.56	0.962	5.81	1.22	3.39	0.500	3.11	0.459	3.54	0.610	0.665	0.599	0.194
1204B 10R2W 50-54	2B		4.68	1.70	5.63	0.961	5.83	1.22	3.29	0.500	2.99	0.442	3.60	0.640	1.25	0.624	0.357
1204B 10R4W 43-47	2B		5.26	1.87	6.26	1.07	6.34	1.33	3.60	0.545	3.32	0.495	3.81	0.676	0.957	0.699	0.178
1204B 12R1W 65-69	2B		5.47	1.91	6.51	1.12	6.78	1.41	3.96	0.603	3.64	0.531	4.07	0.725	1.30	0.742	0.372
1204B 13R1W 118-122	2B		5.66	2.00	6.71	1.17	6.93	1.46	4.01	0.603	3.67	0.541	4.10	0.740	1.33	0.747	0.487
1204B 14R1W 18-22	2B		4.72	1.73	5.57	0.980	5.84	1.22	3.32	0.503	3.02	0.448	3.46	0.602	1.14	0.603	0.199
1204B 14R1W 87-91	2B		4.45	1.61	5.29	0.919	5.47	1.16	3.17	0.481	2.89	0.431	3.33	0.589	0.624	0.579	0.160
1204B 17R1W 107-110	3		4.56	1.67	5.49	0.962	5.65	1.19	3.26	0.492	2.98	0.439	3.41	0.591	0.812	0.605	0.263
1204B 17R2W 11-15	3		4.77	1.74	5.66	0.979	5.91	1.24	3.42	0.513	3.15	0.459	3.59	0.648	0.862	0.642	0.633

[a] Major oxide contents are in %, and trace element abundances are in ppm.
[b] L.O.I., loss on ignition. ~0.2 g samples were ignited at 1000°C for over 8 hours. L.O.I. was calculated using (weight loss during ignition/weight before ignition)*100%.
[c] Samples were oxidized prior to analyses, so all iron is reported as Fe^{3+}, i.e., Fe_2O_3.
[d] Total is sum of oxides measured after ignition and oxidation.

leached in a 1:1 mixture of 2N HCl and H_2O_2 for 10 min.

4. Analytical Procedures

4.1. Major and Trace Element Analyses

4.1.1. Whole-Rock Samples

[17] Abundance of major and some trace elements (Table 3a) were analyzed by X-ray fluorescence at the University of Massachusetts at Amherst following the procedure described by *Rhodes* [1996]. Other trace elements (Table 3a) were analyzed by inductively coupled plasma mass spectrometry (ICP-MS) at Massachusetts Institute of Technology using the procedure described by *Huang and Frey* [2003]. Whole rocks from Sites 883 and 884 have been studied by *Regelous et al.* [2003]. For comparison of their data with our data on Sites 1203 and 1204 lavas, their data have been normalized using BHVO standard values reported by *Regelous et al.* [2003] and *Huang and Frey* [2003].

4.1.2. Glass Samples

[18] Major element compositions of glasses were obtained at the University of Bristol (UB) using a JEOL 8600 electron microprobe with 15keV accelerating voltage, a 10nA beam current and 5–10 μm spot size. The results reported in Table 3b are averages of 4 to 10 analyses for each glass.

[19] In situ laser ablation ICP-MS trace element analyses were obtained at UB using a VG Elemental PlasmaQuad 3+ S-option instrument equipped with a 266 nm Nd-YAG laser (VG Microprobe II). The laser beam diameter at the sample surface was ~50 μm, and the laser repetition rate was set to 10Hz. This choice of laser beam conditions reflected the need to obtain good sensitivity in order to achieve low detection limits. Helium gas and then an argon/helium mixture carried the ablated material from the sample cell to the plasma torch. All measurements were made using Thermo Elemental PlasmaLab "time-resolved analysis" data acquisition software with a total acquisition time of 100 s per analysis (50 s for a gas blank and 50 s for laser ablation). The data reduction algorithm is that of *Longerich et al.* [1996]. NIST 610 glass was used for calibration and NIST 612 glass was used to check on instrument linearity. Analyses of the NIST glass standards bracketed the analysis of unknowns in order to correct for instrument drift. The glass standards BCR-2g, BHVO-2g, BIR-1g were analyzed as unknowns as a check of accuracy. Ca was used as internal standard to correct for variations in ablation yield between and during individual analyses of both standards and samples. Data in Table 3b represent averages of a minimum of 6 analyses of each glass fragment, and for comparison with whole-rock data, the glass data have been normalized to the values of BHVO-2 obtained from solution ICP-MS by *Huang and Frey* [2003].

4.2. Isotopic Analyses

[20] Sr-Nd-Pb isotopic ratios were determined in seventeen whole-rock samples (Table 4a). Because isotopic ratios and parent/daughter ratios were likely affected by postmagmatic alteration processes [*Regelous et al.*, 2003], Sr, Nd and Pb isotopic ratios and their parent/daughter ratios were determined on acid leached whole-rock powders.

[21] Whole-rock powders were strongly acid-leached before being digested in HF-HNO_3 for Sr-Nd-Pb isotopic analyses. Specifically, ~0.3 to 0.4 g whole-rock powder was weighed into a precleaned Teflon® beaker, and ~10 mL 6N HCl was added. This beaker was placed in an ultrasonic bath and the HCl was changed every 30 min until the acid was colorless or pale yellow. For most samples, 6 to 9 leaching steps were required. The residue was soaked in deionized H_2O for 30 min, rinsed twice, and dried. The weight loss after acid leaching was between 28 to 80% (Table 4a). Electron microprobe analyses of several residual assemblages showed that only plagioclase, pyroxene and olivine were present.

[22] The leached sample powders were digested in HF-HNO_3. Three separate dissolutions were prepared for: 1) Pb isotope analyses by Thermal Ionization Mass Spectrometry (TIMS); 2) Sr-Nd isotope analyses by TIMS; and 3) parent/daughter abundance ratio determination by ICP-MS. Pb was separated from the sample matrix by anion exchange technique in HBr acid. Sr and Nd were separated by cation exchange technique in HNO_3 and HCl, respectively. Detailed TIMS analytical procedures are described by *Schmitz and Bowring* [2003]. Parent/daughter abundance ratios in the leached powder (Table 4a) were analyzed by ICP-MS using the procedure described in *Huang and Frey* [2003]. Initial Sr-Nd-Pb isotopic ratios in Detroit Seamount lavas are reported in Table 4b.

Table 3b. Glass Analyses[a]

Sample	Interval	Depth, mbsf	Unit[b]	SiO_2	TiO_2	Al_2O_3	FeO	MnO	MgO	Cr_2O_3	CaO	Na_2O	K_2O	P_2O_5	Total
1203A-1	1203A 18R-2 17-21	465.47	1f: base of Unit 1 overlying sediment	49.5	2.21	13.6	13.1	0.22	6.21	0.05	11.2	2.97	0.33	0.19	99.5
1203A-2	1203A 18R-2 21-27	465.51	1f: glass at top of Unit 2 sediment	49.0	2.19	13.6	13.3	0.16	6.18	0.06	11.1	2.97	0.34	0.21	99.1
1203A-3	1203A 19R-2 38-42	475.28	3k: glass in middle of lobe 3k	49.0	2.20	13.6	13.2	0.19	6.17	0.06	11.1	3.00	0.34	0.28	99.1
1203A-4	1203A 20R-1 106-107	484.06	3x: base of lobe, overlying 3y	48.6	2.19	13.3	13.3	0.17	6.20	0.05	11.1	2.92	0.33	0.23	98.4
1203A-4r				48.5	2.20	13.3	13.3	0.14	6.25	0.05	11.0	2.94	0.34	0.27	98.3
1203A-5	1203A 20R-2 58-61	485.08	3ab top of lobe	48.1	1.90	14.8	11.4	0.19	7.12	0.05	11.7	2.94	0.27	0.22	98.7
1203A-6	1203A 31R-1 105-108	580.45	8k: glass in middle of lobe	48.0	1.90	14.8	11.4	0.21	7.17	0.06	11.7	2.95	0.27	0.21	98.7
1203A-7	1203A 31R-2 1-6	580.91	8m top of lobe	49.2	1.97	14.1	12.6	0.23	6.74	0.02	11.3	2.97	0.30	0.26	99.8
1203A-8	1203A 39R-6 57-63	653.97	18f top of lobe	49.0	1.93	14.1	12.8	0.19	6.67	0.06	11.3	2.94	0.30	0.18	99.6
1203A-9	1203A 40R-1 0-3	656.2	18h top of lobe	48.9	2.21	13.5	13.5	0.19	6.22	0.03	11.1	2.98	0.33	0.22	99.1
1203A-10	1203A 40R-1 65-70	656.85	18h bottom of lobe	48.6	1.91	14.9	11.3	0.13	7.21	0.01	11.7	3.01	0.28	0.21	99.3
1203A-11	1203A 40R-2 102-105	657.92	18i base of lobe	48.6	1.88	14.9	11.4	0.17	7.26	0.05	11.8	2.90	0.26	0.19	99.4
1203A-12	1203A 40R-2 142-146	658.32	18j base of lobe	48.7	1.92	15.1	11.4	0.21	7.39	0.10	11.7	2.91	0.29	0.28	100.0
1203A-13	1203A 40R-4 57-65	660.29	18n top of lobe	48.7	1.87	15.0	11.4	0.19	7.26	0.08	11.7	2.97	0.28	0.18	99.7
1203A-14	1203A 40R-4 80-90	660.52	18o top/side of lobe	48.7	1.89	15.0	11.5	0.18	7.28	0.06	11.7	2.94	0.28	0.20	99.7
1203A-15	1203A 45R-2 32-35	704.92	20s top of lobe	47.9	2.39	14.6	12.6	0.29	6.58	0.03	10.9	3.01	0.28	0.24	98.8
1203A-16	1203A 46R-4 0-4	716.98	20aj top of lobe	47.6	2.38	14.4	12.9	0.21	6.52	0.06	10.9	2.99	0.28	0.24	98.5
1204B-1	1204B 1R-3 69-81	814.39	Unit 1 glass fragments	47.0	2.47	15.1	13.1	0.23	6.31	0.03	11.1	3.44	0.39	0.25	99.4
1204B-2	1204B 3R-2 97-100	832.2	Unit 1 lobe boundary	47.2	2.62	14.4	13.8	0.19	6.04	0.02	11.2	3.45	0.44	0.34	99.6
1204B-3	1204B 3R-2 100-106	832.35	Unit 1 lobe boundary	46.8	2.40	15.2	13.1	0.24	6.48	0.04	11.0	3.42	0.40	0.26	99.3
1204B-4	1204B 3R-2 106-110	832.41	Unit 1 lobe boundary	46.2	2.43	14.7	13.1	0.20	6.23	0.07	11.0	3.33	0.40	0.31	97.9
1204B-4r				46.1	2.46	14.6	13.4	0.18	6.20	0.03	11.0	3.35	0.38	0.25	98.0
1204B-5	1204B 15R-1 112-116	926.72	Unit 2c lobe margin	46.6	2.42	14.9	13.2	0.18	6.36	0.02	11.0	3.36	0.38	0.31	98.7
883-1	883E 20R-5 46-50		Unit 8 top	46.6	2.74	14.0	14.1	0.23	5.85	0.03	11.1	3.43	0.43	0.29	98.8
883-2	883E 22R-2 105-110		Unit 17 lobe margin	46.7	2.72	14.1	14.0	0.19	5.84	0.02	11.1	3.41	0.43	0.34	98.8
883-3	883E 22R-4 112-120		Unit 19-20 boundary	46.9	2.74	14.0	14.1	0.22	5.80	0.04	11.2	3.42	0.44	0.33	99.1
884-1	884E 10R-5 59-62		Unit 11 top	48.2	1.33	14.7	10.8	0.19	7.77	0.05	12.7	3.03	0.12	0.15	99.2
884-2	884E 10R-6 38-40		Unit 11 base	48.1	1.38	14.8	10.7	0.16	7.80	0.07	12.7	2.93	0.12	0.13	98.9
884-3	884E 10R-6 118-121		Unit 13 top	48.3	1.37	14.9	10.7	0.21	7.78	0.04	12.7	2.95	0.12	0.12	99.2

Table 3b. (continued)

Sample	Sc	Cr	Co	Ni	Rb	Sr	Y	Zr	Nb	Ba	La	Ce	Pr	Nd	Sm	Eu	Gd	Tb	Dy	Ho	Er	Tm	Yb	Lu	Hf	Ta	Pb	Th	U
1203A-1	39.6	159	49.9	61.1	3.91	220	33.5	137	9.45	58.6	8.34	21.1	3.37	15.7	4.64	1.54	5.48	0.919	5.79	1.25	3.36	0.531	3.14	0.432	3.47	0.649	0.653	0.638	0.181
1203A-2	39.8	182	49.7	59.0	3.83	220	32.8	138	9.59	58.5	8.31	20.7	3.28	15.9	4.51	1.53	5.33	0.922	5.55	1.19	3.33	0.523	3.11	0.433	3.37	0.665	0.659	0.564	0.187
1203A-3	39.2	179	49.3	58.9	3.94	220	33.3	139	9.68	59.1	8.40	20.9	3.33	15.9	4.49	1.57	5.26	0.897	5.45	1.17	3.34	0.478	2.85	0.408	3.45	0.617	0.658	0.638	0.193
1203A-4	38.3	198	50.6	56.1	4.12	220	31.9	134	9.59	59.9	8.21	21.5	3.34	15.6	4.59	1.53	5.33	0.897	5.45	1.18	3.24	0.470	2.90	0.384	3.41	0.607	0.763	0.579	0.205
1203A-5	39.2	226	46.5	78.0	2.85	231	30.9	124	7.97	47.7	7.48	18.0	2.93	14.3	4.29	1.38	5.04	0.885	5.18	1.16	3.16	0.479	2.79	0.410	3.04	0.520	0.543	0.557	0.136
1203A-6	37.9	247	49.9	81.6	3.00	221	28.0	115	7.89	46.1	6.85	17.2	2.74	12.8	3.66	1.31	4.48	0.765	4.49	0.980	2.78	0.410	2.48	0.383	2.69	0.492	0.517	0.455	0.144
1203A-7	37.4	221	51.2	60.0	3.32	213	28.3	115	7.50	49.5	6.81	16.6	2.67	12.6	3.78	1.30	4.64	0.779	4.55	1.00	2.71	0.418	2.43	0.351	2.73	0.463	0.542	0.458	0.139
1203A-8	37.7	221	49.9	62.2	3.22	212	28.4	114	7.56	49.9	6.66	17.0	2.67	12.9	3.46	1.31	4.48	0.789	4.71	0.976	2.75	0.430	2.48	0.367	2.70	0.495	0.536	0.469	0.136
1203A-9	37.4	182	49.8	58.4	3.90	209	31.5	132	8.98	55.2	7.75	19.7	3.13	14.8	4.17	1.43	5.06	0.856	5.10	1.11	3.04	0.476	2.70	0.375	3.12	0.573	0.775	0.567	0.187
1203A-10	37.9	247	49.7	80.6	3.33	221	27.8	115	7.72	44.5	6.74	17.1	2.72	12.9	3.76	1.30	4.35	0.762	4.50	1.02	2.81	0.423	2.48	0.340	2.76	0.541	0.514	0.499	0.162
1203A-11	37.5	237	46.0	79.3	2.88	217	28.3	118	7.70	44.4	6.76	16.5	2.68	12.6	3.64	1.27	4.42	0.779	4.80	1.03	2.80	0.442	2.56	0.374	2.73	0.476	0.459	0.486	0.142
1203A-12	38.1	248	49.0	82.9	2.94	217	28.6	116	7.74	40.6	6.58	16.6	2.55	12.5	3.91	1.26	4.51	0.760	4.39	1.00	2.69	0.378	2.32	0.350	2.70	0.480	0.516	0.448	0.139
1203A-13	37.5	247	48.8	84.7	3.00	219	28.2	114	7.78	41.4	6.44	16.4	2.55	12.8	3.43	1.24	4.27	0.714	4.53	0.993	2.71	0.367	2.30	0.333	2.64	0.445	0.556	0.490	0.133
1203A-14	38.0	244	46.9	79.6	2.77	216	28.4	116	7.49	39.9	6.51	16.5	2.63	12.5	3.68	1.19	4.47	0.747	4.63	1.00	2.70	0.422	2.43	0.359	2.72	0.463	0.489	0.432	0.139
1203A-15	36.8	202	49.3	89.8	3.20	193	34.7	132	8.39	42.2	6.87	18.7	2.97	13.9	4.12	1.43	5.12	0.861	5.53	1.12	3.49	0.500	3.07	0.424	3.09	0.528	0.552	0.488	0.141
1203A-16	38.6	203	49.2	77.6	3.20	194	34.2	132	8.36	42.6	6.95	18.8	2.94	13.6	4.19	1.47	5.04	0.846	5.63	1.23	3.38	0.490	3.04	0.426	3.22	0.545	0.542	0.505	0.166
1204B-1	39.4	161	49.2	63.2	4.26	214	39.0	162	10.2	63.0	8.60	21.8	3.56	17.2	4.87	1.62	5.58	0.996	6.28	1.31	3.55	0.561	3.38	0.501	3.73	0.619	0.699	0.647	0.171
1204B-2	42.4	162	50.0	50.0	4.63	211	41.8	174	10.9	67.5	9.14	23.9	3.76	18.2	5.11	1.74	5.96	1.07	6.52	1.43	3.93	0.593	3.48	0.515	3.90	0.721	0.808	0.602	0.197
1204B-3	40.3	148	46.1	59.1	3.80	218	41.3	169	9.88	60.8	8.98	21.2	3.49	17.5	5.00	1.69	6.30	1.06	6.37	1.40	3.88	0.615	3.54	0.543	4.03	0.661	0.644	0.631	0.162
1204B-4	39.1	154	46.3	68.0	4.00	217	40.9	165	9.79	62.6	8.83	21.9	3.60	17.4	5.12	1.70	5.92	1.03	6.29	1.40	3.93	0.592	3.39	0.527	3.91	0.671	0.715	0.643	0.163
1204B-5	38.9	157	47.9	63.9	4.08	217	39.8	161	9.77	62.5	8.83	21.8	3.47	17.5	5.31	1.65	5.79	0.998	6.16	1.34	3.89	0.549	3.29	0.464	3.60	0.681	0.663	0.639	0.186
883-1	41.6	145	45.4	41.0	4.61	204	41.6	174	10.7	66.1	9.20	23.7	3.70	17.6	5.35	1.74	6.00	1.06	6.50	1.42	4.12	0.605	3.77	0.515	3.64	0.658	0.664	0.615	0.196
883-2	41.9	150	46.1	45.2	4.54	206	41.5	174	10.7	67.0	9.33	24.1	3.80	18.5	5.42	1.72	6.35	1.07	6.77	1.40	3.99	0.612	3.72	0.519	3.90	0.709	0.709	0.697	0.215
883-3	42.3	151	48.4	46.7	4.71	205	41.5	176	10.8	65.0	9.15	23.8	3.72	18.5	5.36	1.74	6.41	1.08	6.43	1.44	4.03	0.620	3.71	0.522	3.88	0.639	0.718	0.697	0.199
884-1	46.8	307	49.3	75.3	1.21	132	31.5	79	2.98	20.3	2.66	7.62	1.37	7.50	2.65	0.898	3.91	0.646	4.57	1.00	3.09	0.465	2.73	0.401	2.07	0.229	0.297	0.176	0.0473
884-2	46.4	301	49.3	83.9	1.39	131	31.7	78	3.11	20.4	2.79	7.79	1.45	7.93	2.83	0.948	4.23	0.694	4.94	1.06	3.29	0.493	2.94	0.444	2.19	0.226	0.302	0.191	0.0497
884-3	44.8	294	49.2	80.5	1.26	132	31.4	79	3.01	20.4	2.89	8.46	1.53	8.24	2.82	0.971	4.22	0.692	4.91	1.05	3.29	0.487	3.03	0.432	2.06	0.244	0.342	0.197	0.0593

[a] Major oxides were analyzed by electron microprobe, and are reported in %. Trace elements were analyzed by LA-ICP-MS, and are reported in ppm.
[b] See footnote of Table 2b.

Table 4a. Sr-Nd-Pb Isotopic Ratios and Parent/Daughter Ratios

Sample	Unit	Weight Loss,[a] %	$\frac{^{143}Nd}{^{144}Nd}$	±2 sigma	$\frac{^{87}Sr}{^{86}Sr}$	±2 sigma	$\frac{^{206}Pb}{^{204}Pb}$	±2 sigma	$\frac{^{207}Pb}{^{204}Pb}$	±2 sigma	$\frac{^{208}Pb}{^{204}Pb}$	±2 sigma	In Leached Residue				In Unleached Whole Rock			
													$\frac{Sm}{Nd}$	$\frac{Rb}{Sr}$	$\frac{U}{Pb}$	$\frac{Th}{Pb}$	$\frac{Sm}{Nd}$	$\frac{Rb}{Sr}$	$\frac{U}{Pb}$	$\frac{Th}{U}$
1203A 17 R4W 43-47	1	48	0.513080	0.000006	0.703218	0.000023	18.721	0.003	15.473	0.002	37.947	0.005	0.41	0.0046	0.33	0.14	0.30	0.038	0.92	0.67
1203A 20 R3W 10-14	3	37	0.513079	0.000006	0.703198	0.000013	18.362	0.004	15.487	0.004	37.986	0.010	0.41	0.001	0.06	0.075	0.29	0.003	0.18	0.67
1203A 31 R1W 46-50	8	28	0.513085	0.000006	0.703105	0.000010	18.312	0.002	15.476	0.002	37.927	0.004	0.39	0.0025	0.13	0.13	0.30	0.005	0.39	0.72
1203A 32 R4W 76-80	11	36	0.513077	0.000007	0.703102	0.000008	18.266	0.004	15.462	0.003	37.838	0.008	0.40	0.0016	0.16	0.27	0.29	0.006	0.22	0.65
1203A 38 R1W 123-126	16	36	0.513112	0.000006	0.703035	0.000011	18.177	0.002	15.454	0.002	37.733	0.004	0.42	0.0034	0.14	0.15	0.32	0.008	0.19	0.53
1203A 49 R3W 50-54	21	38	0.513078	0.000010	0.703046	0.000008	18.299	0.002	15.469	0.002	37.903	0.005	0.40	0.0005	0.088	0.10	0.31	0.0010	0.29	0.88
1203A 54 R4W 74-78	23	40	0.513047	0.000006	0.703162	0.000008	18.590	0.002	15.484	0.002	38.130	0.005	0.36	0.0007	0.24	0.14	0.28	0.0010	0.37	0.97
1203A 59 R2W 69-73	24	33	0.513093	0.000007	0.703113	0.000008	18.206	0.002	15.467	0.002	37.784	0.004	0.43	0.0005	0.08	0.11	0.30	0.0020	0.23	0.69
1203A 63 R4W 19-22	26	54	0.513065	0.000009	0.703085	0.000008	18.629	0.008	15.468	0.006	38.023	0.014	0.33	0.004	0.46	0.10	0.27	0.0040	0.61	1.02
1203A 65 R4W 9-13[b]	29	60	0.513045	0.000006	0.703188	0.000010	19.073	0.003	15.515	0.002	38.380	0.005	0.32	0.031	1.19	0.26	0.28	0.077	0.43	0.92
1203A 66 R2W 8-10	30	80	0.513047	0.000008	0.703202	0.000015	18.775	0.002	15.490	0.002	38.140	0.005	0.33	0.032	0.72	0.08	0.27	0.109	0.48	0.95
1203A 68 R4W 40-43	31	50	0.513079	0.000005	0.703146	0.000008	19.111	0.003	15.534	0.002	38.196	0.006	0.33	2E-05	0.91	0.79	0.30	0.131	0.46	0.48
1204A 10 R2W 108-112	2	44	0.513096	0.000006	0.702915	0.000007	18.261	0.004	15.457	0.004	37.823	0.008	0.35	0.013	0.28	0.56	0.29	0.018	0.49	1.22
1204B 3 R2W 41-44	1	40	0.513101	0.000005	0.702853	0.000008	18.231	0.003	15.448	0.003	37.847	0.007	0.37	0.016	0.12	0.26	0.29	0.049	0.62	0.70
1204B 7 R3W 68-72	2A	40	0.513090	0.000007	0.702999	0.000010	18.328	0.003	15.476	0.002	37.871	0.005	0.38	0.054	0.34	0.69	0.29	0.27	1.59	1.45
1204B 10 R4W 43-47	2B	39	0.513078	0.000006	0.702910	0.000008	18.162	0.001	15.457	0.001	37.793	0.003	0.34	0.009	0.13	0.14	0.29	0.02	0.19	0.73
1204B 17 R1W 107-110	3	52	0.513093	0.000007	0.702940	0.000013	18.318	0.003	15.447	0.002	37.928	0.006	0.35	0.025	0.10	0.25	0.29	0.353	0.32	0.75
LE unleached			0.513036	0.000006	0.703205	0.000008	18.308	0.002	15.469	0.002	37.905	0.005	0.29	0.0059	0.22	0.65				
LE A					0.703114	0.000007	18.285	0.008	15.472	0.006	37.881	0.017	0.40	0.0027	0.15	0.30				
LE B			0.513077	0.000007	0.703117	0.000018							0.40	0.0022	0.16	0.29				
LE C					0.703124	0.000010	18.271	0.003	15.454	0.003	37.819	0.007	0.39	0.0018	0.15	0.26				
LE D					0.703118	0.000018	18.271	0.003	15.457	0.002	37.827	0.006								
LE E					0.703120	0.000007														
LE F					0.703124	0.000007							0.40	0.0016	0.16	0.27				
LE G					0.703109	0.000007														
LE H					0.703115	0.000007														
LE I			0.513077	0.000007	0.703113	0.000008	18.266	0.004	15.462	0.003	37.838	0.008	0.40	0.0016	0.16	0.27				
Standard sample values[c]																				
MIT			0.511856		0.710265		16.937		15.493		36.713									
From Keller et al.			0.511876		0.710248		16.937		15.493		36.705									
From Regelous et al.			0.511872		0.710223		16.9403		15.4974		36.7246									

[a] Weight loss during acid leaching.

[b] Pb isotopic ratios in this sample are average of two independent analyses, and U/Pb and Th/Pb ratios are average of three independent analyses: Measured $^{206}Pb/^{204}Pb$, $^{207}Pb/^{204}Pb$, and $^{208}Pb/^{204}Pb$ are 19.072, 15.530, 38.415, and 19.074, 15.500, 38.345, respectively. Measured U/Pb ratios in residue are 1.04, 1.30, and 1.23, and Th/Pb ratios are 0.24, 0.25, and 0.29.

[c] Values are reported for standard samples: La Jolla Nd standard (for Nd), NBS-987 (for Sr) and NBS-981 (for Pb).

Table 4b. Age-Corrected (to 76 Ma) Sr-Nd-Pb Isotopic Ratios[a]

Sample	Unit	$^{143}Nd/^{144}Nd$	±2 sigma	$^{87}Sr/^{86}Sr$	±2 sigma	$^{206}Pb/^{204}Pb$	±2 sigma	$^{207}Pb/^{204}Pb$	±2 sigma	$^{208}Pb/^{204}Pb$	±2 sigma
1203A 17 R4W 43-47	1	0.512953	0.000009	0.703204	0.000023	18.477	0.013	15.461	0.002	37.913	0.005
1203A 20 R3W 10-14	3	0.512952	0.000009	0.703195	0.000013	18.320	0.005	15.485	0.004	37.968	0.010
1203A 31 R1W 46-50	8	0.512964	0.000009	0.703097	0.00001	18.216	0.005	15.471	0.002	37.896	0.004
1203A 32 R4W 76-80	11	0.512950	0.000015	0.703097	0.000008	18.152	0.007	15.457	0.003	37.774	0.009
1203A 38 R1W 123-126	16	0.512982	0.000009	0.703025	0.000011	18.075	0.005	15.449	0.002	37.697	0.004
1203A 49 R3W 50-54	21	0.512955	0.000012	0.703044	0.000008	18.233	0.004	15.466	0.002	37.879	0.005
1203A 54 R4W 74-78	23	0.512936	0.000008	0.70316	0.000008	18.412	0.009	15.476	0.002	38.096	0.005
1203A 59 R2W 69-73	24	0.512960	0.000010	0.703111	0.000008	18.147	0.004	15.464	0.002	37.758	0.004
1203A 63 R4W 19-22	26	0.512963	0.000011	0.703073	0.000008	18.289	0.019	15.452	0.006	37.999	0.014
1203A 65 R4W 9-13	29	0.512946	0.000008	0.703095	0.000011	18.183	0.045	15.473	0.003	38.316	0.006
1203A 66 R2W 8-10	30	0.512945	0.000010	0.703106	0.000016	18.241	0.027	15.465	0.002	38.121	0.005
1203A 68 R4W 40-43	31	0.512976	0.000007	0.703146	0.000008	18.432	0.034	15.502	0.003	38.002	0.011
1204A 10 R2W 108-112	2	0.512988	0.000008	0.702876	0.000007	18.056	0.011	15.447	0.004	37.688	0.010
1204B 3 R2W 41-44	1	0.512986	0.000008	0.702805	0.000008	18.143	0.005	15.444	0.003	37.784	0.008
1204B 7 R3W 68-72	2A	0.512972	0.000009	0.702837	0.000013	18.078	0.013	15.464	0.002	37.705	0.010
1204B 10 R4W 43-47	2B	0.512972	0.000008	0.702883	0.000008	18.067	0.005	15.452	0.001	37.759	0.003
1204B 17 R1W 107-110	3	0.512984	0.000009	0.702865	0.000014	18.244	0.005	15.444	0.002	37.868	0.007
LE Unleached		0.512945	0.000011	0.703187	0.000009	18.145	0.008	15.461	0.002	37.747	0.009
LE I		0.512950	0.000015	0.703097	0.000008	18.152	0.007	15.457	0.003	37.774	0.009

[a] The 2 sigma uncertainty in parent/daughter ratios is taken to be 5%. The 2 sigma uncertainty in age-corrected isotopic ratios is estimated considering both uncertainty in TIMS analyses and uncertainty in parent/daughter ratio analyses.

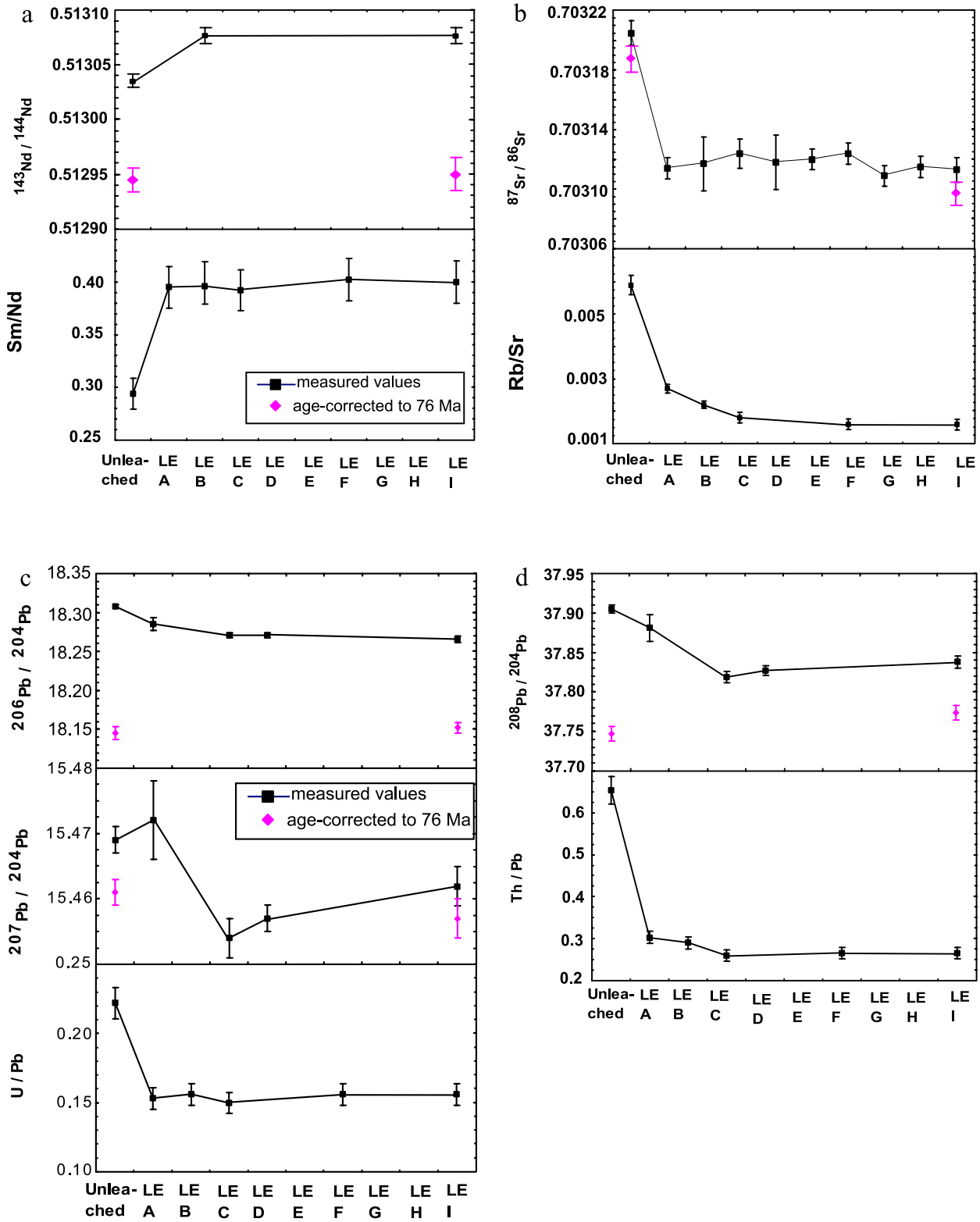

Figure 4. Sr-Nd-Pb isotopic ratios and parent/daughter ratios in samples from different leaching steps. See section 4.3 text for details. The important result is that these isotopic and parent/daughter ratios are relatively constant after three acid leaching steps. The isotope data reported in Tables 4a and 4b were obtained on rock powders that were subjected to 6–9 leaching steps.

4.3. Effects of Acid Leaching on Isotopic Ratios

[23] In order to assess the effects of alteration on isotopic ratios, we carried out a nine step-leaching experiment on one sample, 1203A 32R4W 76-80 (Table 4a). We prepared a series of precleaned centrifuge tubes labeled as LE-A through LE-I, and ~0.4 g sample 1203A 32R4W 76-80 was weighed into each tube; 10 mL 6N HCl was added to each tube, and the tubes were shaken. Then the tubes were placed in an ultra-sonic bath. After 30 min, the acid was decanted from each tube. For Tube LE-A, the leaching step was followed by two steps of rinsing with 10 mL deionized H_2O. Tube LE-B was subjected to two leaching steps, Tube LE-C to three leaching steps, etc. for Tubes LE-D to LE-I with Tube LE-I experiencing nine leaching steps. The color of HCl was colorless after six leaching steps. Sr-Nd-Pb isotopic compositions and Rb/Sr, Sm/Nd, Th/U and U/Pb ratios in this series of unleached and leached powders are reported in Table 4a. As indicated in Figure 4, these isotopic ratios and parent/daughter ratios are relatively constant after two (or three for Rb/Sr and Th/Pb) acid leaching steps. The higher Sm/Nd but lower Rb/Sr, Th/Pb and U/Pb ratios in the leached powders reflect removal of fine-grained groundmass and alteration phases during acid leaching (Figure 4). We assume that the parent/daughter ratios of the leached powders are those of the unaltered mineral assemblage and use them for age correction. After age-correction to 76 Ma, the unleached sample and sample LE I have similar (within 2 σ uncertainty) initial $^{143}Nd/^{144}Nd$, $^{206}Pb/^{204}Pb$ and $^{207}Pb/^{204}Pb$ ratios, but significantly different $^{87}Sr/^{86}Sr$ and $^{208}Pb/^{204}Pb$ ratios (Table 4b; Figure 4).

[24] The similar initial $^{143}Nd/^{144}Nd$ ratios in leached and unleached powders is consistent with the immobility of REE during postmagmatic alteration. The different initial $^{87}Sr/^{86}Sr$ and $^{208}Pb/^{204}Pb$ ratios in leached and unleached powders clearly reflect the disturbance of the Rb-Sr and Th-Pb systems during postmagmatic alteration (Table 4b). Given the evidence for Pb mobility [e.g., *Bach et al.*, 2003; *Regelous et al.*, 2003], the difference in initial $^{208}Pb/^{204}Pb$ probably reflects loss of Pb (and consequently high Th/Pb) during postmagmatic alteration. However, it is surprising that leached and unleached powders have similar initial $^{206}Pb/^{204}Pb$ and $^{207}Pb/^{204}Pb$ ratios (Table 4b; Figure 4c). Since the Th/Pb ratio in leached and unleached powders changed by more than a factor of 2, but U/Pb ratio changed by only a factor of ~1.5 (Figures 4c and 4d), it is possible that both Pb and U were mobile during alteration, but that the U/Pb ratio was not changed dramatically.

5. Results

5.1. Classification of Basalt Type

[25] The whole-rock samples are altered to variable extent as indicated by their Loss on Ignition (L.O.I.) (Table 3a), and the presence of secondary minerals. Among the 69 analyzed whole-rock samples, 54 samples have L.O.I. > 2% (hereafter described as strongly altered samples), and 15 samples have 0.4% < L.O.I. < 2% (hereafter described as moderately altered samples). In contrast, the sums of major elements in the 36 glass samples are greater than 97.9%, and 24 samples have sums greater than 99% (Table 3b, T. Thordarson et al., manuscript in preparation, 2004). This confirms the visual inspections that these glasses are unaltered. Rock classification using the total alkalis–silica criteria can be unreliable for altered rocks, because of the mobility of Na and K during postemplacement alteration (Figure 5a). However, the composition of unaltered glasses enables unambiguous alkali-silica classification for 7 of the 22 flow units recovered at Detroit Seamount during ODP Leg 197 and 5 cooling units recovered during ODP Leg 145 (Figure 3b). Out of 29 whole-rock samples from Site 1204 and 6 from the nearby Site 883 (data from *Regelous et al.* [2003]), 30 samples are within the alkalic field (Figure 5a). The remaining 5 samples are in the tholeiitic field close to the Macdonald-Katsura line. They include 3 samples from Hole 1204B (2 from Unit 2 and 1 from Unit 1) and 2 from Unit 2 at Hole 1204A. However, glasses from Units 1 and 2 at Hole 1204B are within the alkalic field (Table 3b, Figure 5b). Therefore we infer that the three whole-rock samples from Hole 1204B in the tholeiitic field lost alkalis during post magmatic alteration. Although no glass is available from Unit 2 at Hole 1204A, 7 of the 9 Unit 2 whole-rock samples are within the alkalic field. Therefore we classify all lavas from Sites 1204 and 883 as alkalic basalt.

[26] In contrast, glasses from Sites 884 and 1203, whole rocks from Site 884 and moderately altered (L.O.I. < 2%) whole rocks from Site 1203 are tholeiitic basalt. Highly altered (L.O.I. > 2%) whole rocks from Site 1203 range from the tholeiitic to the alkalic field. Three highly altered whole-rock samples from Site 1203 Unit 20

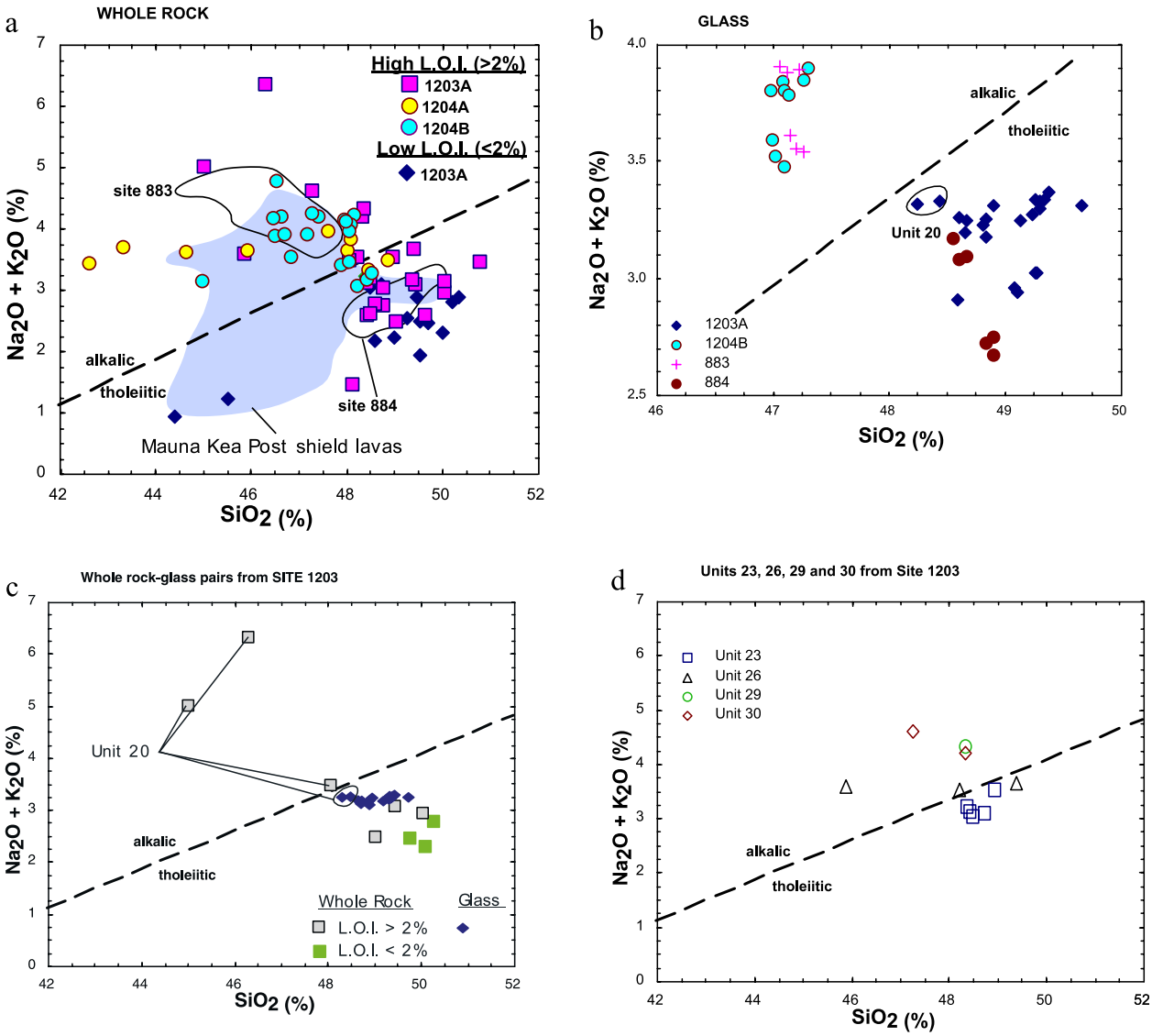

Figure 5. $Na_2O + K_2O$ versus SiO_2 (all in wt%). The dashed line shows the alkalic-tholeiitic boundary of *Macdonald and Katsura* [1964], using the equation Total Alkalis = $0.37SiO_2 - 14.43$ [*Carmichael et al.*, 1974]. The Macdonald-Katsura line is based on data for total iron measured as FeO and Fe_2O_3; consequently, for our analyses, total iron is assumed to be 10% Fe^{3+} and 90% Fe^{2+}. (a) Whole-rock data. All the Detroit Seamount lavas with low L.O.I. (<2%) are within the tholeiitic field, and those with high L.O.I. (>2%) range from tholeiitic to alkalic basalt. See text for details. Shown for comparison is the field (shaded) for late shield to postshield stage lavas from Mauna Kea [*Frey et al.*, 1990, 1991]. Whole-rock fields for Sites 883 and 884 are from *Regelous et al.* [2003]. (b) Glass data. Compositions of unaltered glasses (Table 3b) clearly show that all lavas from Sites 883 and 1204 are alkalic basalt, whereas lavas from Site 884 are tholeiitic. Glasses are available in several units (Units 1, 3, 8, 18, and 20) at Site 1203, and they are also tholeiitic. Detroit Seamount glass data are from this study and T. Thordarson et al. (manuscript in preparation, 2004). (c) Whole-rock–glass pairs from submarine lava flow units at Site 1203. Except for the three samples from Unit 20, which are highly altered (L.O.I. ranges from 5–11%), the other whole-rock samples (three highly altered and three moderately altered) are within the tholeiitic field. As discussed in the text, we classify Unit 20 as a tholeiitic unit (see Figure 5b) and conclude that the high total alkali contents in Unit 20 whole rocks are a result of alteration. (d) The subaerial lava flows Units 23, 26, 29, and 30 at Site 1203 are highly altered (L.O.I. > 2%) and are within the alkalic field or straddle the alkalic-tholeiitic boundary line. No unaltered glass is available from these units; however, on the basis of their high abundances of incompatible elements, they are classified as alkalic basalt (see text).

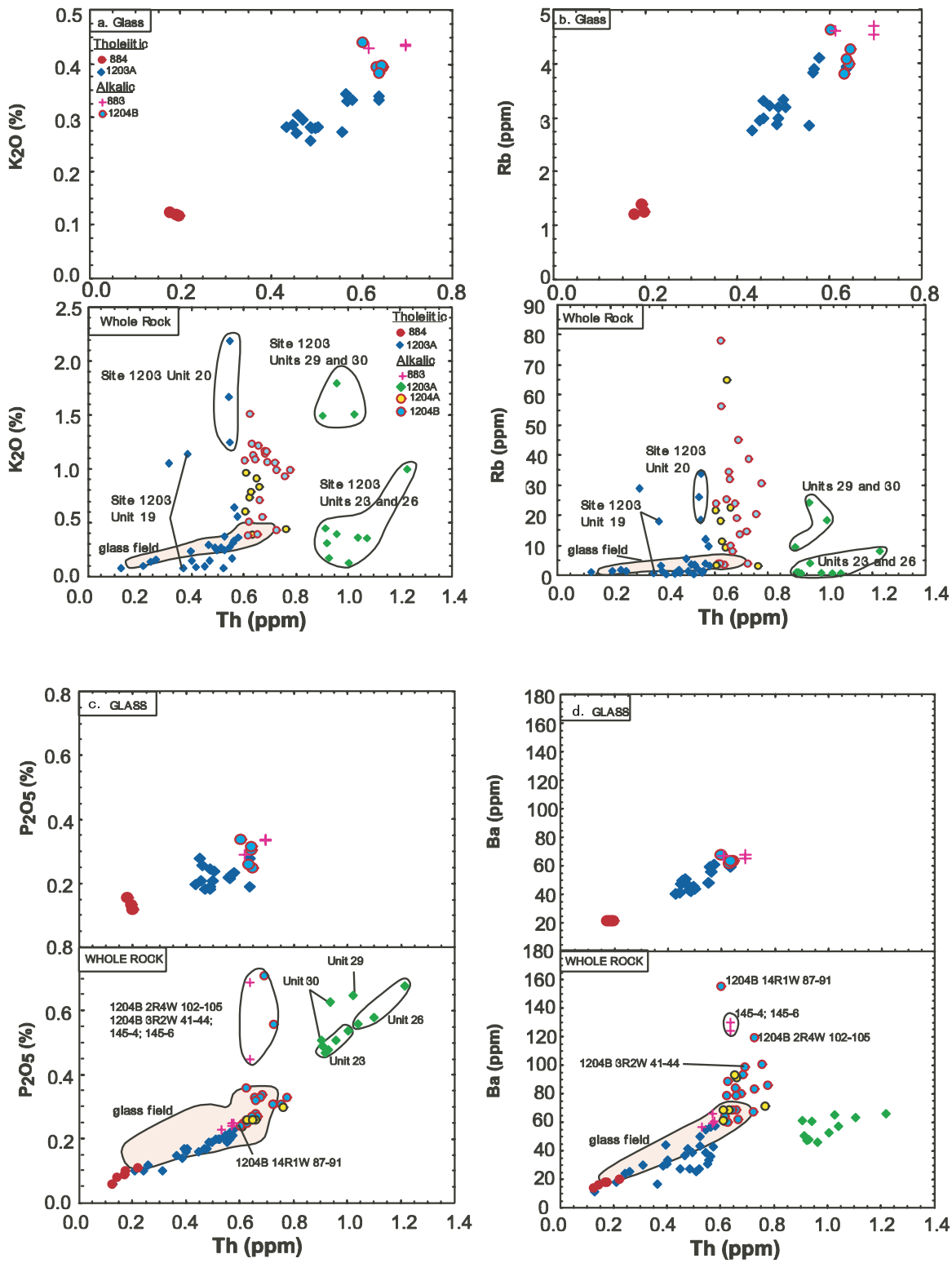

Figure 6. Th (ppm) versus (a) K_2O (wt.%), (b) Rb (ppm), (c) P_2O_5 (wt.%) and (d) Ba (ppm) in glasses and whole rocks.

(L.O.I. ranges from 5–11%) are within alkalic field (Figure 5c); however the two glass samples from this unit are within the tholeiitic field (Figure 5c). In addition, whole-rock and glass samples from this unit have incompatible element abundances similar to other tholeiitic basalts (Tables 3a and 3b). We classify Unit 20 as tholeiitic basalt.

[27] Whole-rock samples from the thick compound pahoehoe Units 23, 26, 29 and 30 at Site 1203 (Figure 2) lie within the alkalic field or are close to alkalic-tholeiitic boundary line (Figure 5d). No unaltered glass is available from these units, but whole-rock samples from these units have high abundances of incompatible elements, such as Ti and Zr (Table 3a); hence we conclude that they represent alkalic basalt underlying the main tholeiitic basalt succession in Hole 1203A (Figure 2).

5.2. Compositional Effects of Alteration

[28] Our objectives are to understand the magmatic evolution of lavas forming Detroit Seamount. Because these lavas are ~76–81 Myr old, the igneous geochemical characteristics of the whole rocks have been affected by postmagmatic processes. For submarine erupted lavas, these are submarine alteration processes. For now submerged but subaerially erupted lavas, both subaerial and submarine alteration processes have occurred. In this section, we discuss the effect of alteration on whole-rock chemical compositions.

[29] A direct approach to evaluate compositional changes of whole rocks caused by postmagmatic alteration is comparison of unaltered glass and whole-rock compositions. Our discussion begins with elements that are known to be mobile, e.g., K and Rb, but also Ba and P, and concludes with assessment of changes in ratios of highly incompatible elements.

[30] K (as K_2O) and Rb are incompatible elements, and their abundance in unaltered tholeiitic and alkalic basalt glasses are positively correlated with Th abundance (Figures 6a and 6b). However, whole-rock samples do not define linear trends in Th-K_2O and Th-Rb diagrams, which is best explained as the result of K and Rb mobility during alteration. Most Site 1204 whole-rock samples are from oxidizing zones defined by *Shipboard Scientific Party* [2002b], and they have higher K_2O and Rb content than the unaltered glass samples at a given Th abundance (Figures 6a and 6b). In contrast, tholeiitic whole-rock samples from Site 1203 range to higher and lower K_2O and Rb contents than unaltered glass samples at a given Th abundance (Figures 6a and 6b). For example, three whole-rock samples from Unit 20 at Site 1203 deviate from the trend formed by unaltered glasses to higher K_2O and Rb content. Their L.O.I. varies from 5% to 11%. Hence we conclude that K_2O and Rb were added during alteration. Two samples from Unit 19 at Site 1203 exhibit contrasting alteration trends. Sample 1203A 42R1W 88-92 deviates from the glass trends to higher K_2O and Rb content, and sample 1203A 42R5W 40-44 trends to lower K_2O and Rb content (Figures 6a and 6b). Their L.O.I. are 5% and 4%, respectively (Table 3a). We infer that K_2O and Rb were added to sample 1203A 42R1W 88-92, and lost from sample 1203A 42R5W 40-44 during alteration.

[31] Among the four alkalic, incompatible element-enriched units at the bottom of Hole 1203A, Units 29 and 30 have higher contents of K_2O and Rb than Units 23 and 26 (Figures 6a and 6b). K_2O/P_2O_5 is sensitive to alteration, and unaltered Hawaiian lavas have $K_2O/P_2O_5 > 1$ [e.g., *Huang and Frey*, 2003]. Therefore the low and variable K_2O/P_2O_5 in Units 23 and 26 (8 of 9 samples range from 0.24 to 0.92) compared to that of Units 29 and 30 (2.3 to 2.9) indicate that K_2O and Rb were removed from Units 23 and 26 during postmagmatic alteration. This inference is important in subsequent evaluation of the role of phlogopite during the petrogenesis of these alkalic lavas.

[32] P is an incompatible element, and its content (as P_2O_5) in unaltered glasses is positively correlated with Th abundance (Figure 6c). Most whole-rock samples form a positive trend in Th versus P_2O_5 diagram which overlaps with the trend formed by the unaltered glasses. Six whole-rock samples (labeled in Figure 6c) deviate from the trend to higher P_2O_5 content. Their P_2O_5 contents, 0.5 to 0.7%, could be explained by secondary apatite, up to 1 wt%.

[33] Mobility of Ba has been observed in altered oceanic crust [e.g., *Staudigel et al.*, 1995]. Most whole rocks from Detroit Seamount form a positive trend in a Th-Ba plot, overlapping with the trend formed by unaltered glasses (Figure 6d). However, several whole-rock samples deviate from the trend to high Ba abundance (Figure 6d). The high Ba abundance in Sample 1204B 14R1W 87-91

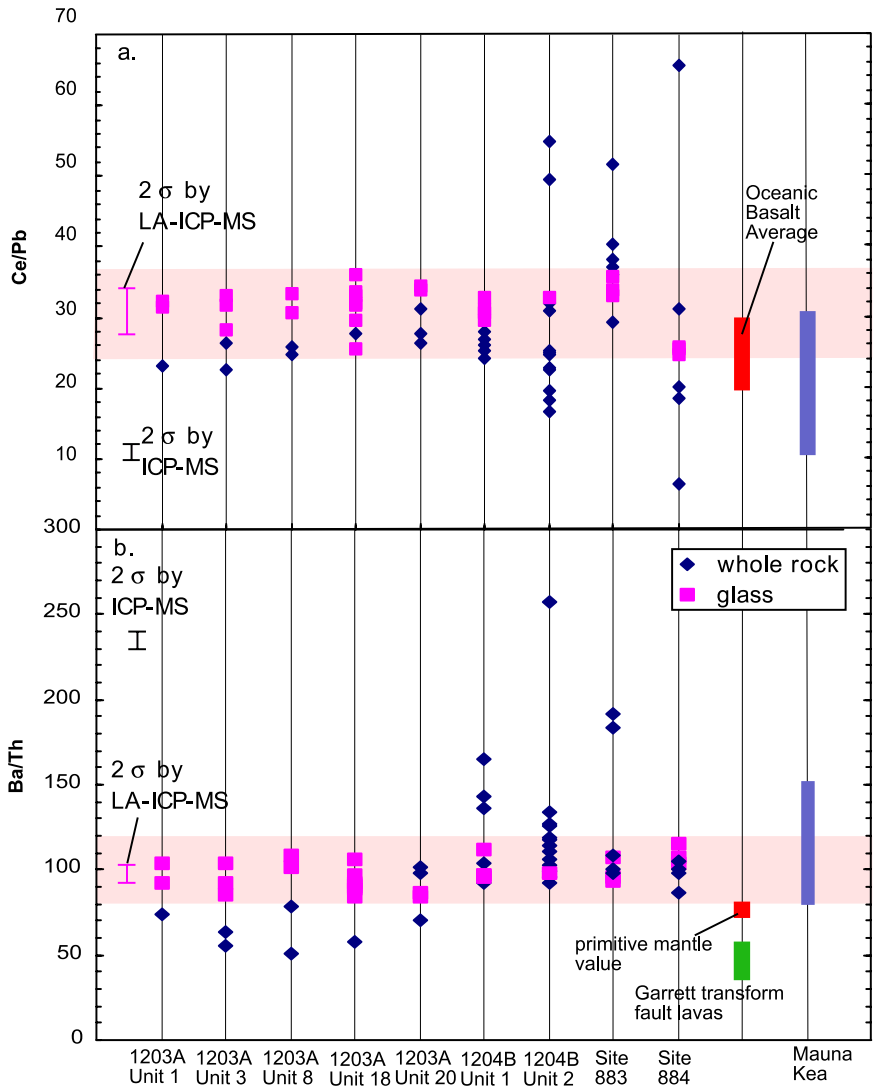

Figure 7. Highly incompatible element ratios: Ce/Pb and Ba/Th. Blue diamond: whole-rock data. Pink square: glass data. Site 883 and 884 data are normalized using the BHVO standard values reported by *Regelous et al.* [2003] and *Huang and Frey* [2003]. The pink fields show the glass range. Data for primitive mantle [*Hofmann*, 1988; *Sun and McDonough*, 1989], average oceanic basalt [*Hofmann*, 1986], Garrett transform fault lavas [*Wendt et al.*, 1999], and Mauna Kea shield lavas [*Huang and Frey*, 2003] are shown for comparison.

has been confirmed by both ICP-MS and XRF analyses (Table 3a). This sample is highly altered and contains large irregular domains of clay after glass.

[34] Ce/Pb and Ba/Th ratios are not readily changed by most magmatic processes; consequently, Ce/Pb and Ba/Th ratios are relatively uniform in unaltered oceanic basalt [e.g., *Hofmann and White*, 1983; *Hofmann*, 1986]. However, due to the mobility of Pb and Ba during alteration processes, these ratios may vary significantly in altered whole rocks. Comparison of unaltered glasses and whole rocks shows that each of these ratios are quite variable in the whole-rock samples, even among samples from the same unit, but relatively uniform in the unaltered glasses (Figure 7). For example, the average value of Ce/Pb in unaltered glasses from Detroit Seamount is 31 ± 6, which is close to the average value of oceanic basalt (25 ± 5) [*Hofmann*, 1986] and that of Mauna Kea lavas

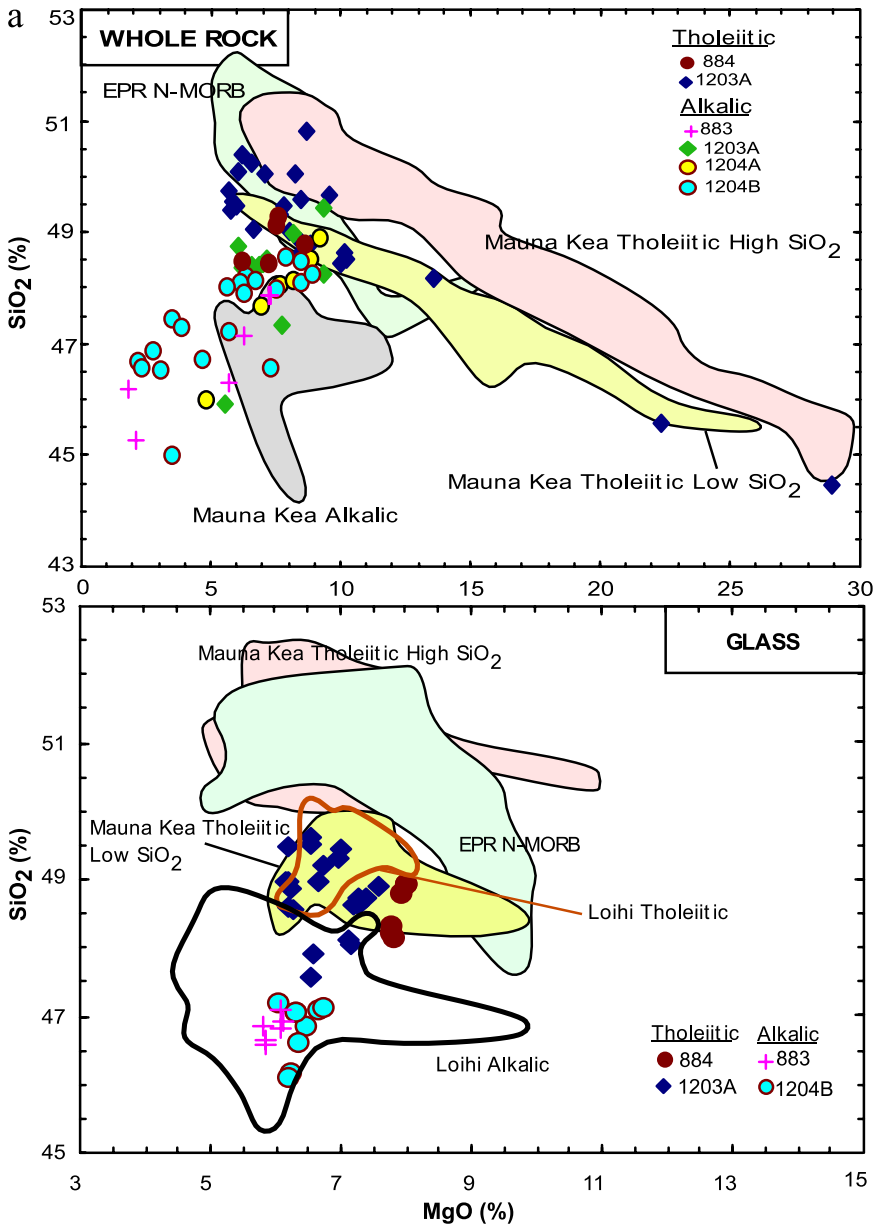

Figure 8. MgO content versus other oxide contents (all in wt.%). For each element, there are two panels: whole-rock data and glass data. Only samples with L.O.I. less than 7% are plotted. Whole-rock data are plotted after converting Fe_2O_3 to FeO. Data sources are as follows: Detroit Seamount whole rocks (Sites 1203 and 1203: this study; Sites 883 and 884: *Regelous et al.* [2003]); Detroit Seamount glasses (this study and Thordarson et al., manuscript in preparation, 2004); EPR N-MORB whole rock (downloaded data from PET DB); EPR N-MORB glass [*Niu and Batiza*, 1997; *Niu et al.*, 1999; *Regelous et al.*, 1999]; Loihi glass [*Garcia et al.*, 1993, 1995, 1998]; Mauna Kea whole rock [*Rhodes*, 1996; *Rhodes and Vollinger*, 2004], and Mauna Kea glass [*Stolper et al.*, 2004]. In the SiO_2 panels the Mauna Kea fields are divided into Low and High SiO_2 groups; these groups are combined in other panels.

(29 ± 8) [*Huang and Frey*, 2003]. The highly variable Ce/Pb ratio (6–66) in the whole-rock samples (Figure 7a) most likely results from the mobility of Pb during alteration. The Ba/Th ratio in unaltered glasses from Detroit Seamount is 98 ± 17, but the Ba/Th ratio ranges widely (50–257) in the whole-rock samples, reflecting Ba mobility during alteration (Figure 7b). Primitive mantle values of 74 and 82 are reported by *Hofmann* [1988] and *Sun and McDonough* [1989], respectively.

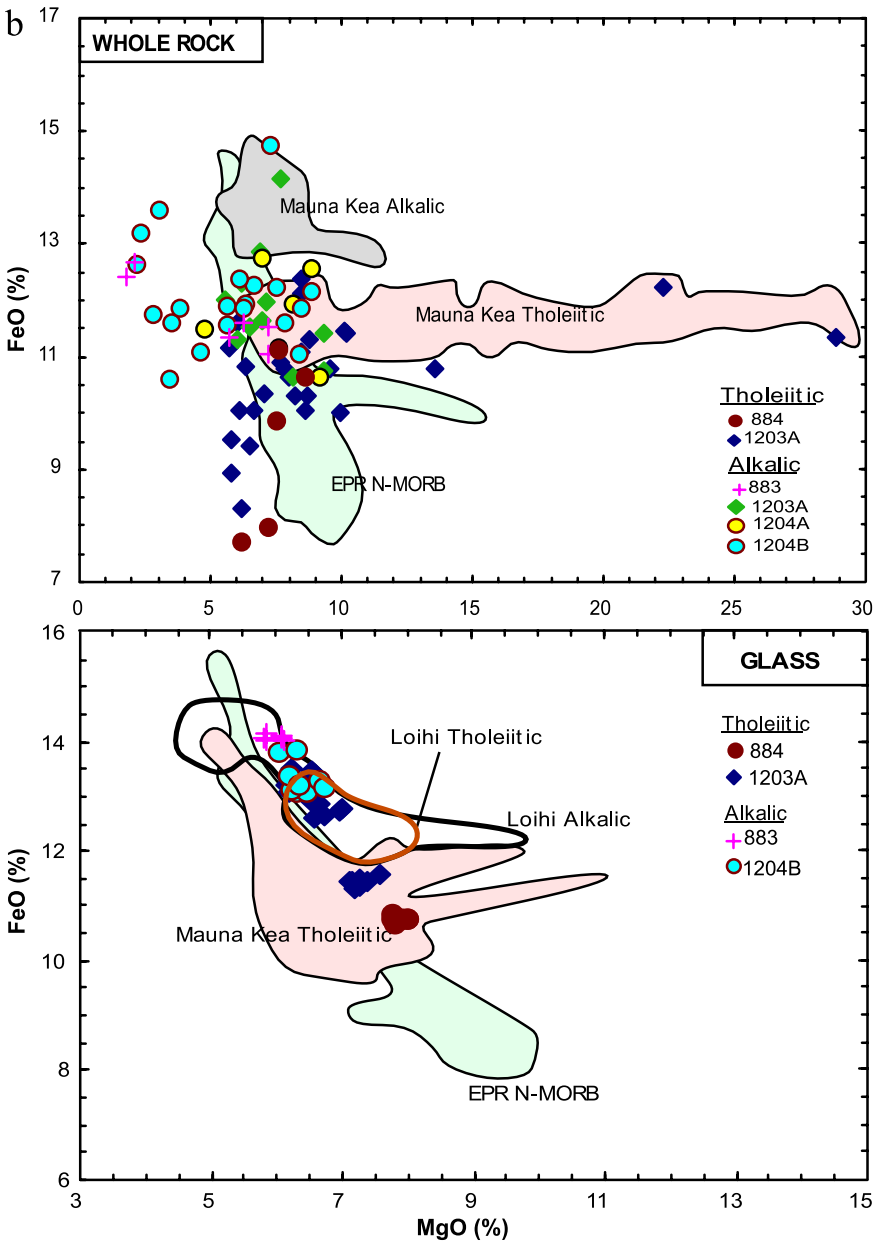

Figure 8. (continued)

5.3. Major Elements: Comparison With Hawaiian Lavas and MORB

[35] We use MgO variation plots to compare and contrast the composition of the basalt from the four ODP drill sites at Detroit Seamount as well as to compare with mid-ocean basalt (MORB) from the East Pacific Rise (EPR) and basalt from Mauna Kea Volcano and Loihi Seamount, which have well studied shield to postshield and preshield to shield transitions, respectively. Our principal objective is to use the well known differences in major element composition between MORB and Hawaiian magmas [e.g., *Albarede*, 1992] to determine the affinities of the magmas erupted at Detroit Seamount.

5.3.1. SiO_2

[36] For whole rocks and glasses with 5–10% MgO, SiO_2 contents increase from Mauna Kea and Loihi alkalic basalt (postshield and preshield stages, respectively) to Mauna Kea (low SiO_2 group) and Loihi tholeiitic basalt (shield stages). The highest SiO_2 contents (>50%) are in EPR MORB and the high SiO_2 group lavas of Mauna

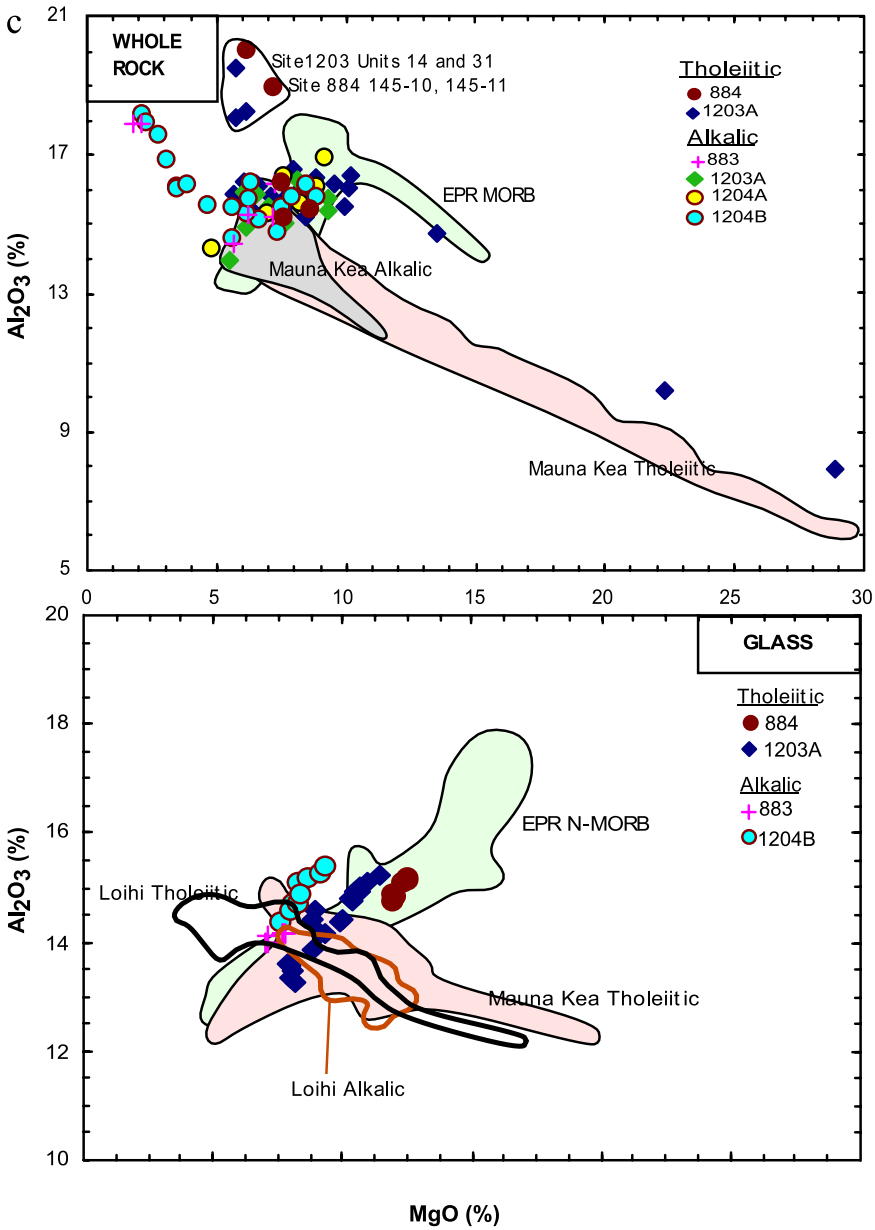

Figure 8. (continued)

Kea Shield lavas (Figure 8a). In contrast to the negative MgO-SiO_2 trend defined by Hawaiian tholeiitic shield lavas, a trend reflecting olivine addition, subtraction and fractionation [e.g., *Yang et al.*, 1996; *Rhodes and Vollinger*, 2004], most Detroit Seamount lavas define a broad positive trend (Figure 8a). Only the olivine-rich samples from Units 11 and 16 at Site 1203 fall on an olivine-control trend. Alkalic basalt, whole rocks and glasses, from Sites 883 and 1204 has relatively low SiO_2 content that overlaps the range of alkalic postshield lavas from Mauna Kea and preshield stage lavas from Loihi. Tholeiitic glasses from Sites 884 and 1203 overlap with the low-SiO_2 tholeiitic shield lavas from Mauna Kea volcano (Figure 8a).

5.3.2. Total Iron as FeO*

[37] For whole rocks with 7–10% MgO, the trend of increasing FeO* contents is opposite to that for SiO_2; i.e., EPR N-MORB have the lowest FeO* abundances and Hawaiian tholeiitic basalt generally has lower FeO* abundance than Hawaiian alkalic basalt. For Detroit Seamount lavas, the whole-rock data for FeO* are scattered widely.

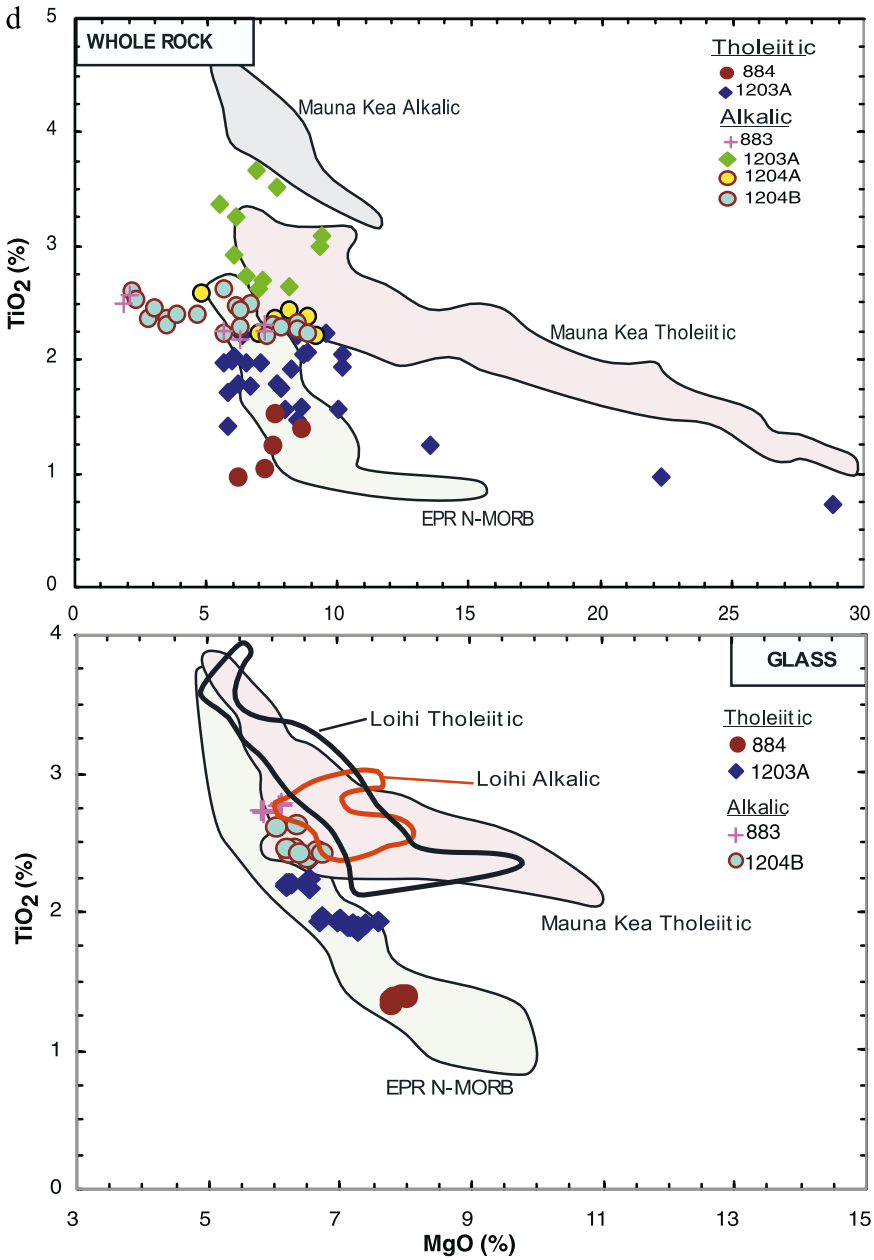

Figure 8. (continued)

The FeO* content of tholeiitic basalt from Sites 1203 and 884 varies from ~7% to 13%, which is similar to EPR N-MORB. The olivine-rich units 11 and 16 at Site 1203 overlap with Mauna Kea shield stage tholeiitic basalt (Figure 8b). The alkalic lavas from Sites 883, 1203 and 1204 overlap with the Mauna Kea tholeiitic field but a few samples range to high FeO* (>13%) and are within the field of Mauna Kea alkalic basalt. A negative MgO-FeO* trend is well defined by Detroit Seamount glasses with the highest FeO* in alkalic basalt from Sites 883 and 1204. This trend parallels the trends for EPR N-MORB and Mauna Kea glasses (Figure 8b).

5.3.3. Al_2O_3

[38] In the context of the MORB-related versus Hawaiian plume-related alternatives proposed for Detroit Seamount lavas [*Keller et al.*, 2000; *Regelous et al.*, 2003], MgO versus Al_2O_3 is especially important because the parental magmas for N-MORB and Hawaiian shield lavas differ significantly in Al_2O_3. For MgO >8%, the Al_2O_3

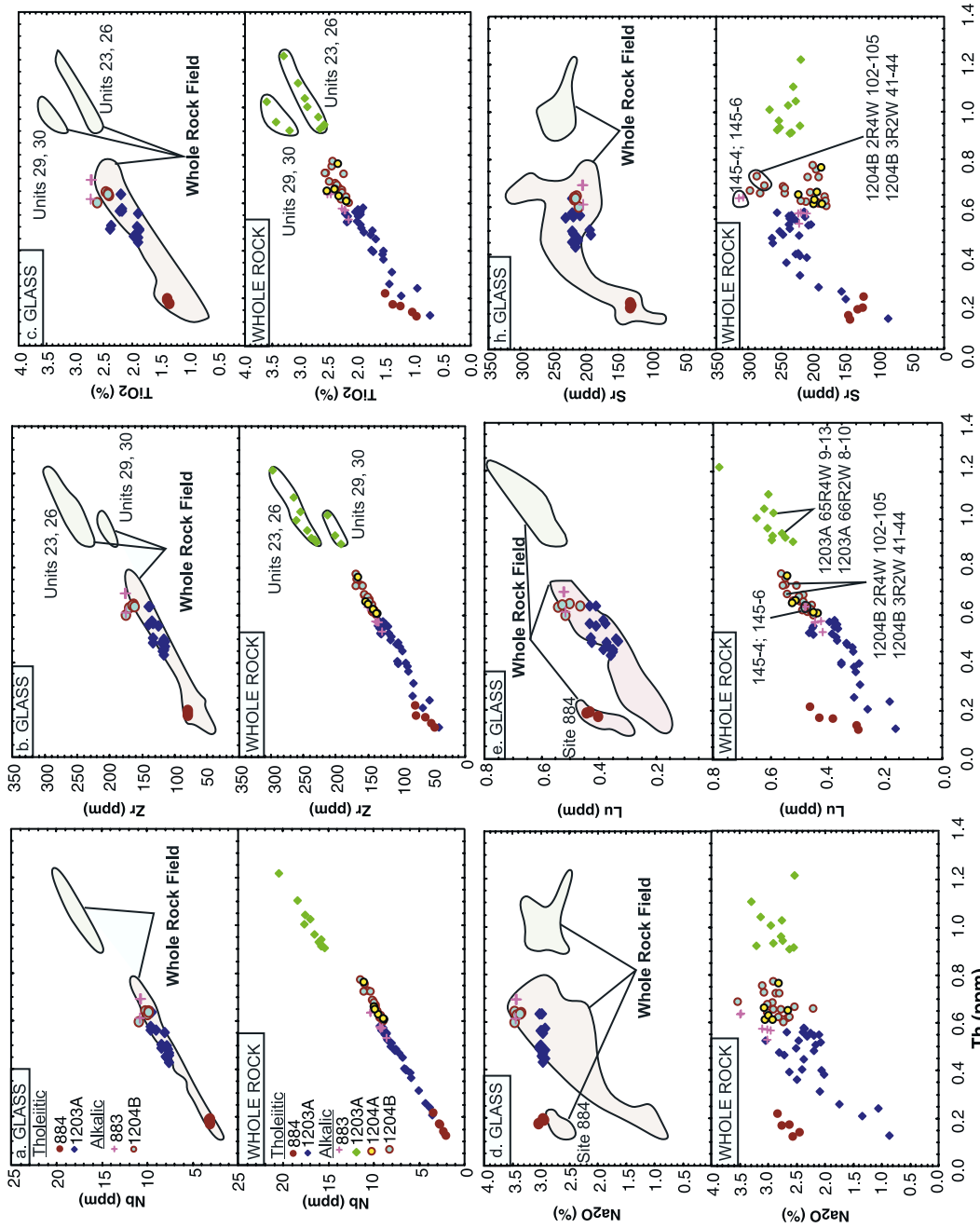

Figure 9. Th abundance (in ppm) versus selected incompatible element abundances (in ppm or %). For each element, there are two panels: whole-rock data and glass data. Only samples with L.O.I. less than 7% are plotted. Whole-rock trace element abundances have been adjusted using Plotted Value = Measured Value/(1-L.O.I.). Whole-rock fields are shown in glass panels for comparison. Site 883 and 884 whole-rock data are from *Regelous et al.* [2003].

Table 5. Ti/Zr, Ba/Th, and Zr/Hf in Alkalic Lavas at Site 1203

Unit	Sample	Ti/Zr	Ba/Th	Zr/Hf
23	1203A 52R 6W 23-27	68.7	51.5	44.4
23	1203A 53R6W 123-127	66.7	51.2	45.0
23	1203A 54R4W 74-78	67.2	52.2	45.4
23	1203A 55R1W 109-113	67.5	48.1	44.4
23	1203A 58R2W 94-98	70.9	55.2	43.5
26	1203A 62R1W 101-105	69.9	53.9	43.6
26	1203A 62R2W 88-92	72.0	54.9	43.7
26	1203A 63R4W 19-22	71.2	57.6	43.5
29	1203A 65R4W 9-13	105.3	63.5	40.2
30	1203A 66R2W 8-10	107.4	64.5	40.9
30	1203A 67R4W 10-14	103.4	67.5	40.5

content of MORB exceeds that for Hawaiian shield lavas (e.g., Figure 8c) [see also *Albarede*, 1992, Figure 2]. Unfortunately, this distinction diminishes as MgO content decreases, because at ~7% MgO the positive Al_2O_3-MgO trend of MORB caused by plagioclase fractionation intersects the negative trend of Hawaiian shield lavas caused by olivine fractionation (Figure 8c). The ~5.8 to 8.0% MgO glasses from Detroit Seamount are in the region of overlap between the Mauna Kea and EPR N-MORB fields. However, the positive MgO-Al_2O_3 trend for Detroit Seamount glasses is similar to the plagioclase fractionation trend of N-MORB. In contrast, the three high MgO (olivine-rich) samples from Units 11 and 16 at Site 1203 define a negative trend that is intermediate between the Mauna Kea shield and EPR MORB fields.

[39] The five lavas with atypically high Al_2O_3 at ~5.7 to 7.2% MgO (Site 1203, Units 14 and 31 and samples 145-10 and 145-11 from Site 884, Figure 8c) are rich (>7 vol.%) in plagioclase phenocrysts (Table 2a) [*Regelous et al.*, 2003; *Shipboard Scientific Party*, 2002a].

5.3.4. TiO_2

[40] It is well known that the primary magmas for Hawaiian tholeiitic lavas contain higher abundances of TiO_2 (and incompatible trace elements) than primary magmas for N-MORB [e.g., *Frey and Roden*, 1987; *Albarede*, 1992]. For Detroit Seamount lavas, there is a range in TiO_2 at a given MgO content: TiO_2 content increases in the order Site 884 < Site 1203 (tholeiitic) < Site 1204 ~ Site 883 < Site 1203 (alkalic) (Figure 8d). Tholeiitic lavas from Sites 884 and 1203 overlap with the N-MORB field. Note that the alkalic lavas from Site 1203 have lower TiO_2 content than alkalic lavas from Mauna Kea (Figure 8d).

5.3.5. Summary

[41] Alkalic basalt with relatively low SiO_2 content and high contents of FeO* and TiO_2 at Detroit Seamount is consistent with the tholeiitic to alkalic basalt transition that is characteristic of the late shield and postshield stages of Hawaiian volcanoes [e.g., *Frey et al.*, 1990, 1991]. On the other hand, Site 884 lavas with low TiO_2 and P_2O_5 contents are similar to MORB. Although MORB and Hawaiian shield stage lavas with >8% MgO content differ significantly in Al_2O_3 [*Albarede*, 1992], evolved MORB and Hawaiian lavas with ~6–8% MgO have similar Al_2O_3 content. Therefore we cannot use Al_2O_3 content to establish a MORB or Hawaiian affinity for the glasses from Detroit Seamount which have ~6–8% MgO. However, as in MORB, plagioclase fractionation was an important process controlling the compositions of Detroit Seamount lavas.

5.4. Incompatible Elements

[42] In both whole rocks and glasses, abundances of incompatible elements that are immobile during alteration, such as Nb, Zr and TiO_2, are positively correlated with Th abundance (Figures 9a–9c). Generally, the lowest abundance of these incompatible elements are in Site 884 lavas and the three high MgO lavas from Site 1203 (from Units 11 and 16) (Tables 3a and 3b). Alkalic lavas from Sites 1204 and 883 have incompatible element abundance intermediate between tholeiitic lavas from Sites 1203 and 884 and alkalic lavas from Site 1203. The highest abundances are in the 4 thick compound pahoehoe units, Units 23, 26, 29 and 30, in the lower part of the Site 1203 core (Figure 2). The combination of high incompatible element abundances and their location within the alkalic field or straddling the alkalic-tholeiitic boundary line in Figure 5d shows that these lavas are alkalic basalt. These 4 alkalic basalt units define two separate trends in the Zr and TiO_2 versus Th plots (e.g., Figures 9b and 9c). The Ti/Zr ratio in most lavas from Detroit Seamount ranges from 86–109, which is close to the primitive mantle value of 116 [*Sun and McDonough*, 1989]; however, alkalic Units 23 and 26 from Site 1203 have a lower Ti/Zr ratio (67–72). Also Zr/Hf in Units 23 and 26 (44–45) differ from those in Units 29 and 30 (40–41) (Table 5).

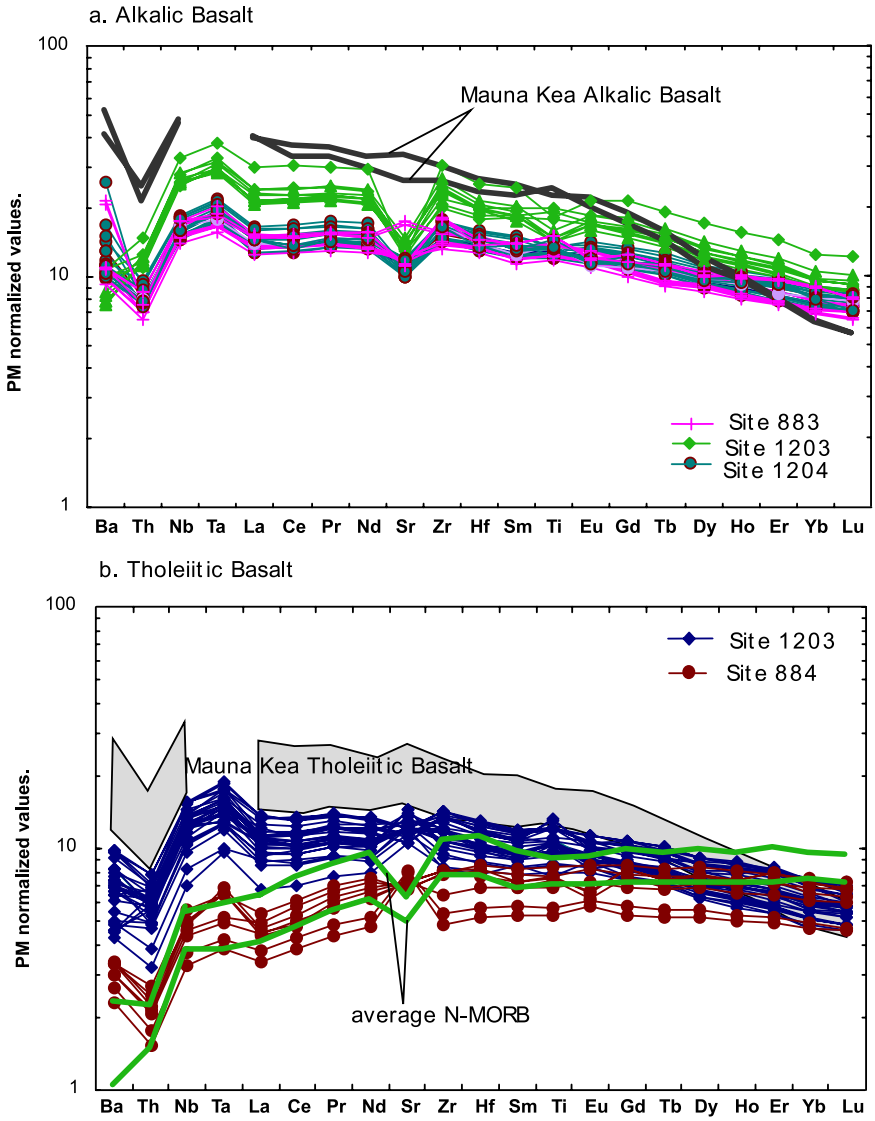

Figure 10. Primitive mantle normalized incompatible element abundances for lavas from Detroit Seamount: (a) alkalic lavas and (b) tholeiitic lavas. In order to minimize the effect of crystal fractionation, only lavas with 6% < MgO < 9% are plotted, except for Site 883 glass samples, whose MgO contents are ~5.8%. Both glass and whole-rock data are plotted. In each group, glass data overlap with whole-rock data. Mauna Kea data are from *Huang and Frey* [2003]. Primitive mantle values are from *Hofmann* [1988]. Average N-MORB data are from *Hofmann* [1988] and *Sun and McDonough* [1989].

[43] Abundance of other moderately incompatible elements, such as Na (as Na_2O) and Lu, versus Th abundance define more complex trends (Figures 9d and 9e). Except for the three high MgO lavas (from Site 1203 Units 11 and 16), which have the lowest Th, Lu and Na_2O abundance, tholeiitic lavas (glasses and whole rocks) from Sites 1203 and 884 have similar Lu and Na_2O abundance. This result is surprising because Site 884 lavas have the lowest abundance of highly incompatible elements. Also, whole-rock data for Site 884 tholeiitic lavas and Site 1203 alkalic lavas overlap in Na_2O content. However, alkalic glasses from Sites 883 and 1204 have higher Na_2O content than tholeiitic glasses from Sites 884 and 1203.

[44] Trends defined by Ba and Sr versus Th abundance are also complex (Figures 6d and 9f). Site 1203 alkalic lavas have variable Th abundances but relatively uniform Sr and Ba abundances. The Sr data for glasses show that Sr abundances are similar in alkalic glasses from Sites 883 and 1204 and tholeiitic glasses from Site 1203 (Figure 9f). This is a surprising result given the relative enrichment of other incompatible elements in these alkalic glasses.

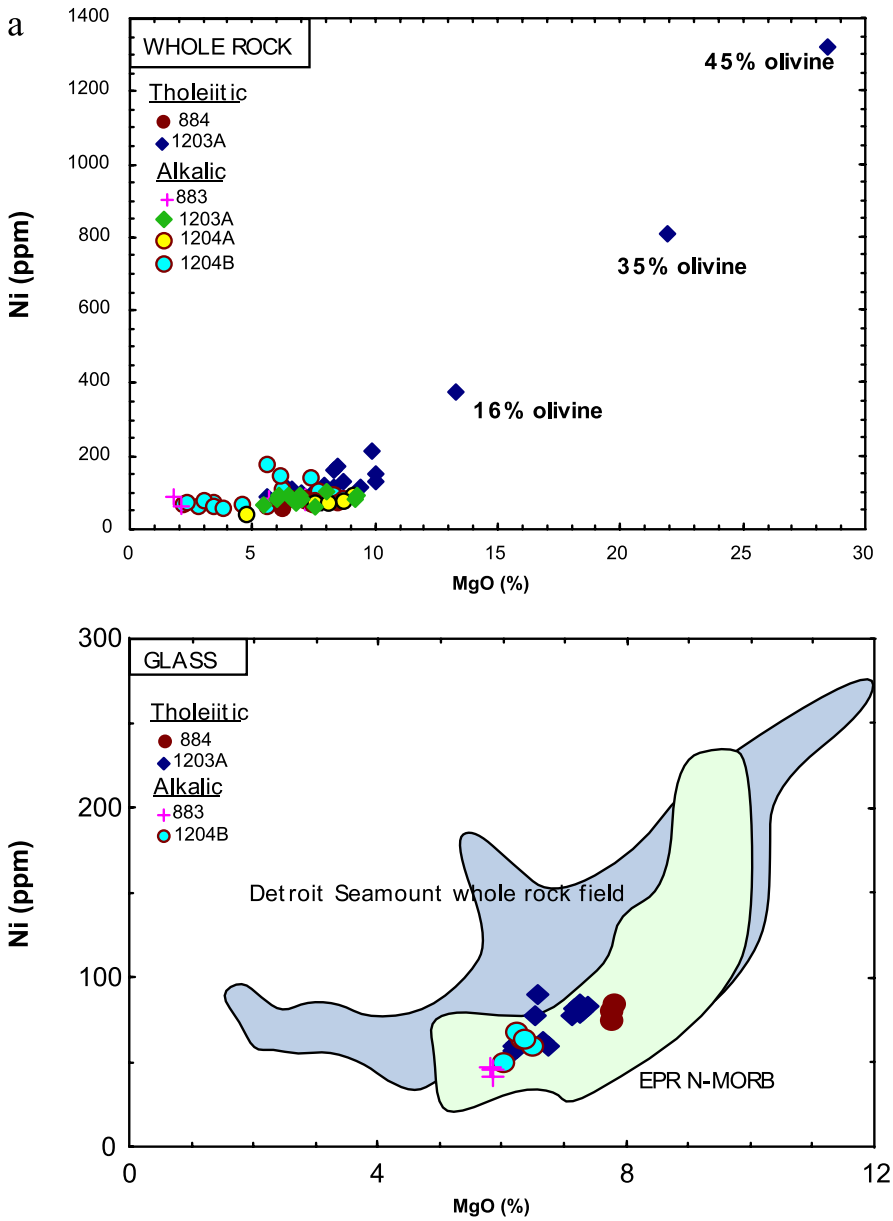

Figure 11. MgO content (in wt%) versus Ni and Sc abundances (in ppm). For each element, there are two panels: whole-rock data and glass data. Only samples with L.O.I. less than 7% are plotted. Whole-rock fields are shown in glass panels for comparison. As shown, three samples contain large proportion of olivine phenocryst (>15 vol.%), and the positive trend in Figure 11a is a result of olivine addition. See the Figures 8a–8d caption for other data sources. Koolau data are from *Frey et al.* [1994].

[45] In a primitive mantle normalized trace element diagram, the relative enrichment in highly incompatible elements decreases in the order Mauna Kea alkalic lavas > Site 1203 alkalic lavas > Sites 1204 and 883 alkalic lavas (Figure 10a). Also relative to alkalic basalt from Mauna Kea, Detroit Seamount alkalic basalt has more pronounced depletion in Sr and flatter patterns. For tholeiitic lavas, incompatible element abundance decrease in the order Mauna Kea tholeiitic lavas > Site 1203 tholeiitic lavas > Site 884 tholeiitic lavas (Figure 10b). As pointed out by *Regelous et al.* [2003], the Site 884 tholeiitic lavas, both whole rocks and glasses, form convex upward trends which are similar to average MORB (Figure 10b). However, the relative depletion in Sr that is characteristic of average MORB does not occur in Mauna Kea or Detroit Seamount lavas.

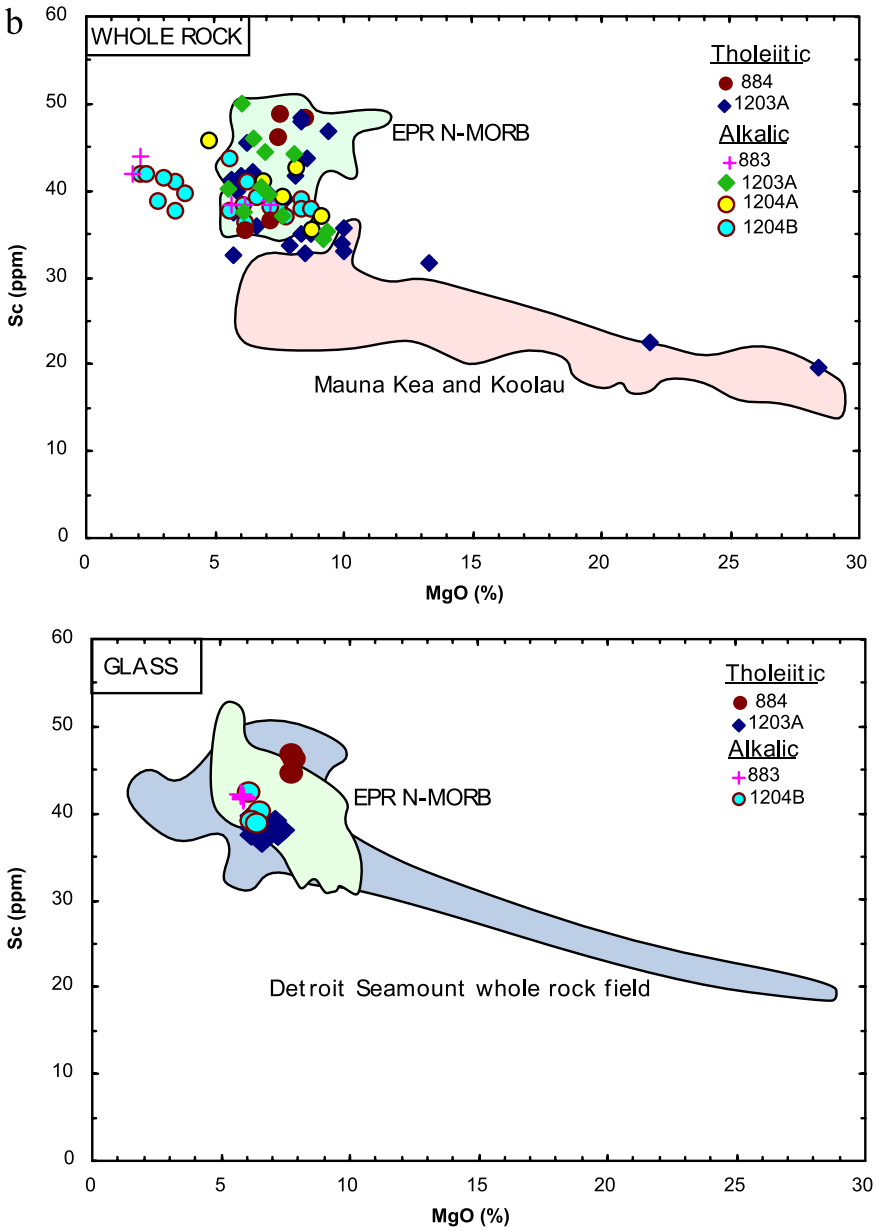

Figure 11. (continued)

5.5. First Series Transition Metals: Ni and Sc

[46] Abundance of Ni is positively correlated with MgO content in the glasses; tholeiitic glasses from Sites 884 and 1203 typically have higher Ni abundance than alkalic glasses from Sites 883 and 1204 (Figure 11a). The highest Ni abundances are in the three olivine-rich whole-rock samples from Units 11 and 16 at Site 1203.

[47] An inverse MgO-Sc trend reflecting olivine control is typical of Hawaiian shield lavas [e.g., *Frey et al.*, 1994; *Huang and Frey*, 2003]. The three MgO-rich samples from Units 11 and 16 at Site 1203 show this trend (Figure 11b). Most importantly, at a given MgO content, the Sc abundance in EPR N-MORB exceeds that of Hawaiian lavas. The majority of Detroit Seamount samples (whole rocks and glasses) have >35 ppm Sc; hence they are within the MORB field (Figure 11b).

5.6. Summary: Incompatible Elements and First Series Transition Metals

[48] The abundance of highly incompatible, relatively immobile elements, such as Nb, La, and Th

are highly correlated in Detroit Seamount lavas. There is, however, a large range from Site 884 tholeiitic basalt which are MORB-like to moderately incompatible element-rich alkalic basalt in the lower part of the Hole 1203A core. For a given lava type, tholeiitic or alkalic, lavas from Detroit Seamount are less enriched in highly incompatible elements than Mauna Kea lavas. In detail, the alkalic lavas from Site 1203 have several characteristics, relative depletion in Ba and Sr and two groups of Ti/Zr and Zr/Hf ratios, which reflect a distinctive petrogenesis. Finally, at a given MgO content, Sc abundances distinguish MORB and Hawaiian tholeiitic basalt. Lavas from Detroit Seamount have relatively high Sc abundance which overlaps with the MORB field.

5.7. Sr-Nd-Pb Isotopic Ratios

[49] Initial Sr-Nd-Pb isotopic ratios in Detroit Seamount lavas are reported in Table 4b. Because of low Rb/Sr ratios in the leached residues, which are plagioclase, pyroxene and olivine, the age correction on $^{87}Sr/^{86}Sr$ in most samples is very small (Tables 4a and 4b). Correction for $^{143}Nd/^{144}Nd$ are significant but the variability is similar for unleached and leached samples (Tables 4a and 4b). In contrast, the scatter of Pb isotopic ratios, especially $^{206}Pb/^{204}Pb$, decreases after age-correction (Tables 4a and 4b).

[50] In a Sr-Nd diagram, Sites 883, 884 and 1204 lavas plot close to the age-corrected EPR MORB field (Figure 12a). Among Detroit Seamount lavas, Site 884 lavas have the highest $^{143}Nd/^{144}Nd$ and lowest $^{87}Sr/^{86}Sr$ ratios, and overlap with the 76 Ma MORB field. In contrast, Site 1203 tholeiitic and alkalic lavas are similar and overlap with the age-corrected Hawaiian rejuvenated stage lava and North Arch lava field which is intermediate between the EPR MORB and Mauna Kea shield fields (Figure 12a).

[51] In Pb isotopic diagrams, Site 883, 1203 and 1204 lavas scatter around the Hawaiian shield field defined by lavas from Mauna Kea and Mauna Loa (Figure 12b). Compared with Site 1203 tholeiitic lavas, Site 1203 alkalic lavas are offset to higher $^{208}Pb/^{204}Pb$ ratio at a given $^{206}Pb/^{204}Pb$ ratio. In detail, Units 23 and 26 lie on an extension of the preshield stage Loihi field, which has higher $^{208}Pb/^{204}Pb$ ratio at a given $^{206}Pb/^{204}Pb$ ratio than the Mauna Kea field; Units 29 and 30 have even higher $^{208}Pb/^{204}Pb$ ratio at a given $^{206}Pb/^{204}Pb$ ratio (Figure 12b). It is important to point out that Sample 1203A 65R4W 9-13 from Unit 29 at Site 1203, which has the highest age-corrected $^{208}Pb/^{204}Pb$ ratio, has been carefully analyzed with two separate analyses for the isotopic ratios and three separate analyses for parent/daughter ratios. These multiple analyses yield similar Pb isotopic ratios and parent/daughter ratios (Table 4a). Compared with Site 1204 lavas, Site 883 lavas are offset to slightly lower $^{207}Pb/^{204}Pb$ ratio at a given $^{206}Pb/^{204}Pb$ ratio.

[52] Site 884 lavas are offset from the Hawaiian shield field to lower $^{207}Pb/^{204}Pb$ and $^{208}Pb/^{204}Pb$ ratios at a given $^{206}Pb/^{204}Pb$ ratio (Figure 12b). Relative to the EPR MORB field defined by data obtained by the triple spike technique, Site 884 lavas clearly have lower $^{207}Pb/^{204}Pb$ and trend to lower $^{206}Pb/^{204}Pb$ and $^{208}Pb/^{204}Pb$. Consequently, *Regelous et al.* [2003] concluded that Site 884 lavas are not similar to EPR MORB or Hawaiian shield stage lavas. However, as indicated in Figure 12b, Detroit Seamount lavas form trends pointing to the field defined by Garrett transform fault lavas, which have low Pb isotopic ratios [*Wendt et al.*, 1999]. The positive trend of Detroit Seamount in a $^{206}Pb/^{204}Pb$ versus $^{87}Sr/^{86}Sr$ diagram is unlike the negative trend defined by Hawaiian shield stage lavas, and it extrapolates toward the field defined by Garrett transform fault lavas (Figure 12c).

[53] In summary, lavas recovered from 4 drill sites are characterized by different age-corrected isotopic ratios. Even in the same drill hole, Hole 1203A, alkalic lavas and tholeiitic lavas have different age-corrected $^{208}Pb/^{204}Pb$ ratios. Compared with modern Hawaiian shields, Detroit Seamount lavas have lower $^{87}Sr/^{86}Sr$ and higher $^{143}Nd/^{144}Nd$ ratios, that range from MORB-like to similar to that in Hawaiian rejuvenated stage lavas and North Arch lavas. Trends of Detroit Seamount lavas in $^{206}Pb/^{204}Pb$ versus $^{208}Pb/^{204}Pb$ and, especially, $^{207}Pb/^{204}Pb$ extend to lower ratios than typical of EPR MORB, but they extend toward the field defined by Garrett transform fault lavas which have $^{206}Pb/^{204}Pb$ less than 18.

6. Discussion

6.1. Role of Crystal Fractionation

[54] Although the isotopic heterogeneity (Figure 12) and compositional changes caused by post-magmatic alteration preclude definition of liquid lines of descent, some geochemical trends provide compelling evidence that olivine and plagioclase fractionation and accumulation were significant processes during the evolution of lavas forming

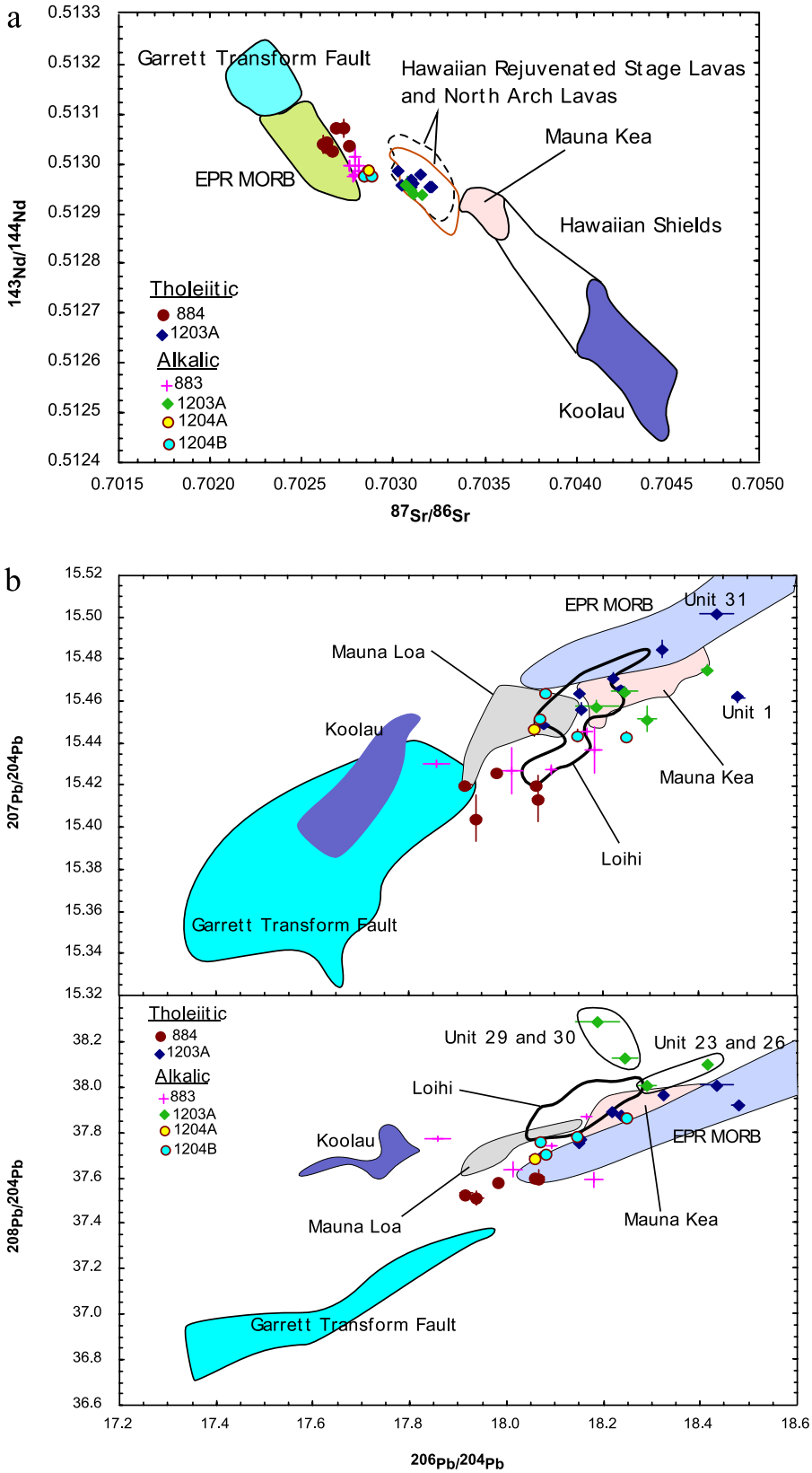
a
Garrett Transform Fault
Hawaiian Rejuvenated Stage Lavas and North Arch Lavas
Mauna Kea
EPR MORB
Hawaiian Shields
Koolau
Tholeiitic
884
1203A
Alkalic
883
1203A
1204A
1204B
143Nd/144Nd
87Sr/86Sr
b
EPR MORB
Unit 31
Mauna Loa
Unit 1
Koolau
Mauna Kea
Loihi
Garrett Transform Fault
Unit 29 and 30
Unit 23 and 26
207Pb/204Pb
208Pb/204Pb
206Pb/204Pb

Figure 12

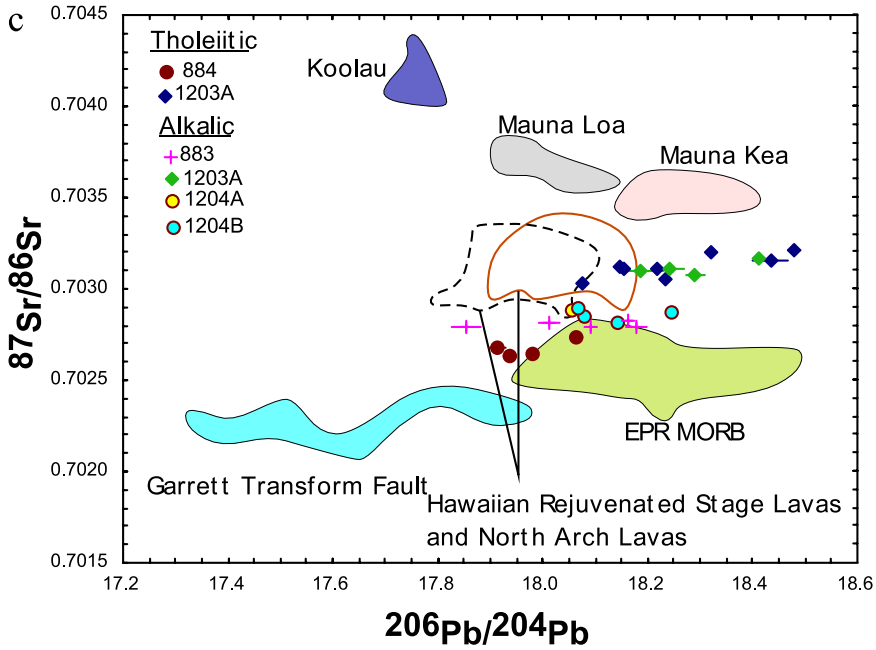

Figure 12. (continued)

Detroit Seamount. For example, olivine fractionation is shown by the MgO-Ni correlation (Figure 11a) and plagioclase fractionation is indicated by the positive MgO-Al_2O_3 correlation for glasses (Figure 8c), the hyperbolic trend of Th-Sr for whole rocks and glasses (Figure 9f) and the positive Eu/Eu*-Sr/Nd correlation (Figure 13). This is a significant result because the compositions of Hawaiian shield lavas are dominantly controlled by olivine fractionation with a relatively minor role for plagioclase and clinopyroxene [e.g., *Huang and Frey*, 2003; *Rhodes and Vollinger*,

Figure 12. (a) Sr-Nd isotopic ratios for Detroit Seamount lavas. (b) Pb-Pb isotopic ratios for Detroit Seamount lavas. (c) Values of $^{206}Pb/^{204}Pb$ versus $^{87}Sr/^{86}Sr$ for Detroit Seamount lavas. For comparison, fields are shown for EPR MORB, Garrett transform fault lavas, two extreme Hawaiian shields (Mauna Kea and Koolau), and Hawaiian rejuvenated stage lavas. All data points and fields have been age-corrected to 76 Ma, except for Site 884 lavas, which have been age-corrected to 81 Ma. A 2-sigma error bar is indicated unless the symbol is larger than the error bar. For the relatively young Hawaiian shield stage lavas and EPR MORB, parent/daughter ratios for age corrections should be those of the magma source. As a crude estimate of these ratios for tholeiitic basalt, we use average parent/daughter ratios in unaltered lavas (see Table 6). For the Sr and Pb isotopic systems this approach leads to overestimates for the age correction, and for the Nd isotopic system the age corrections are underestimates. Parent/daughter ratios in Koolau and Mauna Kea lavas are average values of relatively unaltered samples ($K_2O/P_2O_5 > 1.3$) from *Frey et al.* [1994] and *Huang and Frey* [2003]. Parent/daughter ratios in Mauna Loa are average values of relatively unaltered samples ($K_2O/P_2O_5 > 1.3$) from *Hofmann and Jochum* [1996]. Parent/daughter ratios in EPR-MORB are average N-MORB values from *Sun and McDonough* [1989]. Parent/daughter ratios in Garrett transform fault lavas are average values of lavas with $^{206}Pb/^{204}Pb < 18$ [*Wendt et al.*, 1999]. Because rejuvenated stage and North Arch alkalic basalt were formed by low extents of melting [e.g., *Yang et al.*, 2003], which may lead to significant changes in parent/daughter ratios, we used two sets of parent/daughter ratios for Hawaiian Rejuvenated Stage lavas: N-MORB values for the orange solid line and Mauna Kea values for the black dashed line. Our selection of U/Pb and Th/Pb ratios in EPR MORB results in $^{238}U/^{204}Pb$ and $^{232}Th/^{204}Pb$ values of 10 and 26, respectively, which are about 2 times the values used by *Regelous et al.* [2003]. Data sources: Koolau: *Roden et al.* [1994], *Lassiter and Hauri* [1998]; Mauna Kea: J. G. Bryce et al. (Sr, Nd, and Os isotopes in a 2.84 km section of Mauna Kea Volcano: Implications for the geochemical structure of the Hawaiian plume, submitted to *Geochemistry, Geophysics, Geosystems*, 2004; hereinafter referred to as Bryce et al., submitted manuscript, 2004), *Lassiter et al.* [1996], *Abouchami et al.* [2000], *Eisele et al.* [2003]; Mauna Loa: *Abouchami et al.* [2000]; Loihi: *Garcia et al.* [1993, 1995, 1998], *Norman and Garcia* [1999]; EPR MORB: *Niu et al.* [1999], *Regelous et al.* [1999], *Castillo et al.* [2000]; Hawaiian rejuvenated stage and North Arch lavas: *Stille et al.* [1983], *Roden et al.* [1984], *Tatsumoto et al.* [1987], *Chen and Frey* [1985], *Lassiter et al.* [2000], *Frey et al.* [2000]; Garrett transform fault lavas: *Wendt et al.* [1999]; Site 883 and 884 lavas: *Keller et al.* [2000], *Regelous et al.* [2003]. EPR MORB fields in Pb-Pb plots are taken from *Regelous et al.* [2003].

Table 6. Parent/Daughter Ratios Used to Calculate Initial Ratios for Fields in Figure 12

	Koolau	Mauna Kea	Mauna Loa	Loihi	EPR-MORB	GTF[a]
Rb/Sr	0.015	0.021	–	–	0.0062	0.0040
Sm/Nd	0.26	0.27	–	–	0.36	0.39
Th/Pb	0.52	0.97	0.55	0.80	0.40	0.22
U/Pb	0.15	0.31	0.17	0.27	0.16	0.15

[a] GTF, Garrett transform fault lavas.

2004]. In contrast, like Detroit Seamount lavas, MORB compositions are typically controlled by plagioclase and olivine [e.g., *Langmuir et al.*, 1992].

6.2. Significance of Alkalic Basalt Deep in the Hole 1203A Core

6.2.1. Preshield or Postshield Stage Alkalic Lavas?

[55] In Hole 1203A, there is an upward change from intercalated alkalic and tholeiitic basalt to solely tholeiitic basalt (Figure 2). Specifically, four thick, ranging from 8 to 63 m, subaerially erupted compound pahoehoe alkalic flow units underlie a ~300 m thick sequence of submarine erupted tholeiitic lava flows interbedded with volcaniclastic rocks. Although this alkalic to tholeiitic transition is expected in the preshield to shield transition at a single volcano, it could also reflect interfingering of lavas from two adjacent volcanoes at different growth stages. For example, shield stage tholeiitic lavas from Mauna Loa volcano overlie late-shield to postshield stage alkalic lavas from Mauna Kea volcano in the drill cores recovered by the Hawaii Scientific Drilling Project (HSDP) [*Rhodes*, 1996; *Rhodes and Vollinger*, 2004]. Did alkalic and tholeiitic lavas at Site 1203 erupt from the same volcano? Although there are erosional contacts between some units, such as Units 5 and 6, Units 23 and 24, Units 27 and 28, we cannot confidently use the contact relations in the non-continuous core

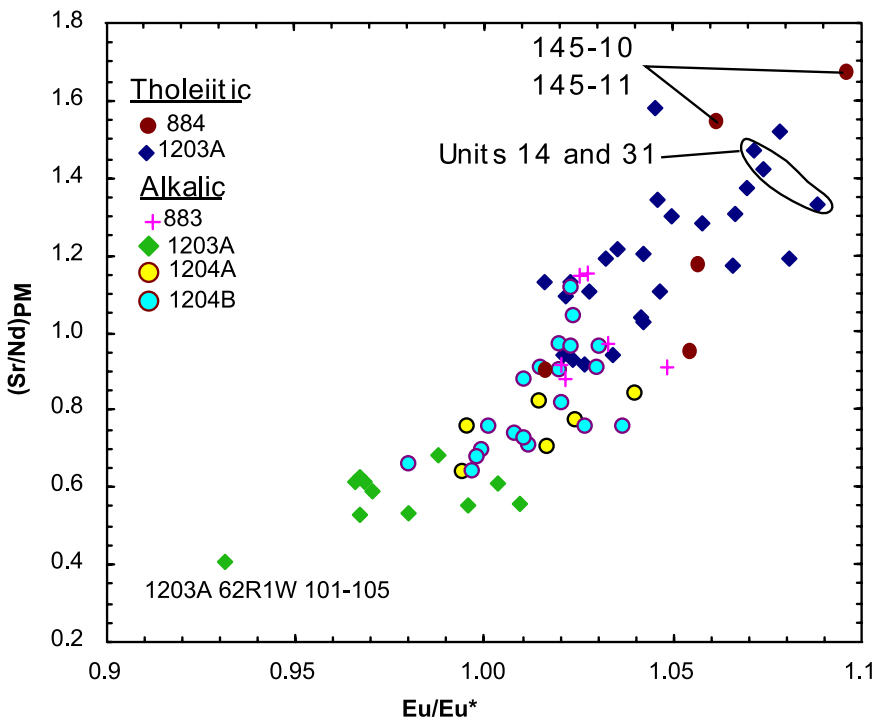

Figure 13. $(Sr/Nd)_{PM}$ versus Eu/Eu* for Detroit Seamount lavas (whole rocks). Eu/Eu* = $2*[Eu]_{PM}/([Gd]_{PM} + [Sm]_{PM})$. Subscript PM indicates normalization to primitive mantle values from *Sun and McDonough* [1989]. These ratios are sensitive to plagioclase fractionation, and the range from >1 to <1 indicates accumulation and loss of plagioclase, respectively. Because Gd abundances for glasses are not reported, glasses are not included. The labeled units with high $(Sr/Nd)_{PM}$ also have anomalously high Al_2O_3 (Figure 8c).

Table 7. Partition Coefficients of Selected Elements Between Phlogopite and Melt

											K_2O, %	
Reference	Melt Type	Ba	Th	Zr	Hf	Ti	Sr	La	Ce	Y	In Melt	In Phlogopite
Villemant et al. [1981]	trachyte	10.0		2.5	1.8		0.7					
Adam et al. [1993]	basanite	2.9		0.13			0.22			<1	2.74	7.28
LaTourrette et al. [1995]	basanite	3.68	0.0014	0.017	0.19	1.768	0.159	0.028		0.018	2.15	7.91
Foley et al. [1996]	alkaline lamprophyre	3.48	0.0145	0.023			0.183		0.0078	0.007	2.5	8.87
Schmidt et al. [1999]	lamproite	1.03	0.00002	0.012		0.87	0.038		0.00002		8.7	9.9
	lamproite	1.61	0.000005	0.017		0.92	0.058		0.00002		9	9.8
	lamproite	0.56	0.0002	0.009		0.827	0.016		0.0002		8.6	9.7
Green et al. [2000]	basanite	3.34		0.008	0.09	0.7	0.21	0.007		0.018	2.15	9.16

containing numerous volcaniclastic units to determine if there is a regional uncomformity between the alkalic and overlying tholeiitic lavas. Therefore we evaluate isotopic differences between these units. The tholeiitic lavas from Mauna Loa in the HSDP core are clearly isotopically distinct from the underlying alkalic to transitional Mauna Kea lavas [e.g., *Lassiter et al.*, 1996, Figure 6]. Therefore the similar age-corrected $^{87}Sr/^{86}Sr$ and $^{143}Nd/^{144}Nd$ ratios of the Site 1203 alkalic and tholeiitic lavas (Figure 12a) are evidence against the hypothesis of interfingering between two adjacent volcanoes at different growth stages. We cannot preclude the possibility that lavas from two adjacent volcanoes were similar in Sr and Nd isotopic ratios (e.g., Kilauea and Mauna Kea in Figure 6 of *Lassiter et al.* [1996]), but the subtle isotopic differences between alkalic and tholeiitic lavas at Site 1203 (Figures 12a and 12b) are typical of isotopic differences found in lavas from a single volcano (e.g., *Lassiter et al.* [1996] and *Blichert-Toft et al.* [2003] for Mauna Kea). Particularly interesting, these alkalic lavas have high $^{208}Pb/^{204}Pb$ at a given $^{206}Pb/^{204}Pb$ (Figure 12b), which is a distinct characteristic of preshield stage Loihi lavas [e.g., *Garcia et al.*, 1993, 1995].

[56] Could these alkalic lava flows represent preshield stage lavas of Detroit Seamount? There are two examples of preshield stage lavas among Hawaiian volcanoes: Loihi Seamount and the submarine part of Kilauea volcano [*Garcia et al.*, 1993, 1995; *Lipman et al.*, 2002; *Sisson et al.*, 2002]. In contrast to these submarine eruptives, the four alkalic flow units at Hole 1203A are subaerially erupted compound pahoehoe lavas. However, modern Hawaiian volcanoes are built on Cretaceous oceanic crust with a water depth of ~4 km; in contrast, the near-ridge setting of Detroit Seamount at ~80 Ma indicates that the seamount initiated in a shallow water depth environment. This inference is consistent with the inferred eruption environment of Site 1203 lavas (Figure 3). Since the maximum thickness of Loihi Seamount is ~3.5 km, and the alkalic to tholeiitic transition occurs within the top several hundred meters [*Garcia et al.*, 1995], it is possible that the preshield stage includes 2–3 km of alkalic basalt. The average water depth of zero age oceanic crust is less than 3 km in both North Pacific and North Atlantic oceans [e.g., *Parsons and Sclater*, 1977; *Stein and Stein*, 1992]. Therefore, if Detroit Seamount grew rapidly relative to subsidence of the young oceanic lithosphere, it is possible that its preshield stage included a subaerial growth stage. However, as discussed earlier, the upward transition from subaerial to submarine eruptives at Hole 1203A requires a subsequent decrease in accumulation rate relative to subsidence rate as the volcano aged.

6.2.2. Petrogenesis of Alkalic Lavas at Site 1203

[57] The four alkalic units form two compositional groups whose differences provide keys to understanding their petrogenesis. Specifically, relative to lavas from Units 29 and 30, lavas from Units 23 and 26 have lower K_2O and Rb abundances (Figures 6a and 6b), lower Ba/Th, Ti/Zr and higher Zr/Hf ratio (Table 5). Common phenocryst phases, such as plagioclase and olivine, do not affect these ratios, but phlogopite, a mineral that fractionates Ba/Th, Ti/Zr and Zr/Hf (Table 7), occurs in preshield stage alkalic Kilauea lavas [*Sisson et al.*, 2002]. For these Site 1203 alkalic lavas, a difficulty with inferring a petrogenetic role for phlogopite as a residual or fractionating mineral is that phlogopite is not a phenocryst phase, presumably because of the low K_2O contents (<1.8%) (Table 3a). Melts saturated with phlogopite typically have more than 2% K_2O (Table 7); however, *Mengel and Green* [1986] infer that only 1.6% K_2O is required to

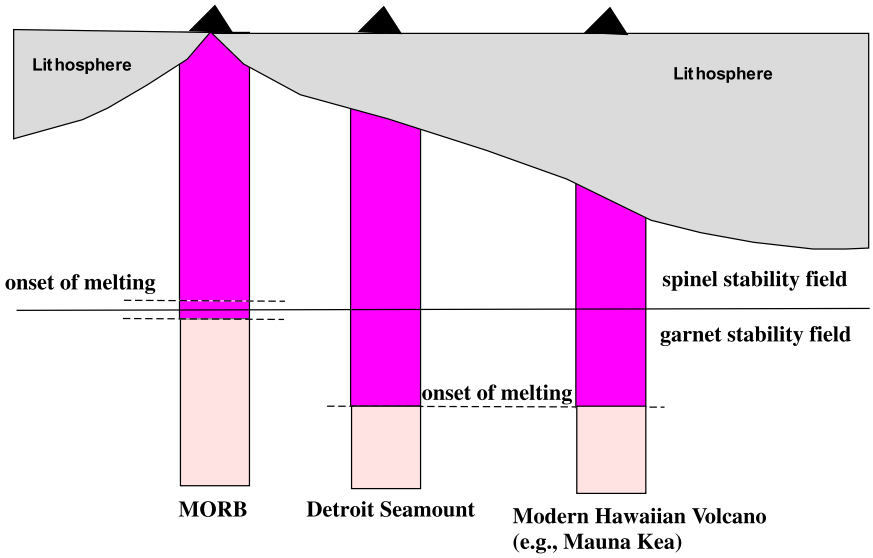

Figure 14. Schematic diagram showing melting column length for EPR MORB, Detroit Seamount, and Mauna Kea, i.e., the depth interval from onset of melting to the lithosphere. The mean pressure of melt segregation increases from MORB to Detroit Seamount lavas to Mauna Kea lavas.

saturate a SiO_2-undersaturated nephelinite with phlogopite. The K_2O content in Units 29 and 30 ranges from ~1.5 to 1.8%, but is less than 1% in Units 23 and 26 (Figure 6a; Table 3a). As discussed in section 5.2, the low K_2O content in Units 23 and 26 reflects K_2O loss during alteration. If we assume that K_2O contents of Units 29 and 30 reflect magmatic ratios (K_2O/P_2O_5 = 2.3–2.9, with K_2O = 1.5–1.8%), it is possible that phlogopite was a residual phase during partial melting. Although phlogopite may not be stable during the high temperature melting typically inferred for a plume environment [*Class and Goldstein*, 1997; *Sisson et al.*, 2002], the presence of fluorine increases the thermal stability of phlogopite [e.g., *Foley et al.*, 1986].

[58] A specific scenario was postulated by *Sisson et al.* [2002] to explain the generation of submarine nephelinite to basanite lavas at Kilauea Volcano. They suggested that these alkalic lavas formed by low degree melting of phlogopite-bearing garnet pyroxenite cumulates formed during high pressure solidification of plume-derived magmas. If these melts bearing a residual phlogopite signature, i.e., relatively low Ti/Zr and Ba/Th and high Zr/Hf, interact with peridotite or mix with a peridotite-derived melt, their high K_2O content would be diminished. Hence they would no longer be phlogopite-saturated, but they could retain the trace element signature of residual phlogopite. This hypothesis is consistent with the geochemical data for the alkalic lavas from Site 1203.

6.3. Melt Segregation Pressure of Detroit Seamount Lavas

[59] On the basis of plate reconstruction, *Mammerickx and Sharman* [1988] and *Lonsdale* [1988] suggested that Detroit Seamount was built on a relatively young and thin lithosphere (Figure 1a). The paleolatitude [*Tarduno et al.*, 2003] and the oceanic paleodepth of Detroit Seamount [*Caplan-Auerbach et al.*, 2000] are consistent with this inference. Therefore during formation of Detroit Seamount decompression melting is likely to have continued to a shallower depth and the mean pressure of melt segregation was lower than that during formation of modern Hawaiian volcanoes which are constructed on thick (~100–110 km [*Li et al.*, 2004]) Cretaceous oceanic lithosphere (Figure 14). Are the compositional data for Detroit Seamount lavas consistent with this interpretation? If the mean pressure of melt segregation increases from MORB to Detroit Seamount lavas to Mauna Kea lavas (Figure 14), these lava groups should show systematic differences in compositional parameters sensitive to pressure.

6.3.1. SiO_2 and Total Iron

[60] The SiO_2 and FeO contents of partial melts of peridotite are a function of melt segre-

gation pressure and extent of melting [e.g., *Walter*, 1998; *Stolper et al.*, 2004, Figure 13]. *Regelous et al.* [2003] noted that compared to young Emperor Seamounts, whole-rock tholeiitic basalt compositions from Detroit Seamount are offset to lower total iron at a given MgO content; consequently, they inferred that melt segregation at Detroit Seamount occurred at relatively low pressure beneath thin lithosphere. Consistent with this inference, whole-rock FeO and SiO_2 contents for tholeiitic basalt from Detroit Seamount overlap with MORB field, but inexplicably, the SiO_2 content of the associated glasses do not (Figures 8a and 8b).

[61] There is also evidence that the depth of melt segregation changes during growth of a Hawaiian volcano. Compared with tholeiitic shield stage lavas from Mauna Kea, postshield stage alkalic lavas from Mauna Kea have higher total iron content but lower SiO_2 content (Figures 8a and 8b). This result was used to infer that these alkalic lavas were generated by lower extent of partial melting at higher pressure [e.g., *Yang et al.*, 1996]. Similarly, at Detroit Seamount, the alkalic lavas have higher FeO* and lower SiO_2 contents than tholeiitic lavas (Figures 8a and 8b). Hence we infer that compared with tholeiitic lavas from Detroit Seamount, the alkalic lavas were generated by a lower degree of melting at higher pressure.

6.3.2. Sc

[62] Sc is compatible in garnet and clinopyroxene [e.g., *Irving and Frey*, 1978; *Hart and Dunn*, 1993; *Blundy et al.*, 1995, 1998; *van Westrenen et al.*, 1999]. Hawaiian lavas have lower Sc abundance than MORB at a given MgO content [*Frey et al.*, 1994] (Figure 11b). If the source of Hawaiian lavas has a Sc abundance similar to the source of MORB, the lower Sc abundances in Hawaiian shield lavas can be explained as a result of more residual garnet [*Frey et al.*, 1994]. At a certain MgO content, Detroit Seamount lavas have higher Sc abundance than Mauna Kea and Koolau lavas (Figure 11b), which implies less residual garnet for Detroit Seamount lavas. This result is consistent with the hypothesis that Detroit Seamount lavas segregated at lower mean pressure than Hawaiian shield stage lavas.

[63] The similar Sc abundance of alkalic and tholeiitic basalt (Figure 11b) from Detroit Seamount is inconsistent with the inferred higher pressure of melt segregation for the alkalic basalt based on SiO_2 and total iron contents. However, Sc is an incompatible element during melting of peridotite; therefore the unexpectedly high Sc abundance of the alkalic basalt may reflect the combination of a lower extent of melting and higher pressure of melt segregation. In fact, alkalic and tholeiitic basalt from Mauna Kea Volcano also have similar Sc abundances [see *Huang and Frey*, 2003, Figure 5e].

6.3.3. Na_2O/TiO_2 and Tb/Yb

[64] During mantle melting, the partition coefficient of sodium (as Na_2O) between clinopyroxene and melt increases with increasing pressure [e.g., *Kinzler*, 1997; *Putirka*, 1999; *Longhi*, 2002]; that is, the proportion of jadeite component in clinopyroxene increases with increasing pressure. In contrast, the partition coefficient of titanium (as TiO_2) is not strongly dependent on pressure; it may decrease slightly with increasing pressure [e.g., *Longhi*, 2002]. Therefore the Na_2O/TiO_2 ratio yields information on the pressure of melt segregation with relatively lower Na_2O/TiO_2 ratio indicating higher mean pressure of melt segregation [e.g., *Putirka*, 1999, Figure 5]. The ratio of Tb/Yb in a melt can also be used as an indicator for pressure of melt segregation because $(D_{Tb}/D_{Yb})^{garnet/melt} \ll (D_{Tb}/D_{Yb})^{clinopyroxene/melt}$ [e.g., *van Westrenen et al.*, 1999]. Hence a higher proportion of residual garnet results in higher Tb/Yb ratio due to the compatibility of Yb in garnet.

[65] Compared with EPR N-MORB, Mauna Kea lavas have lower Na_2O/TiO_2 but higher Tb/Yb ratios at a certain MgO content (Figure 15). These differences in Na_2O/TiO_2 and Tb/Yb ratios show that relative to EPR N-MORB, Mauna Kea lavas segregated at a higher pressure, although source heterogeneity in these ratios may also contribute to this difference. As indicated in Figure 15, Na_2O/TiO_2 decreases and Tb/Yb increases from Site 884 tholeiitic lavas to Site 1203 tholeiitic lavas and Site 883 and 1204 alkalic lavas to Site 1203 alkalic lavas. Site 884 lavas are distinct and overlap with the low pressure end of the EPR N-MORB field. All other Detroit Seamount lavas overlap with the low Na_2O/TiO_2 and high Tb/Yb (relatively high pressure) end of the MORB field. This observation is consistent with the hypothesis that the mean pressure of melt segregation decreases from Mauna Kea lavas to Detroit Seamount

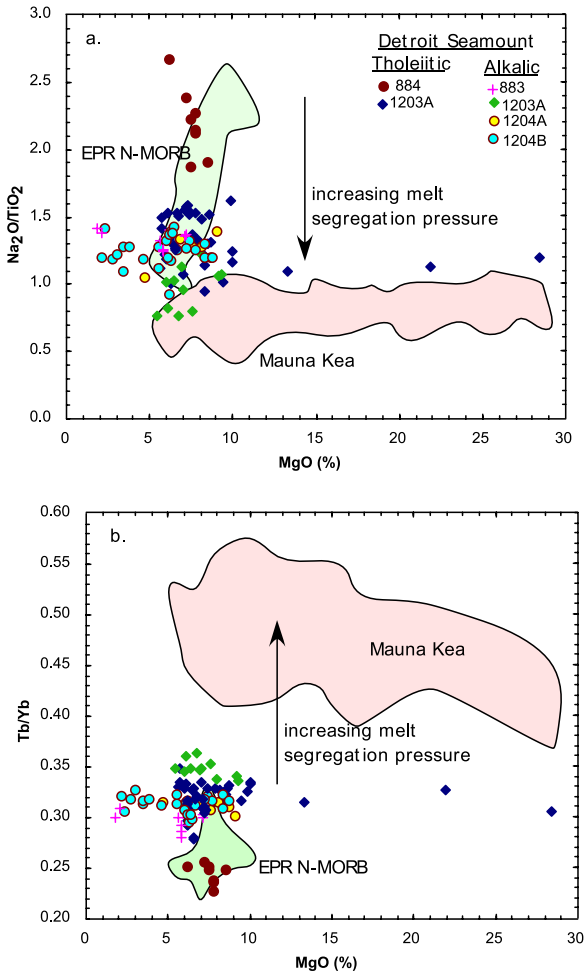

Figure 15. (a) MgO versus Na_2O/TiO_2 and (b) Tb/Yb. Both whole-rock and glass data from Detroit Seamount are plotted. See the Figures 8a–8d and 10 captions for data sources.

lavas to MORB. The lower Na_2O/TiO_2 and higher Tb/Yb ratios in Site 1203 alkalic lavas relative to Site 1203 tholeiitic lavas indicate that the former segregated at higher pressure.

6.3.4. Summary

[66] In summary, compositional indicators of mean pressure of melt segregation, such as Sc abundance and ratios of Na_2O/TiO_2 and Tb/Yb, show that tholeiitic lavas from Detroit Seamount are more similar to MORB than young Hawaiian shield lavas. This similarity to MORB is inferred to reflect segregation of Detroit Seamount lavas at low pressure beneath thin lithosphere. The extremes are expressed in Site 884 lavas (lowest pressure) and Site 1203 alkalic lavas (highest pressure).

6.4. Did Detroit Seamount Lavas Sample a Depleted MORB-Related Component or a Depleted Plume Component?

6.4.1. Controversy About the Origin of Detroit Seamount Lavas

[67] Studies of lavas recovered from Sites 883 and 884 during ODP Leg 145 have led to two different interpretations for the depleted component found in Detroit Seamount lavas. *Keller et al.* [2000] used age-corrected Sr-Nd-Pb isotopic ratios in Detroit Seamount lavas, especially Site 884 lavas, to conclude that lavas forming Detroit Seamount are "indistinguishable from mid-ocean ridge basalt". Hence they proposed that the Hawaiian plume interacted with young and hot lithosphere and "entrained enough of the isotopically depleted upper mantle to overwhelm the chemical characteristics of the plume itself". In contrast, using a high precision triple spike technique, *Regelous et al.* [2003] argued that the Pb isotopic compositions of Site 884 lavas are not similar to either EPR MORB or modern Hawaiian shield stage lavas [*Regelous et al.*, 2003, Figure 6] (Figure 12b). They argued that the Site 884 lavas were derived from a depleted plume component that is not sampled by modern Hawaiian volcanoes. On the basis of Nd-Hf isotopic correlation, *Kempton et al.* [2002], *Thompson et al.* [2002], and *Frey et al.* [2005] also suggest that Detroit Seamount lavas sampled a depleted plume component. With additional data for lavas from Detroit Seamount, our objective is to evaluate these alternative hypotheses.

6.4.2. Constraints From Sr-Nd Isotopes

[68] Age-corrected Sr and Nd isotopic ratios of basalt from 3 of the 4 drill sites on Detroit Seamount (Sites 883, 884 and 1204) overlap with the field calculated for 76 Ma EPR MORB (Figure 12a). A new observation is that both tholeiitic (Site 884) and alkalic basalt (Sites 883 and 1204) overlap with the MORB field, but alkalic basalt has slightly higher $^{87}Sr/^{86}Sr$ and lower $^{143}Nd/^{144}Nd$ than tholeiitic basalt. The simplest interpretation is that a depleted MORB-like component, perhaps slightly heterogeneous in $^{87}Sr/^{86}Sr$ and $^{143}Nd/^{144}Nd$, was melted to various extents to form Detroit Seamount lavas.

6.4.3. Constraints From Pb Isotopes

[69] In plots of Pb isotopic ratios, our new data for Sites 1203 and 1204 basalt confirm the observation

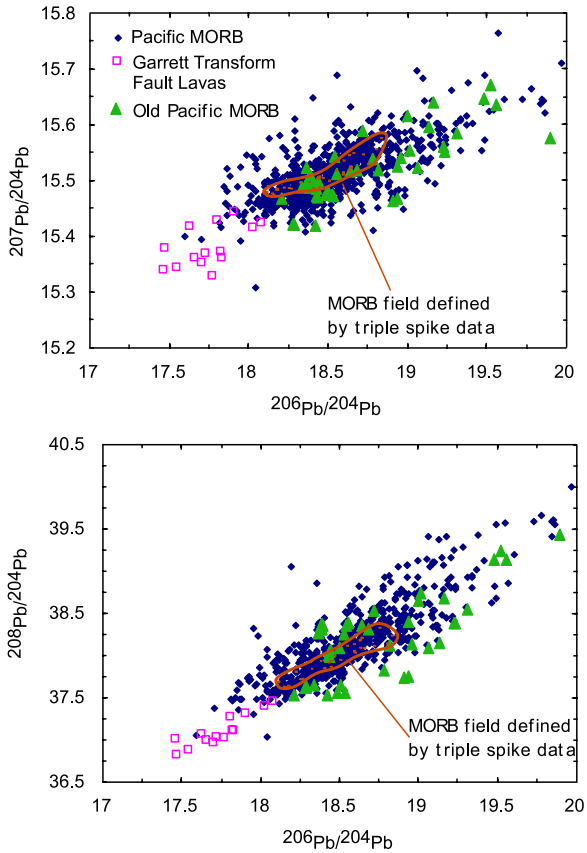

Figure 16. Pb isotopic plots for Pacific MORB. Data are downloaded from PeT DB. The red field with dots is the EPR MORB field defined by data obtained using the triple-spike technique [*Galer et al.*, 1999]. The low $^{206}Pb/^{204}Pb$ (<18) end of the Pacific MORB field is defined by Garrett transform fault lavas [*Wendt et al.*, 1999]. Pacific MORB with $^{206}Pb/^{204}Pb$< 18 are also reported by *Barrett* [1983], *White et al.* [1987], *Fornari et al.* [1988], *Hanan and Schilling* [1989], *Castillo et al.* [1998], *Sturm et al.* [1999], and *Haase* [2002]. Old Pacific MORB are shown for comparison, and they do not differ from young Pacific MORB. Data sources: *Bass et al.* [1973], *Hickey-Vargas* [1991], *Castillo et al.* [1991, 1992, 1994], and *Janney and Castillo* [1997].

by *Regelous et al.* [2003] that for a given $^{206}Pb/^{204}Pb$ ratio, most lavas from Detroit Seamount have lower $^{207}Pb/^{204}Pb$ ratios than EPR MORB data obtained using the triple-spike technique (Figure 12b). *Regelous et al.* [2003] noted that measured $^{207}Pb/^{204}Pb$ in Site 884 lavas, ranging from 15.43 to 15.46, are lower than data for most EPR MORB. Consequently, the difference in $^{207}Pb/^{204}Pb$ between Site 884 lavas and EPR MORB is not a result of an inaccurate age-correction. In addition, as emphasized by *Regelous et al.* [2003] the $^{206}Pb/^{204}Pb$ for lavas from Site 883 and 884 extend to considerably lower ratios (<18) than the EPR MORB field defined by data obtained using the triple-spike technique.

[70] Is the field defined by triple-spike data representative of young Pacific MORB? In order to answer this question, we used the Web database Pet DB (http://www.petdb.org/index.jsp). Three important results arise from assessing Pb isotopic ratios for the 996 samples (Figure 16). (1) The EPR MORB field defined by data obtained by the triple-spike technique is representative of the Pacific MORB database, but it does not include the extremes. (2) Although the database for old Pacific MORB (distant from active spreading centers) is sparse, Pb isotopic ratios of such lavas are similar to young Pacific MORB (Figure 16). (3) Pacific MORB with $^{206}Pb/^{204}Pb$ < 18 are very unusual. The majority of Pacific MORB with low $^{206}Pb/^{204}Pb$ (<18) erupted at a spreading center in the Garrett transform fault (Figure 16). *Wendt et al.* [1999] proposed that Garrett transform fault lavas reflect two-stage melting of a MORB source; i.e., initial melting at the EPR axis followed by melting of the residue to generate the incompatible element-depleted Garrett transform fault lavas. Therefore, if the low $^{206}Pb/^{204}Pb$ (<18) component in Detroit Seamount lavas is a MORB-related component, as suggested by *Keller et al.* [2000], it is not typical Pacific MORB. Sampling of this atypical component may occur only at high extents of melting, such as achieved in the two-stage melting scenario proposed for lavas erupted in the Garrett transform fault [*Wendt et al.*, 1999], and when the Hawaiian plume was near a ridge axis, such as Detroit Seamount at ~80 Ma [*Keller et al.*, 2000].

6.4.4. Constraints From Incompatible Element Abundance Ratios

[71] In both MORB and Hawaiian tholeiitic basalt many incompatible trace element ratios are correlated with radiogenic isotopic ratios [e.g., *Niu et al.*, 2002; *Huang and Frey*, 2003]. Among Hawaiian shield lavas, La/Nb is positively correlated with $^{87}Sr/^{86}Sr$ and negatively correlated with $^{143}Nd/^{144}Nd$; Detroit Seamount tholeiites, like EPR MORB, define opposite correlations (Figures 17a and 17b). Obviously, Detroit Seamount lavas sampled a depleted, low $^{87}Sr/^{86}Sr$, $^{206}Pb/^{204}Pb$ and high $^{143}Nd/^{144}Nd$, La/Nb component that was not sampled by Hawaiian shield stage lavas. Is this depleted component similar to that sampled by Garrett transform fault lavas (Figure 17), as argued on the basis of isotope compositions?

[72] As discussed earlier, tholeiitic basalt from Site 884 has MORB-like incompatible element patterns (Figure 10). There is, however, an important difference between Site 884 lavas and MORB. Relative to MORB, Hawaiian lavas have high Ba/Th (>100) [*Hofmann and Jochum*, 1996; *Huang and Frey*, 2003; *Yang et al.*, 2003]; such ratios are interpreted as characteristic of recycled oceanic lithosphere in the Hawaiian plume [*Hofmann and Jochum*, 1996; *Huang et al.*, 2000; *Sobolev et al.*, 2000]. High Ba/Th ratios are also characteristic of Detroit Seamount glasses, and Site 884 glasses are at the high end of the Ba/Th range in Detroit Seamount lavas (85-113) (Figure 17c). In contrast, Garrett transform fault lavas have low Ba/Th (35-57) which overlap with those of N-MORB [*Wendt et al.*, 1999] (Figure 17c). We therefore speculate that the depleted component sampled by Site 884 lavas has high Ba/Th (>100), and is unrelated to the low $^{87}Sr/^{86}Sr$ and $^{206}Pb/^{204}Pb$ source of Garrett transform fault lavas. Rather, it is an intrinsic component of the plume.

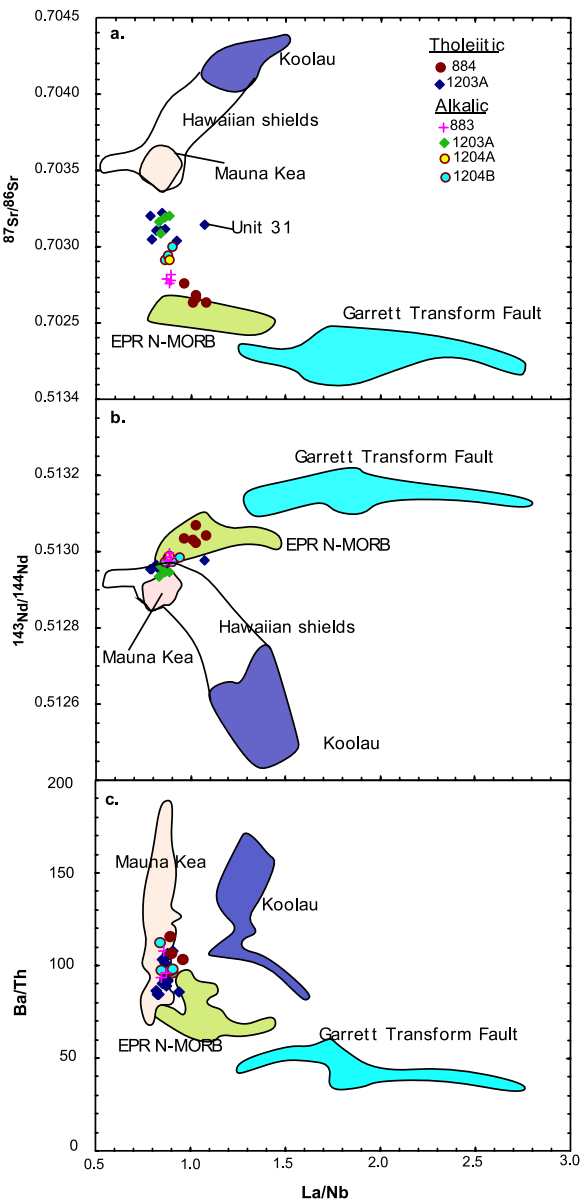

Figure 17. (a and b) La/Nb versus $^{87}Sr/^{86}Sr$ and $^{143}Nd/^{144}Nd$ for Detroit Seamount lavas (whole rocks). Unit 31, a plagioclase-rich unit (Table 2a), at Site 1203 has a high La/Nb ratio, which has been confirmed by three ICP-MS analyses (1.06, 1.07, and 1.10). Note that Hawaiian shield lavas and Detroit Seamount lavas define opposing slopes in the Sr and Nd panels. (c) La/Nb versus Ba/Th for Detroit Seamount glasses. Only Detroit Seamount glass data are plotted to avoid the alteration effect on whole-rock Ba data. The important point is that in this panel, Site 884 data do not overlap with the EPR MORB field. Data sources: Koolau: *Frey et al.* [1994], *Roden et al.* [1994], *Lassiter and Hauri* [1998], S. Huang and F. A. Frey (Temporal geochemical variation within the Koolau shield: A trace element perspective, submitted to *Contributions to Mineralogy and Petrology*, 2004); Mauna Kea: Bryce et al. (submitted manuscript, 2004), *Eisele et al.* [2003], *Huang and Frey* [2003]; Garrett transform fault: *Wendt et al.* [1999]; EPR N-MORB: *Niu et al.* [1999], *Regelous et al.* [1999]. The fields for Hawaiian shields are from *Huang and Frey* [2003].

[73] Young Hawaiian rejuvenated stage lavas also contain a component with low $^{87}Sr/^{86}Sr$, $^{206}Pb/^{204}Pb$ and high $^{143}Nd/^{144}Nd$ and Ba/Th. Such lavas have relatively high incompatible trace element concentrations, and are thought to represent small degrees of melting of plume mantle mixed with melts of a depleted source [e.g., *Yang et al.*, 2003]. *Frey et al.* [2005] argue that the low $^{87}Sr/^{86}Sr$ component in these lavas is the same as that present in Detroit lavas, i.e. it is intrinsic to the plume, and is sampled during a later stage of melting of the Hawaiian plume that previously melted to produce the tholeiitic shields. If this interpretation is correct, it implies that the depleted component has been an integral part of the Hawaiian plume for at least 80 Ma.

6.4.5. Summary

[74] 1. We agree with *Regelous et al.* [2003] that the Pb isotopic data, especially $^{206}Pb/^{204}Pb$ (<18), for Detroit Seamount lavas reflect a depleted component that is not commonly present in either ancient or recent Pacific MORB. Such a component is present in lavas erupted from a spreading center in the Garrett transform fault. Therefore if

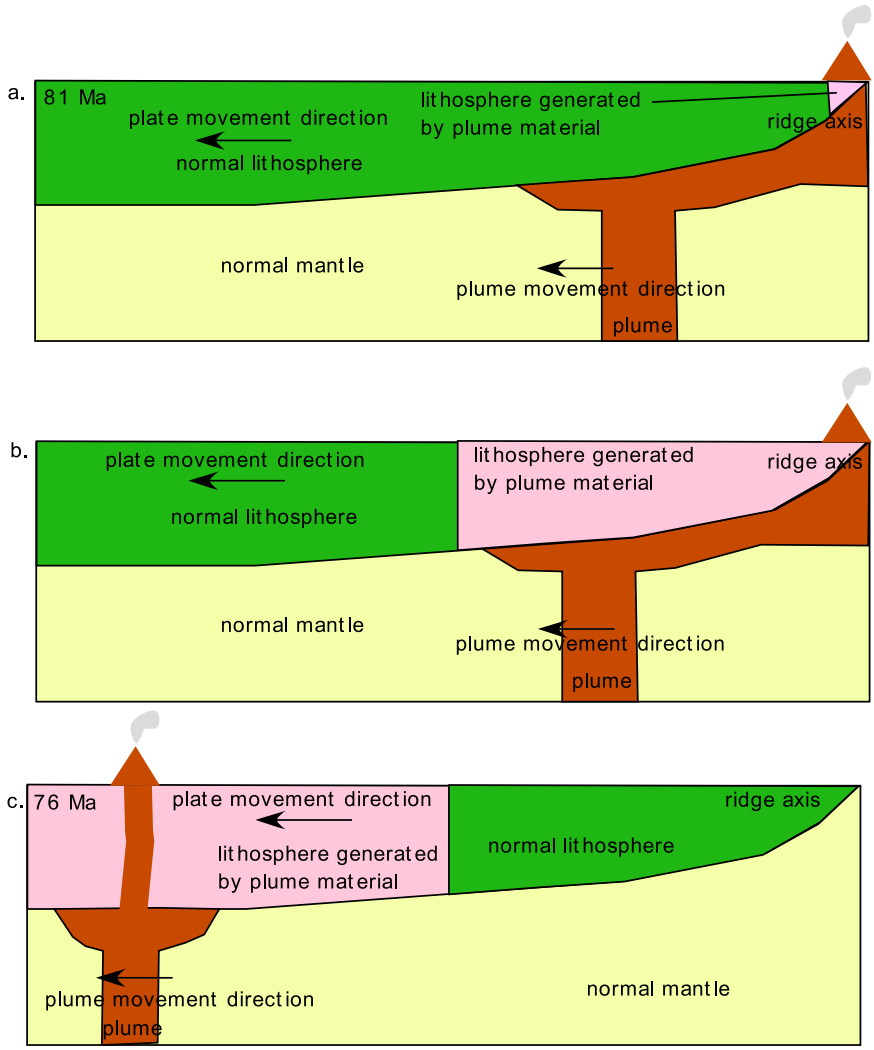

Figure 18. Plume-ridge interactions (adapted from *Sleep* [2002]). Figure 18a shows that when a plume is near a ridge axis, the plume material flows toward the ridge axis, where it melts upon ascent. This scenario may be appropriate for 81 Ma lavas at Site 884. Figure 18b shows the situation where the plume and the lithospheric plate are moving in the same direction, but the plate is migrating faster than the plume. In this case, Figure 18c shows that eventually plume-related magmas and lithosphere created at the ridge axis (Figure 18a) may override the plume and young (76 Ma lavas at Site 1203) lavas may erupt in proximity to old (81 Ma) lavas.

the depleted component arises from a MORB source, it is only sampled under unusual conditions such as the two-stage melting proposed for Garrett transform fault lavas [*Wendt et al.*, 1999] or the proximity of the Hawaiian plume to a ridge axis (Detroit Seamount).

[75] 2. The occurrence at Sites 883 and 1204 of alkalic lavas that have depleted isotopic characteristics shows that the depleted component is not restricted to tholeiitic basalt. In the context of the *Regelous et al.* [2003] hypothesis the depleted plume component with a high solidus temperature was melted to varying extents.

[76] 3. High Ba/Th is a characteristic feature of Hawaiian lavas and the most depleted lavas from Detroit Seamount have Ba/Th ratios exceeding those of MORB (Figure 17c). Their high Ba/Th implies that their source is also characterized by high Ba/Th. Consequently, this source is unlike the source of Garrett transform fault lavas in terms of Ba/Th.

[77] 4. Support for the hypothesis of *Regelous et al.* [2003] that the depleted component is plume related arises from rejuvenated stage Hawaiian lavas. Their Pb isotopic ratios also extend to low $^{206}Pb/^{204}Pb$ ratios [*Fekiacova and Abouchami*,

2003; *Frey et al.*, 2005], and they have high Ba/Th [*Yang et al.*, 2003]. Therefore a depleted plume component may be sampled by rejuvenated stage lavas during a second stage of plume melting [*Ribe and Christensen*, 1999] and during ascent of the plume beneath young and thin oceanic lithosphere, i.e., at Detroit Seamount.

6.5. A Hypothesis for the Geochemical and Age Differences Between Lavas From Site 884 and Site 1203

[78] The age of Site 884 lavas is ~81 ± 1 Ma on the basis of ^{40}Ar-^{39}Ar data for a reverse polarity, tholeiitic basalt [*Keller et al.*, 1995]. At Site 1203, *Duncan and Keller* [2004] obtained an average age of ~76 ± 1 Ma for five normal polarity, tholeiitic lavas. On the basis of its large area (Figure 1b), it is likely that Detroit Seamount consists of several coalesced shields, much like the Big Island of Hawaii. However, an age difference of 5 Myr between Site 1203 and Site 884 is much larger than that for the five shields on the Big Island of Hawaii which all formed over the past 1 Myr. What is the explanation for an age difference of 5 Myr for tholeiitic lavas erupted at sites separated by only 48 km?

[79] It is well-established that near-axis plumes interact with the spreading ridge axis. Using the Galapagos Platform as an analogy, plume-related volcanism in a near-ridge environment is more dispersed and long-lived [e.g., *Sinton et al.*, 1996] than at an intraplate location, such as Hawaii. We propose a scenario that can explain both the old age of Site 884 lavas and their relatively shallow, MORB-like, melt segregation depths (Figure 15). *Sleep* [2002] noted that "off-axis hot spots appear to shut off at the time that an on-axis hot spot becomes active along an axis-approaching track"; i.e., there is a time when volcanism ceases above the hot spot and partial melting of plume material does not occur until ascent at the spreading center (Figure 18a). If the plate moved faster than the plume motion, at some later time the plume was overlain by plume-related lithosphere created at the spreading center (Figure 18b). Perhaps at ~76 Ma, the Hawaiian plume was distant from the spreading center, and intraplate volcanism represented by lavas from Site 883, 1203 and 1204 erupted in close proximity to older Site 884 lavas which erupted at the spreading center (Figure 18c). Melting to a shallow depth at a spreading center for Site 884 lavas implies a large melting extent, and consequently Site 884 magmas sampled a depleted and refractory component with low ^{206}Pb/^{204}Pb.

7. Conclusions

[80] On the basis of studies of drill cores from four drill sites at Detroit Seamount and the comparisons with EPR N-MORB and Mauna Kea lavas, our major conclusions are as follows:

[81] 1. The rapid subsidence rates inferred for Detroit Seamount support the view that this seamount formed on young and thin oceanic lithosphere close to a spreading ridge axis. Also consistent with this inference, major and trace element compositions of Detroit Seamount lavas show that their parental magmas were segregated at a lower pressure than Hawaiian lavas which formed under old and thick oceanic lithosphere.

[82] 2. The upward transition from intercalated alkalic and tholeiitic basalt to solely tholeiitic basalt at Site 1203 may reflect the preshield to shield stage transition, whereas alkalic basalts from Sites 883 and 1204 probably represent postshield stage lavas. Like preshield stage alkalic Kilauea lavas, phlogopite appears to have played an important role in generating the preshield stage alkalic lavas at Site 1203. Also, similar to preshield stage Loihi lavas, Site 1203 alkalic lavas are characterized by high ^{208}Pb/^{204}Pb at a given ^{206}Pb/^{204}Pb.

[83] 3. Both tholeiitic and alkalic Detroit Seamount lavas have lower concentrations of highly incompatible elements, lower ^{87}Sr/^{86}Sr and higher ^{143}Nd/^{144}Nd than the corresponding lava types from young Hawaiian volcanoes. Also Detroit Seamount lavas contain a component with unradiogenic Pb that is not present in Hawaiian shield stage lavas or EPR MORB. Such a component is present in lavas erupted from a spreading center within the Garrett transform fault. However, Site 884 lavas with the most depleted isotopic characteristics have high Ba/Th unlike those of MORB and Garrett transform fault lavas. If the depleted component has high Ba/Th, it is plume-related. Hawaiian rejuvenated stage lavas also have high Ba/Th and define a trend to low ^{87}Sr/^{86}Sr and ^{206}Pb/^{204}Pb, similar to the trend of Detroit lavas (Figure 12c). Rejuvenated stage melts have been proposed as second-stage melts of the Hawaiian plume [*Ribe and Christensen*, 1999]. Therefore this depleted component may be a refractory component of the plume that is only sampled at high degrees of melting, such as occurred at ~81 Ma when the plume was near a spreading center.

[84] 4. The surprisingly large age difference (~81 and 76 Ma) between lavas at two drill sites on Detroit Seamount may reflect the complexity of plume-related volcanism in a near ridge axis environment.

Acknowledgments

[85] We thank the crew and scientific staff of the Joides Resolution during ODP Leg 197 for their help in acquiring and describing lavas from Detroit Seamount. This research was supported by the U.S. Science Support Program. The Ocean Drilling Program is sponsored by the National Science Foundation and participating countries under the management of Joint Oceanographic Institutions, Inc. A grant from the Deutsche Forchungsgemeinschaft is gratefully acknowledged by M. Regelous. We thank S. Bowring for access to the MIT Mass Spectrometer facility and especially F. Dudas for his dedicated efforts obtaining isotopic data, M. Rhodes for access to the XRF facility at UMASS and M. Vollinger for his help in XRF analysis, and B. Grant and R. Kayser for their assistance in ICP-MS analysis. M. Regelous thanks B. Paterson and J. Wade for their help with the LA-ICP-MS and electron probe analyses. This paper benefited from reviews by P. Castillo and T. Sisson, the editorial comments of W. White and R. Duncan, and discussion with S. Parman, A. Hofmann, W. Abouchami, S. Galer, and C. Hawkesworth.

References

Abouchami, W., S. J. G. Galer, and A. W. Hofmann (2000), High precision lead isotope systematics of lavas from the Hawaiian Scientific Drilling Project, *Chem. Geol.*, *169*, 187–209.

Adam, J., T. H. Green, and S. H. Sie (1993), Proton microprobe determined partitioning of Rb, Sr, Ba, Y, Zr, Nb and Ta between experimentally produced amphiboles and silicate melts with variable F content, *Chem. Geol.*, *109*, 29–49.

Albarede, F. (1992), How deep do common basaltic magmas form and differentiate?, *J. Geophys. Res.*, *97*(7), 10,997–11,009.

Bach, W., B. Peucker-Ehrenbrink, S. R. Hart, and J. S. Blusztajn (2003), Geochemistry of hydrothermally altered oceanic crust: DSDP/ODP Hole 504B—Implications for seawater-crust exchange budgets and Sr- and Pb-isotopic evolution of the mantle, *Geochem. Geophys. Geosyst.*, *4*(3), 8904, doi:10.1029/2002GC000419.

Barrett, T. J. (1983), Strontium and lead-isotope composition of some basalts from Deep Sea Drilling Project Hole 504B, Costa Rica Rift, Legs 69 and 70, *Initial Rep. Deep Sea Drill. Proj.*, *69*, 643–650.

Basaltic Volcanism Study Project (1981), *Basaltic Volcanism on the Terrestrial Planets*, 1286 pp., Elsevier, New York.

Bass, M. N., R. Moberly, J. M. Rhodes, C. Shih, and S. E. Church (1973), Volcanic rocks cored in the Central Pacific, Leg 17 Deep Sea Drilling Project, *Initial Rep. Deep Sea Drill. Proj.*, *17*, 429–504.

Blichert-Toft, J., D. Weis, C. Maerschalk, A. Agranier, and F. Albarède (2003), Hawaiian hot spot dynamics as inferred from the Hf and Pb isotope evolution of Mauna Kea volcano, *Geochem. Geophys. Geosyst.*, *4*(2), 8704, doi:10.1029/2002GC000340.

Blundy, J. D., T. J. Falloon, B. J. Wood, and J. A. Dalton (1995), Sodium partitioning between clinopyroxene and silicate melts, *J. Geophys. Res.*, *100*(8), 15,501–15,515.

Blundy, J. D., J. A. C. Robinson, and B. J. Wood (1998), Heavy REE are compatible in clinopyroxene on the spinel lherzolite solidus, *Earth Planet. Sci. Lett.*, *160*, 493–504.

Caplan-Auerbach, J., F. Duennebier, and G. Ito (2000), Origin of intraplate volcanoes from guyot heights and oceanic paleodepth, *J. Geophys. Res.*, *105*(2), 2679–2698.

Carmichael, I. S. E., F. J. Turner, and F. Verhoogen (1974), *Igneous Petrology*, McGraw-Hill, New York.

Castillo, P. R., R. W. Carlson, and R. Batiza (1991), Origin of Nauru Basin igneous complex: Sr, Nd and Pb isotope and REE constraints, *Earth Planet Sci Lett.*, *103*(1–4), 200–213.

Castillo, P. R., P. A. Floyd, and C. France-Lanord (1992), Isotope geochemistry of Leg 129 basalts: Implications for the origin of the widespread Cretaceous volcanic event in the Pacific, *Proc. Ocean Drill. Program Sci. Results*, *129*, 405–513.

Castillo, P. R., M. S. Pringle, and R. W. Carlson (1994), East Mariana Basin tholeiites: Cretaceous intraplate basalts or rift basalts related to the Ontong Java plume?, *Earth Planet Sci Lett.*, *123*(1–4), 139–154.

Castillo, P. R., J. H. Natland, Y. Niu, and P. F. Lonsdale (1998), Sr, Nd and Pb isotopic variation along the Pacific-Antarctic risecrest, 53–57 degrees S: Implications for the composition and dynamics of the South Pacific upper mantle, *Earth Planet Sci. Lett.*, *154*(1–4), 109–125.

Castillo, P. R., E. Klein, J. Bender, C. Langmuir, S. Shirey, R. Batiza, and W. White (2000), Petrology and Sr, Nd, and Pb isotope geochemistry of mid-ocean ridge basalt glasses from the 11°45′N to 15°00′N segment of the East Pacific Rise, *Geochem. Geophys. Geosyst.*, *1*, doi:10.1029/1999GC000024.

Chen, C.-Y., and F. A. Frey (1985), Trace element and isotope geochemistry of lavas from Haleakala Volcano, East Maui: Implications for the origin of Hawaiian basalts, *J. Geophys. Res.*, *90*(B10), 8743–8768.

Clague, D. A., and G. B. Dalrymple (1987), The Hawaiian-Emperor volcanic chain: Part I, Geologic evolution, in *Volcanism in Hawaii*, edited by R. W. Decker, T. L. Wright, and P. H. Stauffer, *U.S. Geol. Surv. Prof. Pap.*, *P 1350*, 5–73.

Class, C., and S. L. Goldstein (1997), Plume-lithosphere interactions in the ocean basins: Constraints from the source mineralogy, *Earth Planet Sci Lett.*, *150*(3–4), 245–260.

Cottrell, R. D., and J. A. Tarduno (2003), A Late cretaceous pole for the Pacific plate: Implications for apparent and true polar wander and the drift of hotspots, *Tectonophysics*, *362*, 321–333.

Dalrymple, G. B., M. A. Lanphere, and D. A. Clague (1980), Conventional and $^{40}Ar/^{39}Ar$ K-Ar ages of volcanic rocks from Ojin (Site 430), Nintoku (Site 432), and Suiko (Site 433) seamounts and the chronology of volcanic propagation along the Hawaiian-Emperor chain, *Initial Rep. Deep Sea Drill. Proj.*, *55*, 659–676.

DePaolo, D. J., E. M. Stolper, D. M. Thomas, and M. O. Garcia (1999), Hawaii Scientific Drilling Project: Core logs and summarizing data, report, Calif. Inst. of Technol., Pasadena.

Duncan, R. A., and R. A. Keller (2004), Radiometric ages for basement rocks from the Emperor Seamounts, ODP Leg 197, *Geochem. Geophys. Geosyst.*, *5*, Q08L03, doi:10.1029/2004GC000704.

Eisele, J., W. Abouchami, S. J. G. Galer, and A. W. Hofmann (2003), The 320 kyr Pb isotope evolution of Mauna Kea

lavas recorded in the HSDP-2 drill core, *Geochem. Geophys. Geosyst.*, *4*(5), 8710, doi:10.1029/2002GC000339.
Fekiacova, Z., and W. Abouchami (2003), Pb isotopic evolution of Koolau volcano (Oahu, Hawaii), *Eos Trans. AGU*, *84*(46), Fall Meet. Suppl., Abstract V32A-0991.
Foley, S. F., W. R. Taylor, and D. H. Green (1986), The role of fluorine and oxygen fugacity in the genesis of the ultrapotassic rocks, *Contrib. Mineral. Petrol.*, *94*(2), 183–192.
Foley, S. F., S. E. Jackson, B. J. Fryer, J. D. Greenough, and G. A. Jenner (1996), Trace element partition coefficients for clinopyroxene and phlogopite in an alkaline lamprophyre from Newfoundland by LAM-ICP-MS, *Geochim. Cosmochim. Acta*, *60*(4), 629–638.
Fornari, D. J., M. R. Perfit, J. F. Allan, R. Batiza, R. M. Haymon, A. M. Barone, W. B. F. Ryan, S. Terri, T. Simkin, and M. A. Luckman (1988), Geochemical and structural studies of the Lamont Seamounts: Seamounts as indicators of mantle processes, *Earth Planet. Sci. Lett.*, *89*(1), 63–83.
Frey, F. A., and M. F. Roden (1987), The mantle source for the Hawaiian Islands: Constraints from the lavas and ultramafic inclusions, in *Mantle Metasomatism*, pp. 423–463, Elsevier, New York.
Frey, F. A., W. S. Wise, M. O. Garcia, H. West, S. T. Kwon, and A. Kennedy (1990), Evolution of Mauna Kea volcano, Hawaii: Petrologic and geochemical constraints on postshield volcanism, *J. Geophys. Res.*, *95*, 1271–1300.
Frey, F. A., M. O. Garcia, W. S. Wise, A. Kennedy, P. Gurriet, and F. Albarede (1991), The evolution of Mauna Kea volcano, Hawaii: Petrogenesis of tholeiitic and alkalic basalts, *J. Geophys. Res.*, *96*, 14,347–14,375.
Frey, F. A., M. O. Garcia, and M. F. Roden (1994), Geochemical characteristics of Koolau Volcano: Implications of intershield geochemical differences among Hawaiian volcanoes, *Geochim. Cosmochim. Acta*, *58*, 1441–1462.
Frey, F. A., D. Clague, J. J. Mahoney, and J. M. Sinton (2000), Volcanism at the edge of the Hawaiian plume: Petrogenesis of submarine alkalic lavas from the North Arch volcanic field, *J. Petrol.*, *41*(5), 667–691.
Frey, F. A., S. Huang, J. Blichert-Toft, M. Regelous, and M. Boyet (2005), Origin of depleted components in lavas related to the Hawaiian hot spot: Evidence from Hf isotope data, *Geochem. Geophys. Geosyst.*, doi:10.1029/2004GC000757, in press.
Galer, S. J. G., W. Abouchami, and J. D. Macdougall (1999), East Pacific Rise MORB through the Pb isotope lookingglass, *Eos Trans. AGU*, *80*(46), Fall Meet. Suppl., F1086.
Garcia, M. O., B. A. Jorgenson, J. J. Mahoney, E. Ito, and A. J. Irving (1993), An evaluation of temporal geochemical evolution of Loihii summit lavas: Results from Alvin submersible dives, *J. Geophys. Res.*, *98*, 535–550.
Garcia, M. O., D. J. P. Foss, H. B. West, and J. J. Mahoney (1995), Geochemical and isotopic evolution of Loihi Volcano, Hawaii, *J. Petrol.*, *36*, 1647–1674.
Garcia, M. O., K. H. Rubin, M. D. Norman, J. M. Rhodes, D. W. Graham, D. W. Muenow, and K. Spencer (1998), Petrology and geochronology of basalt breccia from the 1996 earthquake swarm of Loihi Seamount, Hawaii: Magmatic history of its 1996 eruption, *Bull. Volcanol.*, *59*, 577–592.
Green, T. H., J. D. Blundy, J. Adam, and G. M. Yaxley (2000), SIMS determination of trace element partition coefficients between garnet, clinopyroxene and hydrous basaltic liquids at 2–7.5 GPa and 1080–1200°C, *Lithos*, *53*, 165–187.
Haase, K. M. (2002), Geochemical constraints on magma sources and mixing processes in Easter Microplate MORB (SE Pacific): A case study of plume-ridge interaction, *Chem. Geol.*, *182*(2–4), 335–355.
Hanan, B. B., and J.-G. Schilling (1989), Easter Microplate evolution: Pb isotope evidence, *J. Geophys. Res.*, *94*(6), 7432–7448.
Hart, S. R., and T. Dunn (1993), Experimental clinopyroxene/melt partitioning for 24 trace elements, *Contrib. Mineral. Petrol.*, *113*(1), 1–8.
Hickey-Vargas, R. (1991), Isotope characteristics of submarine lavas from the Philippine Sea: Implications for the origin of arc and basin magmas of the Philippine tectonic plate, *Earth Planet. Sci. Lett.*, *107*(2), 290–304.
Hofmann, A. W. (1986), Nb in Hawaiian magmas: Constraints on source composition and evolution, *Chem. Geol.*, *57*, 17–30.
Hofmann, A. W. (1988), Chemical differentiation of the Earth: The relationship between mantle, continental crust, and oceanic crust, *Earth Planet. Sci. Lett.*, *90*, 297–314.
Hofmann, A. W., and K. P. Jochum (1996), Source characteristics derived from very incompatible trace elements in Mauna Loa and Mauna Kea basalts (Hawaiian Scientific Drilling Project), *J. Geophys. Res.*, *101*, 11,831–11,839.
Hofmann, A. W., and W. M. White (1983), Ba, Rb and Cs in the Earth's mantle, *Z. Naturforssch.*, *38a*, 258–266.
Huang, S., and F. A. Frey (2003), Trace element abundances of Mauna Kea basalt from Phase 2 of the Hawaiian Scientific Drilling Project: Petrogenetic implications of correlations with major element content and isotopic ratios, *Geochem. Geophys. Geosyst.*, *4*(6), 8711, doi:10.1029/2002GC000322.
Huang, S., H.-J. Yang, and F. A. Frey (2000), Understanding the anomalous Ba/Th ratio in Hawaiian shield lavas, *Eos Trans. AGU*, *81*(48), Fall Meet. Suppl., Abstract V11D-06.
Irving, A. F., and F. A. Frey (1978), Distribution of trace elements between garnet megacrysts and host volcanic liquids of kimberlitic to rhyolite composition, *Geochim. Cosmochim. Acta.*, *42*, 771–787.
Janney, P. E., and P. R. Castillo (1997), Geochemistry of Mesozoic Pacific mid-ocean ridge basalt: Constraints on melt generation and the evolution of the Pacific upper mantle, *J. Geophys. Res.*, *102*(3), 5207–5229.
Keller, R. A., R. A. Duncan, and M. R. Fisk (1995), Geochemistry and $^{40}Ar/^{39}Ar$ geochronology of basalt from ODP Leg 45 (North Pacific Transect), *Proc. Ocean Drill. Program Sci. Result*, *145*, 333–343.
Keller, R. A., M. R. Fish, and W. M. White (2000), Isotopic evidence for Late Cretaceous plume-ridge interaction at the Hawaiian hotspot, *Nature*, *405*, 673–676.
Kempton, P. D., P. M. E. Thompson, and A. D. Saunders (2002), Did the ancestral Hawaiian plume interact with a mid-ocean ridge? The isotopic evidence, *Geochim. Cosmochim. Acta.*, *66*(15A), suppl., A392.
Kinman, W. S., and C. R. Neal (2002), The influence of MORB on a plume-generated seamount: The story told by plagioclase phenocrysts from Detroit Seamount lavas, Emperor Seamount Chain, *Eos Trans. AGU*, *83*(47), Fall Meet. Suppl., Abstract T61C-10.
Kinzler, R. J. (1997), Melting of mantle peridotite at pressures approaching the spinel to garnet transition: Application to mid-ocean ridge basalt petrogenesis, *J. Geophys. Res.*, *102*(1), 853–874.
Kirkpatrick, R. J., D. Clague, and W. Freisen (1980), Petrology and geochemistry of volcanic rocks, DSDP Leg 55, Emperor Seamount Chain, *Initial Rep. Deep Sea Drill. Proj.*, *55*, 509–557.
Langmuir, C. H., E. M. Klein, and T. Plank (1992), Petrological systematics of mid-ocean ridge basalt: Constraints on melt generation beneath ocean ridges, in *Mantle Flow and*

Melt Generation at Mid-Ocean Ridges, *Geophys. Monogr. Ser.*, vol. 71, pp. 183–280, AGU, Washington, D. C.

Lanphere, M. A., G. B. Dalrymple, and D. A. Clague (1980), Rb-Sr systematics of basalts from the Hawaiian-Emperor volcanic chain, *Initial Rep. Deep Sea Drill. Proj.*, *55*, 695–706.

Lassiter, J. C., and E. H. Hauri (1998), Osmium-isotope variations in Hawaiian lavas: Evidence for recycled oceanic lithosphere in the Hawaiian plume, *Earth Planet Sci Lett.*, *164*, 483–496.

Lassiter, J. C., D. J. DePaolo, and M. Tatsumoto (1996), Isotopic evolution of Mauna Kea volcano: Results from the initial phase of the Hawaiian Scientific Drilling Project, *J. Geophys. Res.*, *101*, 11,769–11,780.

Lassiter, J. C., E. H. Hauri, P. W. Reiners, and M. O. Garcia (2000), Generation of Hawaiian post-erosional lavas by melting of a mixed lherzolite/pyroxenite source, *Earth Planet. Sci. Lett.*, *178*(3–4), 269–284.

LaTourrette, T., R. L. Hervig, and J. R. Holloway (1995), Trace element partitioning between amphibole, phlogopite, and basanite melt, *Earth Planet. Sci Lett.*, *135*, 13–30.

Li, X., R. Kind, X. Yuan, I. Wölbern, and W. Hanka (2004), Rejuvenation of the lithosphere by the Hawaiian plume, *Nature*, *427*, 827–829, doi:10.1038/nature02349.

Lipman, P. W., T. W. Sisson, T. Ui, J. Naka, and D. K. Smith (2002), Ancestral submarine growth of Kilauea volcano and instability of its south flank, in *Hawaiian Volcanoes: Deep Underwater Perspectives*, *Geophys. Monogr. Ser.*, vol. 128, edited by E. Takahashi et al., pp. 161–192, AGU, Washington, D. C.

Longerich, H. P., S. E. Jackson, and D. Günther (1996), Laser ablation inductively coupled plasma mass spectrometric transient signal data acquisition and analyte concentration calculation, *J. At. Anal. Spectrom.*, *11*, 899–904.

Longhi, J. (2002), Some phase equilibrium systematics of lherzolite melting: I, *Geochem. Geophys. Geosyst.*, *3*(3), 1020, doi:10.1029/2001GC000204.

Lonsdale, P. (1988), Paleogene history of the Kula Plate: Offshore evidence and onshore implications, *Geol. Soc. Am. Bull.*, *100*, 733–754.

Lonsdale, P., J. Dieu, and J. Natland (1993), Posterosional volcanism in the Cretaceous part of the Hawaiian hotspot trail, *J. Geophys. Res.*, *98*, 4081–4898.

Macdonald, G. A., and T. Katsura (1964), Chemical composition of Hawaiian lavas, *J. Petrol.*, *5*(1), 82–133.

Mammerickx, J., and G. F. Sharman (1988), Tectonic evolution of the North Pacific during the Cretaceous Quiet Period, *J. Geophys. Res.*, *93*, 3009–3024.

Mengel, K., and D. H. Green (1986), Stability of amphibole and phlogopite in metasomatized peridotite under water-saturated and water-undersaturated conditions, in *Proceedings of the Fourth International Kimberlite Conference*, vol. 1, edited by J. Ross et al., pp. 571–581, Blackwell Sci., Malden, Mass.

Moore, J. G. (1987), Subsidence of the Hawaiian Ridge, in *Volcanism in Hawaii*, edited by R. W. Decker, T. L. Wright, and P. H. Stauffer, *U.S. Geol. Surv. Prof. Pap.*, *1350 II*, 85–100.

Mueller, R. D., W. R. Roest, J.-Y. Royer, L. M. Gahagan, and J. G. Sclater (1997), Digital isochrons of the world's ocean floor, *J. Geophys. Res.*, *102*(2), 3211–3214.

Niu, Y., and R. Batiza (1997), Trace element evidence from seamounts for recycled oceanic crust in the eastern Pacific mantle, *Earth Planet. Sci. Lett.*, *148*(3–4), 471–483.

Niu, Y., K. D. Collerson, R. Batiza, J. I. Wendt, and M. Regelous (1999), Origin of enriched-type mid-ocean ridge basalt at ridges far from mantle plumes: The East Pacific Rise at 11°20′N, *J. Geophys. Res.*, *104*(B4), 7067–7088.

Niu, Y., M. Regelous, I. J. Wendt, R. Batiza, and M. J. O'Hara (2002), Geochemistry of near-EPR seamounts: Importance of source vs. process and the origin of enriched mantle component, *Earth Planet. Sci. Lett.*, *199*(3–4), 327–345.

Norman, M. D., and M. O. Garcia (1999), Primitive magmas and source characteristics of the Hawaiian Plume: Petrology and geochemistry of shield picrites, *Earth Planet. Sci. Lett.*, *168*(1–2), 27–44.

Parsons, B., and J. G. Sclater (1977), An analysis of the variation of ocean floor bathymetry and heat flow with age, *J. Geophys. Res.*, *82*(5), 803–827.

Putirka, K. (1999), Melting depths and mantle heterogeneity beneath Hawaii and the East Pacific Rise: Constraints from Na/Ti and rare earth element ratios, *J. Geophys. Res.*, *104*(2), 2817–2829.

Rea, D. K., and J. M. Dixon (1983), Late Cretaceous and Paleogene tectonic evolution of the North Pacific Ocean, *Earth Planet. Sci. Lett.*, *65*, 145–166.

Regelous, M., Y. Niu, J. I. Wendt, R. Batiza, A. Greig, and K. D. Collerson (1999), Variations in the geochemistry of magmatism on the East Pacific Rise at 10 degrees 30′N since 800 ka, *Earth Planet. Sci. Lett.*, *168*(1–2), 45–63.

Regelous, M., A. W. Hofmann, W. Abouchami, and S. J. G. Galer (2003), Geochemistry of lavas from the Emperor Seamounts, and the geochemical evolution of Hawaiian magmatism from 85 to 42 Ma, *J. Petrol.*, *44*, 113–140.

Rhodes, J. M. (1996), Geochemical stratigraphy of lava flows sampled by the Hawaii Scientific Drilling Project, *J. Geophys. Res.*, *101*, 11,729–11,746.

Rhodes, J. M., and J. P. Lockwood (Eds.) (1995), *Mauna Loa Revealed: Structure, Composition, History, and Hazards*, *Geophys. Monogr. Ser.*, vol. 92, AGU, Washington, D. C.

Rhodes, J. M., and M. J. Vollinger (2004), Composition of basaltic lavas sampled by phase-2 of the Hawaii Scientific Drilling Project: Geochemical stratigraphy and magma types, *Geochem. Geophys. Geosyst.*, *5*, Q03G13, doi:10.1029/2002GC000434.

Ribe, N. M., and U. R. Christensen (1999), The dynamical origin of Hawaiian volcanism, *Earth Planet. Sci. Lett.*, *171*(4), 517–531.

Roden, M. F., F. A. Frey, and D. A. Clague (1984), Geochemistry of tholeiitic and alkalic lavas from the Koolau Range, Oahu, Hawaii: Implications for Hawaiian volcanism, *Earth Planet. Sci. Lett.*, *69*(1), 141–158.

Roden, M. F., T. Trull, S. R. Hart, and F. A. Frey (1994), New He, Sr, Nd and Pb isotopic constraints on the constitution of the Hawaiian plume: Results from Koolau Volcano, Oahu, Hawaii, *Geochim. Cosmochim. Acta*, *58*, 1431–1440.

Schmidt, K. H., P. Bottazzi, R. Vannucci, and K. Mengel (1999), Trace element partitioning between phlogopite, clinopyroxene and leucite lamproite melt, *Earth Planet. Sci. Lett.*, *168*, 287–299.

Schmitz, M. D., and S. A. Bowring (2003), Ultrahigh-temperature metamorphism in the lower crust during Neoarchean Ventersdorp rifting and magmatism, Kaapvaal Craton, southern Africa, *Geol. Soc. Am. Bull.*, *115*, 533–548.

Sharp, W. D., and D. A. Clague (2002), An older, slower Hawaii-Emperor bend, *Eos Trans. AGU*, *83*(47), Fall Meet. Suppl., Abstract T61C-04.

Shipboard Scientific Party (1993), Site 884, *Proc. Ocean Drill. Program Initial Rep.*, *145*, 209–302.

Shipboard Scientific Party (2002a), Site 1203, *Proc. Ocean Drill. Program Initial Rep.* [CD-ROM], *197*, 171 pp.

Shipboard Scientific Party (2002b), Site 1204, *Proc. Ocean Drill. Program Initial Rep.* [CD-ROM], *197*, 125 pp.

Sinton, C. W., D. M. Christie, and R. A. Duncan (1996), Geochronology of Galapagos seamounts, *J. Geophys. Res.*, *101*(6), 13,689–13,700.

Sisson, T., P. W. Lipman, and J. Naka (2002), Submarine alkalic through tholeiitic shield-stage development of Kilauea volcano, in *Hawaiian Volcanoes: Deep Underwater Perspectives*, *Geophys. Monogr. Ser.*, vol. 128, edited by E. Takahashi et al., pp. 193–220.

Sleep, N. H. (2002), Ridge-crossing mantle plumes and gaps in tracks, *Geochem. Geophys. Geosyst.*, *3*(12), 8505, doi:10.1029/2001GC000290.

Sobolev, A. V., A. W. Hofmann, and I. K. Nikogosian (2000), Recycled oceanic crust observed in ghost plagioclase within the source of Mauna Loa lavas, *Nature*, *404*, 986–990.

Staudigel, H., G. R. Davies, S. R. Hart, K. M. Marchant, and B. M. Smith (1995), Large scale isotopic Sr, Nd and O isotopic anatomy of altered oceanic crust: DSDP/ODP sites 417/418, *Earth Planet. Sci. Lett.*, *130*, 169–185.

Stein, C. A., and S. Stein (1992), A model for the global variation in oceanic depth and heat flow with lithospheric age, *Nature*, *359*(6391), 123–129.

Stille, P., D. M. Unruh, and M. Tatsumoto (1983), Pb, Sr, Nd and Hf isotopic evidence of multiple sources for Oahu, Hawaii basalts, *Nature*, *304*(5921), 25–29.

Stolper, E., S. Sherman, M. Garcia, M. Baker, and C. Seaman (2004), Glass in the submarine section of the HSDP2 drill core, Hilo, Hawaii, *Geochem. Geophys. Geosyst.*, *5*, Q07G15, doi:10.1029/2003GC000553.

Sturm, M. E., E. M. Klein, D. W. Graham, and J. Karsten (1999), Age constraints on crustal recycling to the mantle beneath the southern Chile Ridge: He-Pb-Sr-Nd isotope systematics, *J. Geophys. Res.*, *104*(3), 5097–5114.

Sun, S.-S., and W. F. McDonough (1989), Chemical and isotopic systematics of oceanic basalts: Implications for mantle composition and processes, in *Magmatism in the Ocean Basins*, edited by A. D. Saunders and M. J. Norry, *Geol. Soc. Spec. Publ.*, *42*, 313–345.

Tarduno, J. A., et al. (2002), *Proceedings of the Ocean Drilling Program, Initial Reports* [CD-ROM], vol. 197, 171 pp., Ocean Drill. Program, College Station, Tex.

Tarduno, J. A., et al. (2003), The Emperor Seamounts: Southward motion of the Hawaiian Hotspot plume in Earth's mantle, *Science*, *301*(5636), 1064–1069.

Tatsumoto, M., E. Hegner, and D. M. Unruh (1987), Origin of the West Maui volcanic rocks inferred from Pb, Sr, and Nd isotopes and a multicomponent model for oceanic basalt, in *Volcanism in Hawaii*, edited by R. W. Decker, T. L. Wright, and P. H. Stauffer, *U.S. Geol. Surv. Prof. Pap.*, *1350 II*, 723–744.

Thompson, P. M. E., P. D. Kempton, and A. D. Saunders (2002), The 48 Ma Koko Guyot: Early indications of temporal changes in the composition of the Hawaiian plume, *Eos Trans. AGU*, *83*(47), Fall Meet. Suppl., Abstract T61C-09.

van Westrenen, W., J. Blundy, and B. Wood (1999), Crystal-chemical controls on trace element partitioning between garnet and anhydrous silicate melt, *Am. Mineral.*, *84*, 838–847.

Villemant, B., H. Jaffrezic, J.-L. Joron, and M. Treuil (1981), Distribution coefficients of major and trace elements: Fractional crystallization in the alkali basalt series of Chaine des Puys (Massif Central, France), *Geochim. Cosmochim. Acta.*, *45*, 1997–2016.

Walter, M. J. (1998), Melting of garnet peridotite and the origin of komatiite and depleted lithosphere, *J. Petrol.*, *39*(1), 29–60.

Wendt, J. I., M. Regelous, Y. Niu, R. Hekinian, and K. D. Collerson (1999), Geochemistry of lavas from the Garrett Transform Fault: Insights into mantle heterogeneity beneath the eastern Pacific, *Earth Planet. Sci. Lett.*, *173*, 271–284.

White, W. M., A. W. Hofmann, and H. Puchelt (1987), Isotope geochemistry of Pacific mid-ocean ridge basalt, *J. Geophys. Res.*, *92*, 4881–4893.

Wilson, J. T. (1963), A possible origin of the Hawaiian Islands, *Can. J. Phys.*, *21*, 863–870.

Yang, H.-J., F. A. Frey, J. M. Rhodes, and M. O. Garcia (1996), Evolution of Mauna Kea volcano: Inferences from lava compositions recovered in the Hawaii Scientific Drilling Project, *J. Geophys. Res.*, *101*, 11,747–11,767.

Yang, H.-J., F. A. Frey, and D. A. Clague (2003), Constraints on the source components of lavas forming the Hawaiian North Arch and Honolulu Volcanoes, *J. Petrol.*, *44*, 603–627.